

SEPARATION OF SPIKY TRANSIENTS IN EEG/MEG USING  
MORPHOLOGICAL FILTERS IN MULTI-RESOLUTION ANALYSIS

by

Lin-Sen Pon

B. S. in Electronic Engineering, Chung-Yuan Christian University

M. S. in Electronic Engineering, University of Lowell

Submitted to the Graduate Faculty  
of the School of Engineering  
in partial fulfillment of  
the requirement for the degree of  
Doctor  
of  
Philosophy

University of Pittsburgh  
2002

The Author grants permission  
to reproduce single copies.

---

Signed

## COMMITTEE SIGNATURE PAGE

This dissertation was presented

by

Lin-Sen Pon

It was defended on

Feb 20, 2002

and approved by

(Signature) \_\_\_\_\_  
Committee Chairperson  
Ching-Chung Li, Ph.D. (Electrical Engineering)

(Signature) \_\_\_\_\_  
Committee Co-chairperson  
Robert J. Sclabassi, M.D., Ph.D. (Neurological Surgery, Electrical Engineering)

(Signature) \_\_\_\_\_  
Committee Co-chairperson  
Mingui Sun, Ph.D. (Neurological Surgery, Electrical Engineering)

(Signature) \_\_\_\_\_  
Committee Member  
Robert J. Boston, Ph.D. (Electrical Engineering)

(Signature) \_\_\_\_\_  
Committee Member  
Luis F. Chaparro, Ph.D. (Electrical Engineering)

(Signature) \_\_\_\_\_  
Committee Member  
Delma J. Hebert, Ph.D. (Mathematics)

(Signature) \_\_\_\_\_  
Committee Member  
Mark L. Scheuer, M.D. (Neurology)

(Signature) \_\_\_\_\_  
Committee Member  
Marwan A. Simaan, Ph.D. (Electrical Engineering)

## ABSTRACT

Signature \_\_\_\_\_

Ching-Chung Li, Ph.D.

### SEPARATION OF SPIKY TRANSIENTS IN EEG/MEG USING MORPHOLOGICAL FILTERS IN MULTI-RESOLUTION ANALYSIS

Lin-Sen Pon , Ph.D.

University of Pittsburgh

Epileptic electroencephalographic (EEG) data often contains a large number of sharp spiky transient patterns which are diagnostically important. Background activity is the EEG activity representing the normal pattern from the brain. Transient activity manifests itself as any non-structured sharp wave with dynamically short appearance as distinguished from the background EEG. Generally speaking, the amplitude change of background activity varies slowly with time and spiky transient activity varies quickly with pointed peaks.

In this thesis, a method has been developed to automatically extract transient patterns based on morphological filtering in multiresolution representation. Using a simple structuring element (SE) to match a signal's geometrical shape, mathematical morphology is applied to detect the differences of morphological characteristics of

signals. If a signal contains features consistent with the geometrical feature of the structuring element, a morphological filter can recognize and extract the signal of interest. The multiresolution scheme can be based on the wavelet packet transform which decomposes a signal into scaling and wavelet coefficients of different resolutions. The morphological separation filter is applied to these coefficients to produce two subsets of coefficients for each coefficient sequence: one representing the background activity and the other representing the transients. These subsets of coefficients are processed by the inverse wavelet transform to obtain the transient component and the background component. Alternatively, a morphological lifting scheme has been proposed for separation these two components. Experimental results on both synthetic data and real EEG data have shown that the developed methods are highly effective in automatic extraction of spiky transients in the epileptic EEG data.

The interictal spike trains thus extracted from multiple electrode recordings are further analyzed. Their cross-correlograms are examined according to the stochastic point process model. Our experiment result has been verified by human experts' estimation.

## DESCRIPTORS

EEG	Epilepsy
Interictal Activity	Lifting Scheme
Mathematical Morphology	Multiresolution Analysis
Stochastic Point Process	Transient
Wavelet Packet Transform	Wavelet Transform

## ACKNOWLEDGMENTS

I would like to express my sincere thanks to my advisors Dr. Robert J. Scwabassi and Dr. Mingui Sun of the Laboratory for Computational Neuroscience, University of Pittsburgh, for the guidance and support given to me throughout the course of doctoral studies.

Special thanks to my Dr. C. C. Li in the Electrical Engineering, University of Pittsburgh for his encouragement and help which have been a great inspiration to me and allowed me to stay focused on my studies. I would also like to thank the members of my committee: Dr. Marwan Simaan, Dr. Bob Boston, Dr. Luis Chaparro, Dr. Delma Hebert, Dr. Marker Scheuer and again Dr. Robert Scwabassi and Dr. Mingui Sun for their roles on my dissertation committee.

The data used in this paper has been obtained from a young epilepsy patient who has had a serious symptoms for his entire life. My blessing is dedicated to him and I wish that he will be cured soon.

Most of all I would like to thank my parents and my wife Shu-Ling Yang. Without their endless patience and support I would never have made it this far. My daughter Vanessa and son Kevin, who are not very helpful, but the enjoyment of their presence is a tremendous encouragement.

# TABLE OF CONTENTS

	<u>Page</u>
<b>ABSTRACT</b> . . . . .	<b>iv</b>
<b>ACKNOWLEDGMENTS</b> . . . . .	<b>vi</b>
<b>LIST OF TABLES</b> . . . . .	<b>xi</b>
<b>LIST OF FIGURES</b> . . . . .	<b>xii</b>
<b>NOMENCLATURE</b> . . . . .	<b>xvi</b>
<b>1.0 INTRODUCTION</b> . . . . .	<b>1</b>
1.1 A Brief Review of Existing Approaches for Separation of Signal Components . . . . .	5
1.2 Correlative Analysis of Multiple Electrode Spike Trains . . . . .	10
1.3 Objective of This Research . . . . .	11
1.4 Organization of the Thesis . . . . .	12
<b>2.0 MATHEMATICAL METHODS</b> . . . . .	<b>13</b>
2.1 Mathematical Morphology . . . . .	13
2.1.1 Fundamental Operators of Mathematical Morphology . . . . .	14
2.1.2 Morphological Erosion, Dilation, Closing and Opening . . . . .	18
2.2 Multiresolution Scheme . . . . .	24
2.2.1 Wavelet Transform and Wavelet Packet Transform . . . . .	25
2.2.2 Lifting Scheme . . . . .	29
2.2.3 Morphological Lifting Scheme . . . . .	33

2.3	Stochastic Point Process of Spike Trains . . . . .	34
<b>3.0</b>	<b>METHODS FOR SEPARATION OF SIGNAL COMPONENTS</b>	<b>41</b>
3.1	The Concept of Multi-resolution Morphological Separation Method . . . . .	41
3.1.1	Effect of Using Different Sizes of Structuring Element . . . . .	42
3.1.2	Effect of Using Coarse Scale Signals . . . . .	44
3.1.3	The Comparison Between Varying SE Size and Varying Signal Scale . . . . .	48
3.2	A Separation Method Using Morphological Filtering in Wavelet Packet Transform . . . . .	50
3.2.1	Linear Function . . . . .	50
3.2.2	Morphological Classification . . . . .	51
3.2.2.1	Decomposition . . . . .	53
3.2.2.2	Reconstruction . . . . .	56
3.2.3	Synthetic Spike Signal Using Morphological Wavelet Packet Transform . . . . .	59
3.3	A Separation Method Using Morphological Lifting Scheme . . . . .	64
3.3.1	Decomposition and Reconstruction Processes of the Morpho- logical Lifting Scheme . . . . .	65
3.3.2	Synthetic Spike Signal Using Morphological Lifting Scheme . . . . .	69

<b>4.0</b>	<b>EXPERIMENTAL RESULTS ON EEG/MEG DATA . . . . .</b>	<b>72</b>
4.1	Experiment of Simulation Data . . . . .	72
4.1.1	Results of Simulated Data Using Morphological Filtering in Wavelet Packet Transform . . . . .	72
4.1.2	Results of Simulated Data Using Morphological Lifting Scheme	81
4.2	Separation Results Using Real EEG Data . . . . .	82
4.2.1	Results of Real EEG Data Using Morphological Filter in Wavelet Packet Transform . . . . .	83
4.2.2	Results of Real EEG Data Using Morphological Lifting Scheme	86
4.3	Results of Spike Train Analysis . . . . .	87
4.3.1	Spike Train Analysis Using Subdural EEG Data . . . . .	88
4.3.2	Spike Train Analysis Using Scalp EEG Data . . . . .	91
4.3.3	Spike Train Analysis Using MEG Data . . . . .	103
<b>5.0</b>	<b>DISCUSSIONS . . . . .</b>	<b>113</b>
5.1	Summary . . . . .	113
5.2	Morphological Filtering in Wavelet Packet Decomposition . . . . .	115
5.3	Morphological Filtering in Lifting Scheme . . . . .	118
5.4	Statistical Point Process of Spike Trains . . . . .	120
<b>6.0</b>	<b>CONCLUSIONS . . . . .</b>	<b>123</b>
6.1	Contributions . . . . .	123
6.2	Future Works . . . . .	124

APPENDIX A	Data Acquisition of Subdural EEG Data . . . . .	125
APPENDIX B	Collection of EEG Data . . . . .	134
APPENDIX C	The Montage of EEG Recording . . . . .	138
APPENDIX D	International 10-20 System . . . . .	143
APPENDIX E	The Bi-Directional Spike Detection in EEG Using Morphological Filtering in Wavelet Transform . . . . .	146
BIBLIOGRAPHY	. . . . .	150

## LIST OF TABLES

<u>Table No.</u>	<u>Page</u>
4.1 The Signal-to-Noise Ratio of Synthetic Transient Data for a Single Trial	80
4.2 The Signal-to-Noise Ratio of Synthetic Background Data for a Single Trial . . . . .	80
4.3 The Average Signal-to-Noise Ratio of 500 Trials for Synthetic Transient Data . . . . .	80
4.4 The Average Signal-to-Noise Ratio of 500 Trials for Synthetic Back- ground Data . . . . .	81
B-1 Electrodes on the Frontal Area . . . . .	136
B-2 Electrodes on the Central Area of Brain . . . . .	137
B-3 Electrodes for Muscle and Eye Ball . . . . .	137
B-4 Electrodes for EKG . . . . .	137

## LIST OF FIGURES

Figure No.	Page
2.1 Translation . . . . .	15
2.2 Minkowski Addition . . . . .	16
2.3 Minkowski Subtraction . . . . .	17
2.4 Mathematical Operation: Dilation . . . . .	19
2.5 Mathematical Operation: Erosion . . . . .	20
2.6 Mathematical Operation: Opening . . . . .	21
2.7 Mathematical Operation: Closing . . . . .	22
2.8 Developed Morphological Filter . . . . .	24
2.9 The Schematic Diagram of the Wavelet Transform . . . . .	27
2.10 The Binary Tree Structure of Wavelet Packet Transform . . . . .	28
2.11 The Diagram of Lifting Scheme . . . . .	30
2.12 The Recurrence Times Between Two Spike Train . . . . .	36
2.13 The Correlogram of Two Uncorrelated Spike Trains . . . . .	39
2.14 The Correlogram of Two Correlated Spike Trains . . . . .	40
3.1 The Separation Results Using Varied Structuring Element Applied on a Fixed Scaled Triangular Signal . . . . .	43
3.2 The Separation Results Using a Fixed Size Structuring Element Ap- plied on The Varied Resolution Triangular Signal . . . . .	45

3.3	The Separation Result Using a Half-Resolution Signal And Converting Back to Its Original Scale . . . . .	47
3.4	The Separation Result Using a Quarter-Resolution Signal And Converting Back to Its Original Resolution . . . . .	48
3.5	The Comparison of Varying Structuring Elements and Varying Scale Resolutions . . . . .	49
3.6	The Morphology Wavelet Separation Method . . . . .	52
3.7	A Simulated Signal Containing Two Components: Background Activity And Spiky Transient . . . . .	59
3.8	The First Level Decomposition of Wavelet Transform For a Simulated Signal . . . . .	60
3.9	The First Level Reconstruction of Wavelet Transform For a Simulated Signal . . . . .	61
3.10	The Level Two Decomposition of Wavelet Transform For a Simulated Signal . . . . .	62
3.11	Final Result of a Simulated Signal Using Morphology Wavelet Separation Method . . . . .	63
3.12	Proposed Morphological Lifting Scheme: Decomposition . . . . .	67
3.13	Proposed Morphological Lifting Scheme: Reconstruction . . . . .	68
3.14	The Decomposed Coefficients Representing The Background Activity and Transient Signal Using Morphological Lifting Scheme . . . . .	69
3.15	Separation Result of Simulated Signal by Using Lifting Scheme . . . . .	70
4.1	Simulated EEG Data . . . . .	73

4.2	Separation Results of the Simulated EEG Using Morphology Wavelet Separation Method . . . . .	74
4.3	Power Spectrum of Simulated EEG Data . . . . .	75
4.4	The Separated Result of Simulated EEG Using Low Pass Filter . . . . .	76
4.5	The Experimental Result 1 Using Synthetic EEG . . . . .	77
4.6	The Experimental Result 2 Using Synthetic EEG . . . . .	78
4.7	The Experimental Result 3 Using Synthetic EEG . . . . .	79
4.8	Separation Results of Simulated EEG Data by Using Morphological Lifting Method . . . . .	82
4.9	Three Levels Decomposition Using Wavelet Packet Transform . . . . .	84
4.10	The Separation Result of a Subdural EEG Data by Using Morphology Wavelet Separation Method . . . . .	85
4.11	The Decomposed Coefficients of a Subdural EEG Date Using Morphological Lifting Scheme . . . . .	87
4.12	The Separation Result Using Morphological Lifting Scheme . . . . .	88
4.13	Peaks of Epileptic Spikes . . . . .	89
4.14	Spike Count of Subdural EEG 1 . . . . .	90
4.15	Spike Count of Subdural EEG 2 . . . . .	92
4.16	Spike Count of Subdural EEG 3 . . . . .	93
4.17	The Montage of a Scalp EEG . . . . .	94
4.18	Scalp EEG Data . . . . .	95
4.19	Separated Spiky Transient From a Scalp EEG . . . . .	96
4.20	Spike Count of Scalp EEG Data 1 . . . . .	97

4.21 Spike Count of Scalp EEG Data 2 . . . . .	98
4.22 Correlograms of Spike Trains From Scalp EEG Data . . . . .	99
4.23 Spatial Plot of the Maximum Correlation of the Scalp EEG . . . . .	101
4.24 Montage of MEG Data . . . . .	102
4.25 MEG Data . . . . .	104
4.26 Separated Spiky Signal From MEG Data . . . . .	105
4.27 Spike Count of MEG Data 1 . . . . .	106
4.28 Spike Count of MEG Data 2 . . . . .	107
4.29 Spike Count of MEG Data 3 . . . . .	108
4.30 The Correlogram of MEG . . . . .	109
4.31 The Spatial Plot of the Correlogram Using MEG Data . . . . .	110
4.32 The Correlogram of MEG . . . . .	111
5.1 System of Interictal Spike Analysis . . . . .	114
A-1 Montage of Subdural EEG . . . . .	127
A-2 The A/D Convertor . . . . .	128
D-1 International 10-20 System . . . . .	144
D-2 The Electrode Placements of the 10-20 System . . . . .	145

## NOMENCLATURE

Translation	$A_b = \{A + b : a \in A\}$
Minkowski Addition	$A \oplus B = \{A + b : a \in A, b \in B\} = \bigcup_{b \in B} A_b$
Minkowski Subtraction	$A \ominus B = (A^c \oplus B)^c = \bigcap_{b \in B} A_{-b}$
Erosion	$A \ominus \check{B} = \{z : B_z \subseteq A\} = \bigcap_{b \in B} A_{-b}$
Dilation	$A \oplus \check{B} = \{z : B_z \cap A \neq \emptyset\} = \bigcup_{b \in B} A_{-b}$
Opening	$A \circ B = (A \ominus \check{B}) \oplus B$
Closing	$A \bullet B = (A \oplus \check{B}) \ominus B$

## ABBREVIATIONS

FT	Fourier Transform
MF	Morphological Filter
SE	Structuring Element
WT	Wavelet Transform
IWT	Inverse Wavelet Transform

## 1.0 INTRODUCTION

Epilepsy is a common neurological disease affecting about 0.6% of the population. The syndrome of epileptic seizures involves irregular electrical paroxysmal activities. It manifests itself in the form of abnormal motor and sensory activity in the brain. In particular, this neurological disorder of children which produce delay in the development of their physiological and psychological capabilities. A tool used to investigate these behaviors of the brain is electroencephalography (EEG). The EEG is a non-invasive clinical approach to monitor the electrical activity of the brain. The EEG is collected by placing a set of electrodes on the scalp or directly on the surface of the brain. Such a EEG recording contains the spiky transients of short duration in addition to the background activity. The analysis of these spiky transients between interictal activities represents the transition of epileptic foci inside the brain.

In this thesis, we have developed a novel method to separate the spiky transients  $y$  from the background activity  $x$ , where the observed EEG is  $z = x + y$ . The two components of the observed signal are assumed to be non-stationary. The spatial-temporal aspects of the two components are different. The background activity is considered, in an intuitive sense, to be a dominant and spontaneous signal with relatively moderate amplitude variation. The sharp transient component may be distinguished from the background activity by sharper amplitude changes than the background activity. The transient contains salient patterns. In visual inspection, the background activity appears smoother than these spiky transients. Here we quote the description of the epileptic spike from Chatrian (16) <sup>\*</sup>: “Spike. A transient, clearly distinguished from background activity, with pointed peak at conventional paper

---

<sup>\*</sup>Bracketed references placed superior to the line of text refer to the bibliography.

speeds and a duration from 20 to under 70 msec, i.e., 1/50 to 1/14 sec, approximately. Main component is generally negative relative to other areas. Amplitude is variable.” The spiky transient can be distinguished only by trained experts. This research has investigated the dissimilarity between spiky components and background activity by differentiating their morphological characteristics.

Separation of signal components is an important issue in signal processing. Separation normally includes three processes: decomposition, classification and reconstruction. Decomposition divides a signal into several pieces, with each piece containing partial information of the original signal. Classification is a decision process which requires an intelligent system or knowledge base to categorize the decomposed pieces into different groups. Reconstruction synthesizes several of the signal pieces into one resultant signal. These decomposed pieces still maintain the integrity of the original signal. The complexity of the decomposed signal is equal to the original data, but the decomposition has divided the original signal into several subsignals, each containing less information, but presented in a clear fashion. The classification includes recognition and categorization processes. The recognition process needs prerequisite knowledge to identify the special properties of each class. The simplicity of new data obtained by decomposition will make it easier to assign data into different categories. Classifying the decomposed signal may eliminate some difficulty in recognition when the original signal is used. The reconstruction must have an ability to put all or parts of the classified pieces together into a “new” signal. Once the subsignals are classified into separate categories, it is very likely that one or several categories provides the real target(s) needed for further analysis. To achieve this purpose, the reconstruction process synthesizes the target component into a new signal set and the remaining pieces form another component. The summation of all reconstructed components

provides the original data, which is called a perfect signal reconstruction.

Separating complex data, such as biological data, into different components is a difficult task. Finding the salient transient patterns require the ability to identify their shapes from the underlying EEG signal and extract them amidst the data in the neighboring region. One can group these separated waveforms together to form a new signal where the morphological shapes of the new data are different than the original EEG data. In this sense, the interictal spiky pattern detection is a “hunting” process to separate these salient structures which were overlapped with the background waveforms. To separate a complex-structured signal, e.g. epileptic EEG signal, into two components the first step is to decompose the signal into several parts to reduce the complexity of each part. The most popular decomposition method is by Fourier transformation which decomposes a signal into a set of sinusoidal waves in the spectral domain. The signal is expressed in terms of its frequency information, however, the time information is lost. Other signal decomposition methods, including time-frequency analysis and the wavelet transform, may be used to overcome this difficulty. But the principle of decomposition to break the original signal into several smaller parts has not changed. Classification is the second step to separate the two components from EEG signal. The spectral and statistical properties of target patterns are widely used as the knowledge base to classify the decomposed signal into two categories. Other features are also used in classification criterion, e.g. amplitude, slope, etc. In this thesis, the morphological characteristics are the main features used to separate the transient from the background activity.

In clinical situations, an epilepsy patient may be monitored with an EEG machine for a long time. Imaging techniques, such as MRI and CT, are also used to help physicians understand patient’s situations for the diagnosis. Based on the diagnosis,

physicians will decide what the best therapy is for that patient. Most patients will be treated with drugs which can effectively eliminate or control the syndromes of the epilepsy. But in some instances, these medicines are unable to control the seizure activity. In these cases, more aggressive treatment, such as surgical operations, may be used to treat the patient. Computational evaluations of epileptic EEG data are very critical to these operations. Interictal spiky waveforms are the most recognizable phenomenon to be analyzed to determine the seizure focus. The reason for this is that the epilepsy patient normally generates a significant interictal activity which shows no particular sign of the abnormality in his/her behavior. By analyzing the EEG data collected from different electrodes, the neurologist finds the temporal and spatial relationships between electrodes to determine the focus of epilepsy. In order to collect enough information for analysis, the EEG is normally recorded for a number of days. Epileptologists and neurologists inspect the traces of EEG displayed on the computer screen. The visual examination is tedious and time-consuming even though the data are rendered in 10 to 20 second segments. Thus, the amount of collected EEG sets are very huge. A computer aided tool would help to reduce both the time and energies related to recovery of these data sets. In addition, even with usual analysis, epileptologists tend to focus on only the properties of a few spikes. Thus, due to the significance of the spikes and the amount of required data processing, an automatic recognition and separation method would be very useful.

A complete solution for detecting epileptic spiky transient signal has not been found; part of the reason is that there is no clearly descriptive definition of epileptic spiky patterns. The shapes of these transients vary widely from patient to patient and their appearances embedded in the background activity of EEG cannot be precisely identified. The two categorized components are both non-stationary signals

and are difficult to be modeled by traditional methods. The mixture of these two categorized components makes the problem even more complicated. The ambiguous definition of these waveforms and the laborious identification process involved, make 100% detection of such sharp transients impossible by visual inspection. It has been reported that no two experts score EEG in exactly the same way and sometimes the same expert does not identify some features in the same EEG record if it is presented multiple times (99,26). Over the past two decades, many approaches to automated separation of an EEG signal into two categorized components have been proposed. These approaches are based on either spectral analysis or direct recognition of characteristics. Spectral analysis is a parametric method and characteristic recognition is a direct analysis method. These methods used different measurements, such as statistical distributions, spectral properties and others in order to threshold out the target patterns from the ongoing data. Other newer approaches, such as time-frequency analysis and wavelet transform, are also included to improve the separation results of the spiky transients (80,102). These will be represented in the following subsection.

### **1.1 A Brief Review of Existing Approaches for Separation of Signal Components**

The classical spectral analysis of a stochastic signal is the most widely used method. This method normally treats a whole signal either as stationary or divides the signal into smaller pieces where are stationary. The optimal segmentation is difficult to determine and requires much computational effort. Spectral analysis is heavily dependent on statistical predictability and suffers from the uncertainty principle requiring that higher spectral resolution will decrease the temporal resolution or vice versa. Witte (1991) (103) used the Fourier and the Hilbert transforms to map the

transient signal. Bender (1992) (1) tested the stationarity of the background activity by using an autoregressive model in a constrained condition. Grieszbach (1994) (32) developed an adaptive recursive method based on basic spectral parameters. Wang (1994) (98) studied the “rigidity” of the signal by using spectral analysis.

The parametric method is based on an autoregressive model to represent the background activity. If the model well-represents the background activity, then any signal other than the background activity can be easily distinguished from that activity. Model parameters characterize the statistical properties of the background activity signal. The signal must satisfy the stationarity condition. Then these parameters of a model can be obtained. Models have been developed having adaptive segmentation capability. The drawback of these models is that they are heavily dependent on the stationarity of the signal. Saltzberg (1971) (77) used the mean of correlated activities to separate a signal. Lopes da Silva (1975, 1977) (50, 51) modeled the stationary background activity with an autoregressive prediction filter and detected transients by examining the prediction error. Rappelsberger (1975) (74) analyzed the spectra of a signal by using an autoregressive model. Praetorius (1977) (73) also used this model to evaluate the stationarity of segments. Bodenstein (1977) (7) extracted the features of spiky signals by using an autoregressive model with the ability to adaptively adjust parameters. Michael (1979) (62) presented a segmentation procedure, based on the autocorrelation function, to detect the amplitude and frequency of signals. Isaksson (1981) (39) surveyed the parametric method to detect the occurrence of transient signal. Gath (1992) (24) suggested a multivariate autoregressive model combined with the adaptive segmentation method to track rapid dynamic transient signals. Victor (1992) (97) used a nonlinear autoregressive model to estimate the characteristics of subsignals. Kobayashi (1992) (45) used an autoregressive model to utilize coherence

and phase differences. Florian (1995) (23) used a sequence of autoregressive models to fit EEG segments which exhibited the best local stationarity and then used several spectral factors to analyze the data. Schack (1995) (79) used spectral analysis on the ARMA model. Inouye (1995) (40) investigated the power contribution of transients based on the multivariate autoregressive model. Sankar (1989) (78) applied a linear prediction model and found the model's parameters by minimizing the total errors of the system. This algorithm judged the residuals for a certain number of consecutive samples when their amplitudes were greater than a cutoff threshold and then determined whether the target patterns are spikes.

There are two approaches to the direct analysis: one is to use a set of well defined features (e.g. using the information of amplitude, slope, sharpness, etc.) of the spiky transient, the other is to provide different transient examples (typical or well-recognized patterns) and compare these patterns with EEG data. These two approaches are known as the mimetic method and the template matching, respectively. The drawbacks of the direct analysis methods are: 1) the precise definitions of transient may be lacking; 2) the transients are signal-dependent and so cannot be generalized for other signals; and 3) the typical pattern(s) may not cover all the cases. The use of the mimetic method has been reported by several groups. Smith (1974) (84) created a model based on a criterion governing the slope, apex and lengths on both sides of the apex for detecting two components. Carrie (1972) (9) used the second derivative function to detect the sharp changes in the signal. Chatrian (1974) (16) defined the transient patterns for the EEG signal. Pola (1979) (70) proposed an automatic detection method based on the morphological aspects of the signal. Ktonas (1987) (47) utilized the context information of signals to detect sharp waveforms. Glover (1989) (27) described a knowledge base of spatial and

temporal information for finding sharp transient waveforms. Dingle (1993) (21) and Jones, et al. (1996) (43) used the mimetic approach to build a multistage expert system to detect parameters such as duration, amplitude and sharpness of transients. Considerable effort has been made to use the template matching method. Gotman (1985, 1991) (29, 30) described three general methods to recognize transients. The first one was a mimetic method which identified signal segments fitting a set of pre-defined features. The second method was a parametric method which utilized a small number of parameters, representing statistical properties of the background activity. The transient, whose features are different from those of background activity, will be picked up after all the parameters are tested. The third one was a template matching method which attempted to match the transient with well-defined specific waveform pattern(s). Gotman used the template matching method to separate transient from the original signal. James (1997) (41) applied adaptive noise canceling to enhance nonstationary transients.

Time-frequency analysis (17) and wavelet transforms have also been utilized to improve epileptic spike separation. Finer time-frequency and time-scale resolutions provide better information with respect to the two components. The information helps to model the background activity more precisely or to make the direct analysis of the transient more reliable.

There are several separation processes related to wavelet transform: Mallat (1991) (52) explored the properties of sharp variation and characterized transients. Senhadji (1995) (81) applied a non-orthogonal wavelet transform in a decision machine to separate two components of a signal. Bertrand (1994) (3) used the wavelet transform to represent transient responses. Li (1995) (49) developed an algorithm based on the wavelet transform to detect characteristics of the electrocardiogram. Cha and

Chaparro (10) proposed a polynomial function using mathematical morphology to implement a wavelet representation. A signal was decomposed into several frames, and morphological operations were carried out with adaptive structuring functions applied to different frames. The morphological interpolation is based on these structuring functions derived from orthogonal polynomials. Popescu (1998) (72) trained wavelet “children” to detect the epileptic spikes.

Several investigations have used time-frequency analysis to separate the signal components. Williams (1995) (102) and Choi (1989) (14) suggested that time-frequency analysis is useful in epilepsy research. Martin (1985) (58) used the Wigner-Ville spectral analysis. Meste (1994) (63) linked the wavelet transform to the time-frequency representation to characterize and detect the sharp transients. Blanco (1995, 1997) (4, 5) used a method based on the Gabor transform for simultaneous quantization in the time-frequency domain. An optimal correlation was found that differentiates characterizes the background activity and transient alterations. Wendling (1999) (100) tried to separate the seizure EEG by using time-frequency domain matching processes, in which the warping information between time and frequency is presented as the signature of the epileptic EEG activity.

Artificial neural network (ANN) has also been used to detect epileptic EEG signals. ANNs are known as tools having adaptive and flexible functional ability for human-like pattern recognition. The multi-layer structure of a neural network provides a knowledge system which can be trained to recognize, classify and analyze different patterns of the epileptic EEG data. The trained neural network can detect the epileptic spikes generated from the brain activity. In order to train a neural network, one needs to provide a set of spiky transient pattern, that have been recognized, and whose features have been extracted. These training patterns will affect the

correctness of the spike detection. Khan et al, (44) used an artificial neural network with feature vectors that quantify slope, sharpness and autoregressive parameters extracted from the segmented EEG. An ANN was trained to detect two classes of the EEG data, normal and epileptic. Özdamar et al, (66) designed and evaluated an artificial neural network with two levels. The first level recognizes candidate spikes in separated channels, and the second level properly integrates the spatial information from the first level to increase the detection accuracy. Although a multilayer network may function well for small to medium size pattern recognition tasks, it may be inefficient for larger task, which will need more training. Meanwhile, a proper architecture must be chosen to avoid divergence of reaching conclusions. All of these considerations must be well taken of.

## 1.2 Correlative Analysis of Multiple Electrode Spike Trains

The separated spike trains from multiple electrode EEG recording are useful for the clinical diagnosis. Because of the size of the data set, workload of human experts and the computational effort required, most examinations of epileptic data have been limited to small segments of EEG data. The drawback of using only small segments is that the data may not adequately represent the involved neurophysiological progress. It is desirable to analyze the data of longer periods and explore the spatial transitions of the brain activity. the time instants at which the peak of epileptic peaks occur in an EEG recording can be modeled by stochastic point process. To find the relationship among spike trains monitored by multiple electrodes, correlogram behaves every pair of electrodes have been used. Maximum correlations show tracks of abnormal behavior occurring in the brain. Because each epilepsy source in the brain tissue fires an abnormal signal triggering a sharp spike which travels from the source to the rest area

of the brain, it will cause the neurons there to act abnormally. The timing of spike occurrences in different electrodes describes the trajectory of a spiky signal from one area to another. If the data length is long enough, the statistical correlations between the spike train of a given electrode and that of every other electrode will reveal the trajectory of epileptic spikes which describes the timing relationship of the abnormal activities in the brain.

### 1.3 Objective of This Research

The objective of this research is to develop a new method which is effective and efficient for separating spiky transients and the background data. This is formulated as a problem of detection and extraction of fast rising-and-falling triangular-shape pulses of various amplitude of short durations embedded in a complex-structured background which has relatively slower variation in general but yet contains rapid fluctuations as well. The shape of a target spike transient component is modeled by a triangle with its peak in the middle having a significant amplitude and its has subtended over a specified range. Utilizing the shape features, a morphological filter is considered with a circular disc structuring element (SE), and the morphological filtering applies in multiresolution schemes to capture and extract various target components in multiple resolutions. Spiky transients and background EEG are synthesized with these separated two components on each resolution level. We plan to verify the successful extraction of spike train indirectly by experimentation on multi-electrode epileptic EEGs in connection with the epileptic foci confirmed by expert neurologists.

## 1.4 Organization of the Thesis

The thesis is organized as follows: chapter one provides an overall introduction. The second chapter includes general descriptions of the related mathematical background, including mathematical morphology, wavelet transform, lifting scheme and stochastic point process. Chapter three describes the development of morphological filtering in multiresolution representations, including both wavelet packet transform and lifting schemes, for extracting signal components. Experimental results obtained by using the proposed methods are provided in chapter four. The experiments were performed on simulated data and real epileptic EEG data. Chapter five discusses the advantages and disadvantages of these methods. Chapter six gives conclusions and contributions of this research as well as suggestions for future development. An appendix is included detailing information on the EEG data collection and preprocessing which is needed before the proposed methods are applied.

## 2.0 MATHEMATICAL METHODS

Before detailed descriptions of proposed methods, a general mathematical background is presented. The discussion begins with presenting general concepts of mathematical morphology and continues with an introduction of multiresolution schemes, including the wavelet transform and lifting scheme. Finally, the stochastic point process is discussed.

### 2.1 Mathematical Morphology

Mathematical morphology was introduced by G. Matheron (59) and J. Serra (82). The term of morphology is related to the analysis of the form and structure of a signal and widely applied to biology, geography and image processing. Mathematical morphology involves the set of analytic operations based on a prior geometric shape known as a structuring element (SE). The behaviors of structuring elements operating on a signal have been studied for years. The set of operations corresponding mathematical morphology can be characterized as a morphological filters. Morphological filters have been applied to black-and-white binary images. But the applications of mathematical morphology are not only limited to two dimensional binary image processing. Mathematical morphology has been expanded to apply to gray level images and one dimensional signal by using the concepts of umbra (28, 86, 57, 87). The concept of umbra is that of the points on and below the function, and the realizations are based on max and min operations. The morphological filter is based on a set of algebraic and integral geometry operations and this process is a nonlinear transformation. Using the structuring element (SE), a morphological filter can locally detect, extract, modify and preserve desired geometric features of a signal with respect to

the properties of the structuring element. The input signal is viewed as a set in an Euclidean space, and the morphological filter quantifies the geometrical information of the input signal. Morphological filters have been applied to many applications including pattern recognition (85), non-linear filtering (55,56,11), smoothing operation (18,90), edge detection (64,13), noise suppression (69,12), thinning usage (54), texture analysis (101), biomedical image processing (60,83) and medical applications (94).

### 2.1.1 Fundamental Operators of Mathematical Morphology

Before a further explanation of mathematical morphology, several fundamental concepts are introduced first, including set theory, translation, space definition and basic set operators.

Let the set  $A$  to be a subset of an Euclidean space  $\mathbb{E}$ . A fixed point inside space  $\mathbb{E}$  is assigned as the origin, denoted as  $\bar{0}$ . The second set  $B$  known as structuring element (SE) is also a subset of space  $\mathbb{E}$ . Set  $A$  can have very different spatial aspects which will be described by the set structuring element  $B$ . The shape of the structuring element  $B$  can be defined arbitrarily with respect to the applications. Set  $B$  can extract, eliminate or enhance the different morphological features of set  $A$ . Some basic algebraic operators have been introduced here. These are translation, Minkowski Subtraction, Minkowski Addition and others.

The set  $A$ , a given input signal, is the set needed to be processed and  $B$  is a set called a structuring element (SE). Let  $A_b = \{A + b : a \in A\}$  denote the translation of  $A$  by  $b \in B$ . Let  $\check{B} = \{-b : b \in B\}$  be the reflection of  $B$ . Note that the reflection is simply  $B$  rotating  $B$  by  $180^\circ$  with respect to the origin.  $A^c = \{s : s \neq A\}$  is the complement of  $A$ . The following are the mathematical descriptions for the basic set operators used in mathematical morphology.

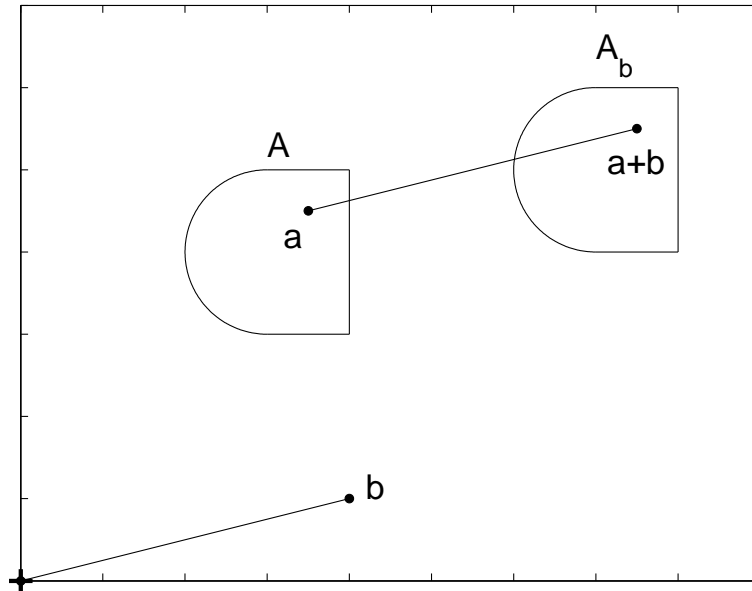


**Figure 2.1** Translation  $A_b$ :  $A$  is translated by element  $b$ , where  $a$  is the element of set  $A$ . The element  $b$  of set  $B$  is a point which has a vector direction from the origin at the left bottom corner. This operation satisfies the translation invariant property.

**Definition 1 (Translation).** Let  $A, B$  be subsets of  $\mathbb{E}$  ( $A, B \subseteq \mathbb{E}$ ) and  $a \in A, b \in B$ .

The translation denoted as  $A_b$  is defined as

$$A_b = \{A + b : a \in A\}, \quad (2-1)$$

where the plus sign refers to vector addition.

Fig. 2.1 demonstrates the translation operation. The set  $A$  is translated by an element  $b \in B$  with respect to its vector direction. It shows that the translation of signal  $A$  is merely shifted by a vector  $b$ . Here the origin is located at the left bottom corner, as marked by “+”.

**Definition 2 (Translation Invariant).** Let  $A, B \subseteq \mathbb{E}$  and  $a \in A, b \in B$ . An operator  $\psi$  is called translation invariant if it satisfies

$$\psi(A_b) = [\psi(A)]_b = \psi(A) + b. \quad (2-2)$$

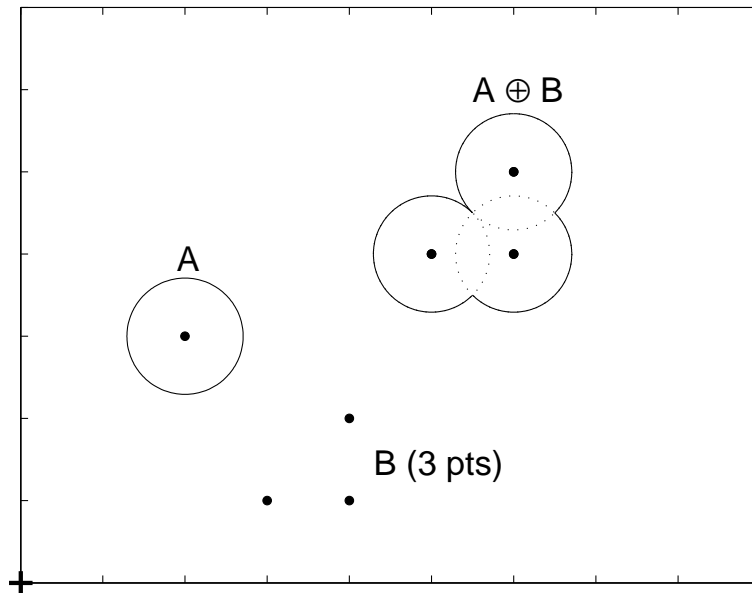


**Figure 2.2** Minkowski Addition  $A \oplus B$ : Set  $A$  is a solid circular disk and set  $B$  contains three points. The origin is located at the left bottom corner. The Minkowski addition has translated and unioned set  $A$  three times with respect to the vector relationships of the elements  $b$  ( $b \in B$ ). The result of the Minkowski addition is a new set, which is like three disk overlapped each other partially.

Fig. 2.1 shows the translation operation of a set  $A$  from  $b$  that satisfies the translation invariant property.

**Definition 3 (Minkowski Addition).** Let  $A, B$  be subsets of  $\mathbb{E}$  ( $A, B \subseteq \mathbb{E}$ ) and  $a \in A, b \in B$ . The Minkowski addition (33), denoted as  $\oplus$ , is defined as follow:

$$A \oplus B = \{a + b : a \in A, b \in B\} = \bigcup_{b \in B} A_b, \quad (2-3)$$

where  $+$  is referred to vector addition.

Fig. 2.2 shows an example of the Minkowski addition. The set  $A$  are the elements in a circular disc and the set  $B$  has three points. The origin  $\bar{0}$  is located at left bottom corner marked as marked by “+”. The disk is translated three times with respect

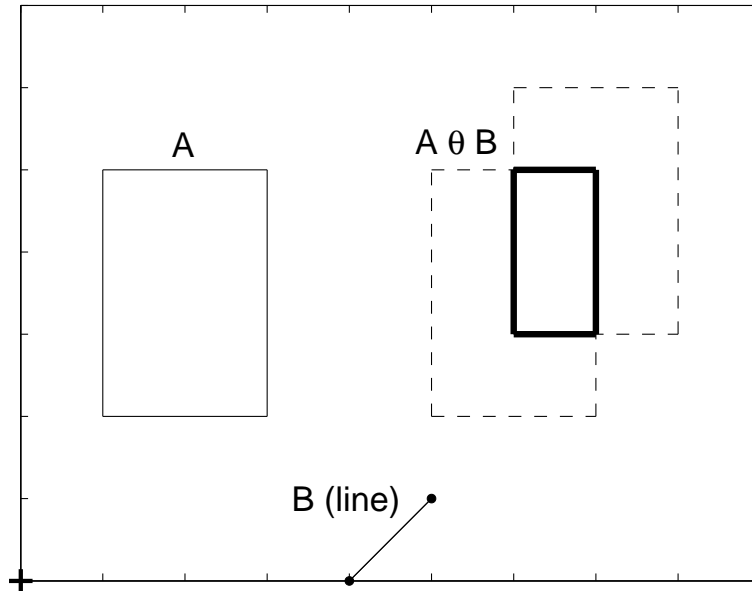


**Figure 2.3** Minkowski Subtraction  $A \ominus B$ : Set  $A$  is a rectangle plate and  $B$  is a line. The origin is located at the left bottom corner. The set  $A$  translated with every elements of the line  $B$  with respect to their vector directions of the origin. The intersection of all the translations is the result of Minkowski subtraction, shown as the thick solid small rectangle.

to set  $B$  and the union of the three translations is the final result of the Minkowski addition.

**Definition 4 (Minkowski Subtraction).** *Let  $A$  and  $B$  be subsets of  $\mathbb{E}$  ( $A, B \subseteq \mathbb{E}$ ) and  $a \in A$ ,  $b \in B$ . Then Minkowski subtraction (61), denoted as  $\ominus$ , is defined as follow:*

$$A \ominus B = (A^c \oplus B)^c = \bigcap_{b \in B} A_b. \quad (2-4)$$

Fig. 2.3 shows an example of the Minkowski subtraction of set  $A$  and  $B$ . In this example, set  $A$  is a rectangular plate and  $B$  is a segment of line. The origin is located at the left bottom corner, as marked by “+”. The plate is translated by each element  $b \in B$  with respect to their vectors. The intersection of these translation is the result

of Minkowski subtraction. It is a smaller rectangle shifted to the right from set  $A$  with respect to structuring element  $B$ .

### 2.1.2 Morphological Erosion, Dilation, Closing and Opening

Four basic mathematical morphological operators are introduced here: these are 1.) dilation, 2.) erosion, 3.) opening, and 4.) closing. These operators are defined as follows (82, 34, 75):

**Definition 5 (Dilation).** *Let  $A$  and  $B$  be the subsets in space  $\mathbb{E}$  ( $A, B \subseteq \mathbb{E}$  and the elements  $a \in A, b \in B$ ). The dilation of  $A$  by a structuring element  $B$  is denoted by  $A \oplus \check{B}$ , and is defined as:*

$$A \oplus \check{B} = \bigcup_{b \in B} A_{-b} \quad (2-5)$$

Fig. 2.4 demonstrates the operation of morphological dilation. The solid line, set  $A$ , is the signal to be processed and the circular disc set  $B$  is the structuring element. The origin is marked by the “+”. In this example, the structuring element is the circular disk with its center being the origin. Morphological dilation uses each element  $a$  of set  $A$  as a center and each center is translated by element  $b$ . The translated signal will be like the signal  $A$  filled with many disks with their center on the set  $A$ . The morphological dilation is the maximum value in the vertical direction. In this figure, it can clearly be seen that the original signal  $A$  has been dilated by the structuring element  $B$ .

**Definition 6 (Erosion).** *Let  $A$  and  $B$  be subsets of  $\mathbb{E}$ . The erosion of  $A$  by a structuring element  $B$  is denoted by  $A \ominus \check{B}$ , and is defined as:*

$$A \ominus \check{B} = \bigcap_{b \in B} A_{-b}, \quad (2-6)$$

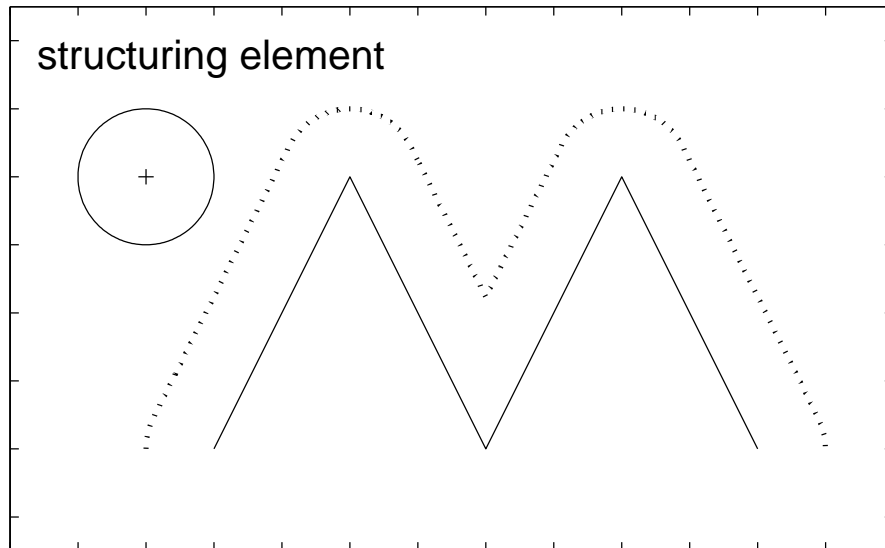


**Figure 2.4** Morphological Dilation: Set  $A$  is triangular signal (shown as solid line) and the structuring element is a circular disk with its center located at the origin, as marked by the “+”. The dash line is the result of morphology dilation operation. The dilation is the maximum point that the circle  $B$  rotating onto the signal  $A$  can reach.

Fig. 2.5 shows the operation of morphological erosion. The solid line, set  $A$ , is the signal to be processed and the circular disc, set  $B$ , is the structuring element. with its center on the origin. Morphological erosion uses every elements of set  $A$  as the center and then translated with element  $b$ . A new translated signal will be like the signal  $A$  filled with many circles with their center on the set  $A$  with the minimum value on the vertical direction. In this figure, it can clearly be seen that the original signal  $A$  has been eroded by the structuring element  $B$ .

**Definition 7 (Opening).** *Let  $A$  and  $B$  be subsets of space  $\mathbb{E}$ . The opening operation of  $A$  by a structuring element  $B$  is obtained by first operating with erosion and then operated on with the dilation. Morphological opening is denoted by  $A \circ B$  defined as:*

$$A \circ B = (A \ominus \check{B}) \oplus B \quad (2-7)$$

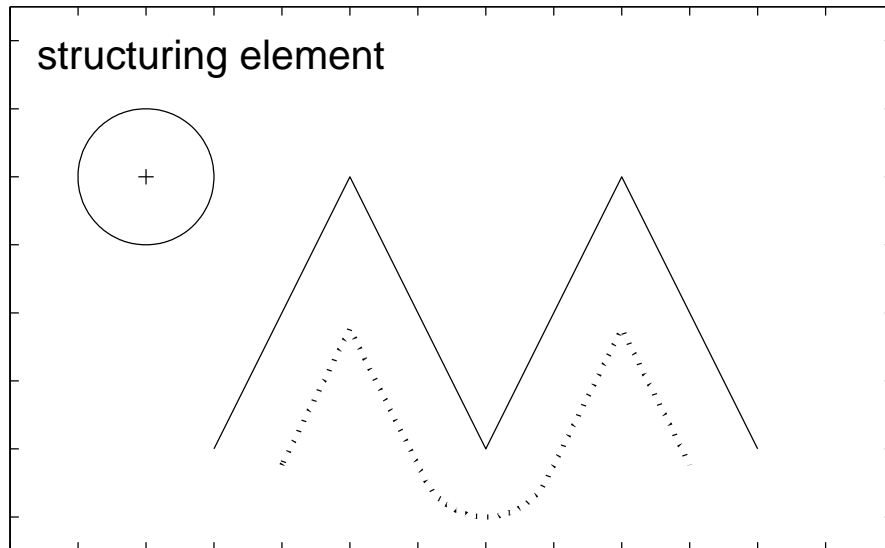


**Figure 2.5** Morphological Erosion: The solid line is the original signal  $A$  and the structuring element is a circular disk where its center is located onto origin (as marked by the “+”). The dash line is the result of erosion  $A \ominus \check{B}$ . Visually, the dash line looks as if the signal  $A$  has been eroded by the disk.

Fig. 2.6 demonstrates the morphological opening operation. Set  $A$ , a triangular signal plotted by a thin solid line, is the signal to be processed. Set  $B$ , a circular disk centered onto the origin, is the structuring element. Both sets are the same as in the previous examples. The origin is marked by the “+”. Signal  $A$  is first eroded by structuring element  $\check{B}$ , where the result is shown as the dash line in the figure. The dash line is then dilated with set  $B$ . The dilation of the dash line is indicated with a thick solid line which is the final result of the morphological opening process. Opening smooths the convex peaks of the signal  $A$ . In this example, there are two convex peaks, which have been smoothed by this operation. It should be noted that the smoothing of the upward peak is equal to the difference between signal  $A$  and a circle just under it with only two points connected.

**Definition 8 (Closing).** *Let  $A$  and  $B$  be subsets in space  $\mathbb{E}$ . The closing of  $A$  by*

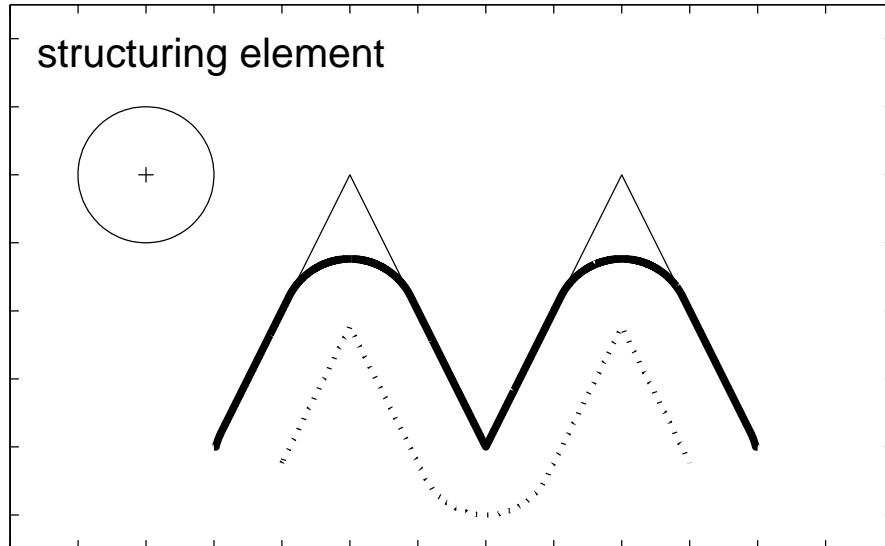


**Figure 2.6** Morphological Opening: The structuring element  $B$  is a circular disk with its center onto the origin as marked by the “+”. The thin solid line is original signal,  $A$ , and the dash line is result by erosion operator and then it was applied by dilation operation. The thick solid line is the final result of applying opening operator on the signal. The opening operation smooths only upward peaks and has no affection on the downward peaks.

*the structuring element  $B$  is obtained by operating with the dilation operator with this result then operated on by the erosion operator. Morphological closing is denoted by  $A \bullet B$ , and is defined as:*

$$A \bullet B = (A \oplus \check{B}) \ominus B \quad (2-8)$$

Fig. 2.7 demonstrates the operation of morphological closing. The thin solid line, set  $A$ , is the signal to be processed and the circular disk, set  $B$ , is the structuring element. Both are the same as in the previous examples. The origin is marked by the “+”. Signal  $A$  is first dilated by the structuring element ( $\check{B}$ ) shown in the Fig. 2.7. Then, the dashed line is then eroded by the structuring element. The result is shown as a thick solid line. In this example, there exists a concave peak in the middle of signal  $A$ , which has been smoothed by morphological closing. Morphological closing has no

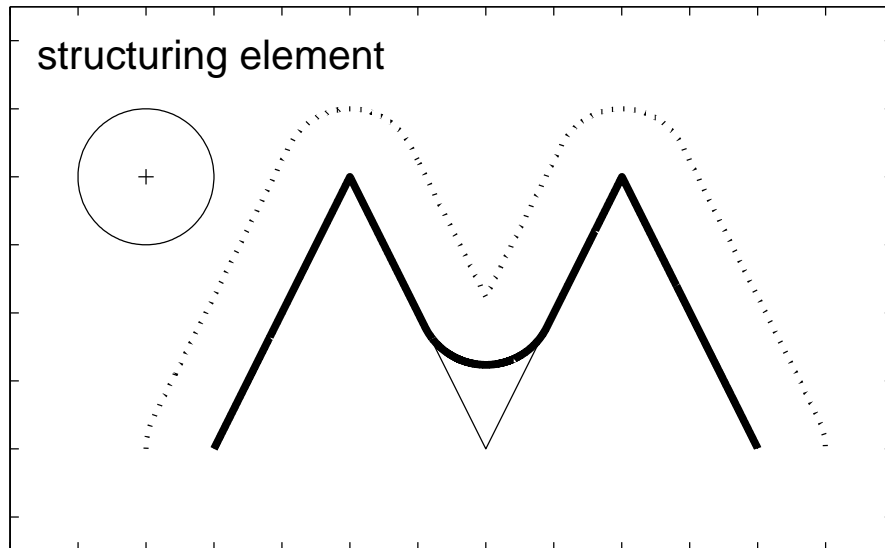


**Figure 2.7** Morphological Closing: The structuring element is a circular disk with its center onto the origin as marked by the “+”. The thin solid line is original signal and the dash line is dilated by the structuring element circle and the result is then applied with erosion operator. The thick solid line indicates the result of the morphological closing. The closing operation only smooths the downward peak and has no affection on the upward peaks.

affect on the convex peak. From this example, it can be seen that the closing operator can smooth downward peaks. Again, it should be noted that the smoothing thick line above the downward peak is a curve part of circular disk connecting only two points above the signal  $A$ . Applying a circular structuring element to a triangular signal, the morphological closing operator smooths the downward peaks without changing the upward peaks. Morphological opening is the reverses of closing, where upward peaks are smoothed and the downward peaks are unchanged.

Mathematical morphology analysis is a combination of several set operators involving a prior defined structuring element. The properties of the different operators will smooth, extract, and separate different parts of a signal with respect to the geometrical shape of the structuring element. By manipulating these operators, one

can design a filter to separate an input signal into two categorized signals. One signal is categorized by the structuring element and other is the residue of the signal. It has been demonstrated that the morphological opening operator can smooth the upward peaks and the closing operator can smooth downward peaks. By defining the structuring element as a circle with its center at the origin, a new morphological operator combining both closing and opening operators may be used to smooth both directional peaks. This combined operator can separate the epileptic spiky activity from the background EEG. This morphological filter is defined as followed:

$$\begin{aligned}
 M_f^B(A) &= (A \circ B) \bullet B = A_m \\
 A_r &= A - A_m \\
 A &\xleftrightarrow{M_f^B} A_m + A_r,
 \end{aligned} \tag{2-9}$$

where  $M_f^B$  is referred as a morphological function with the structuring element  $B$ . The separated component  $A_m$  is the signal categorized by the structuring element and  $A_r$  is the residue. The lengths of both element are the same to each other and the summation of these two are equal to the original signal  $A$ .

The first operation is applied with the morphology opening and then followed by the closing operator. The double arrow means that the morphological operation is merely classified the input signal  $A$  into two categorized groups but the signal features do not change during the operation. The symbol “ $\longleftrightarrow$ ” indicates that the signal on the left side is operated by the morphological filter  $M_f^B$  and right side shows the mathematical operation. Fig. 2.8 shows the result of using this proposed morphological filter. The dash line is the triangular signal and the structuring element is a circular disk with its center on the origin. The thick solid line is the filtered result where it estimates the approximation of the smoothed background with the upward and downward peaks removed from the triangular signal  $A$ . This estimation is apparently

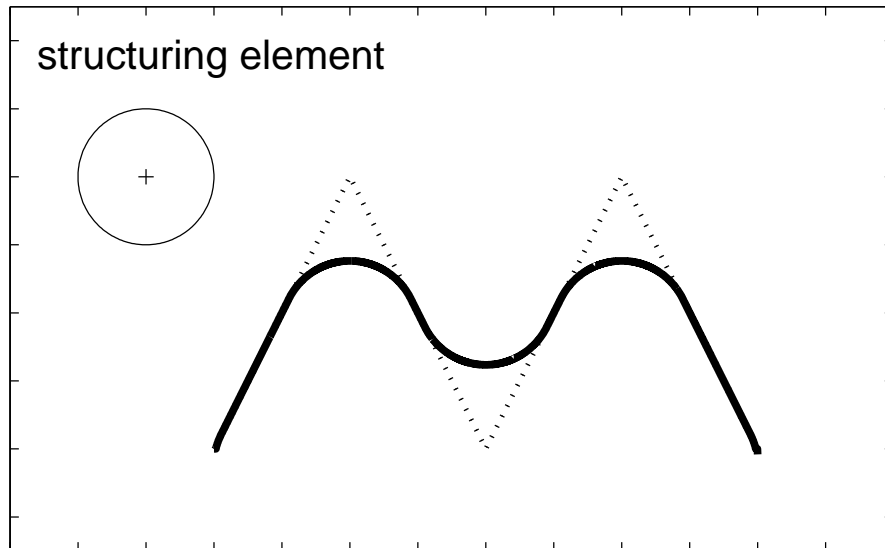


**Figure 2.8** A morphological filter is shown in this figure where the dash line is the original signal and the center of the structuring element disk is located onto the origin marked as “+”. The thick solid line is filtered result which is operated by morphological opening first followed by closing operators. All the peaks of this signal are smoothed by this filter with affecting the non-peak regions.

smoother and its amplitude variation is reduced. The difference between the triangular signal and thick line is sharp signal which representing as the approximation of the spiky transient containing only pointed peak patterns, i.e., the desired result.

## 2.2 Multiresolution Scheme

Multiresolution analysis captures the properties of a signal at different resolutions. The multiresolution analysis schemes are introduced here: There are the wavelet transform, the wavelet packet transform, and the lifting scheme.

### 2.2.1 Wavelet Transform and Wavelet Packet Transform

The wavelet transform is a signal processing method which decomposes a signal into several multiscale components. The concepts of delineating a signal into a spectrum domain is based on the assumption that the signal has a spread in the frequency range over its entire temporal existence. By selecting a subset of the spectral components, the wavelet transform divides a signal into two corresponding signals at each level; represented as two coefficient sets: the approximation coefficient set with lower frequency components and the detail coefficient set with higher frequency components. In our example, each lower level coefficient set is a half scale of higher level one. The approximation coefficients is approximated from the higher level coefficients with similar low frequency properties. The detail coefficients is the fast variation of the higher level coefficients. The coefficients of the wavelet transform maintain the structure of the higher level signal components. The wavelet transform has been used in applications in image, speech processing, medicine (96) and biology fields. These applications have included the detection process (e.g., spikes in EEG, microcalcifications in mammograms) (89), data compress (image compression) (48), data analysis (detecting changes in fMRI (76)) and data processing (wavelet de-noising) (95).

A family of wavelet function  $\psi_{j,n}$  has the property of dilation by a factor  $2^j$  at level  $j$  and shifting by a factor  $n$  in the orthonormal basis of  $\mathbf{L}^2$ . The integral of wavelet  $\psi$  is zero, i.e.,

$$\psi_{j,n}(t) = \frac{1}{\sqrt{2^j}}\psi\left(\frac{t - 2^j n}{2^j}\right), \quad (j, n) \in \mathbf{Z}. \quad (2-10)$$

and

$$\int_{-\infty}^{\infty} \psi(x)dx = 0. \quad (2-11)$$

A scaling function  $\phi_{j,n}$  is family of functions which have an orthonormal basis  $V_j$  for level  $j$ . The scaling function is:

$$\phi_{j,n}(t) = \frac{1}{\sqrt{2^j}} \phi\left(\frac{t - 2^j n}{2^j}\right), \quad (2-12)$$

The filter bank algorithm that calculates the orthogonal wavelet coefficients of a discrete signal  $a_0[n]$  may be described as follows. Let us define the function  $f(t)$  as

$$f(t) = \sum_n a_0[n] \phi(t - n), \text{ where } \phi(t - n) \in V_0. \quad (2-13)$$

The  $V_0$  is a base space and exist  $\phi$  such that  $\phi(t - n)$  is a Riesz basis of  $V_0$ , where  $\phi(t - n)$  is a scaling function and orthonormal. The approximation coefficients,  $a_0[n]$ , which are the weighted average of  $f$  in the neighboring points around location  $n$  are given by:

$$a_0[n] = \langle f(t), \phi(t - n) \rangle = f * \phi. \quad (2-14)$$

While the wavelet coefficients or detail coefficients,  $d_j[n]$ , of function  $f$  are given by:

$$d_j[n] = \langle f(t), \psi_{j,n} \rangle = f * \psi_{j,n}. \quad (2-15)$$

The wavelet transform can also be represented as a filtering function. Fig. 2.9 shows the decomposition and reconstruction processes using the wavelet transform. Let  $x$  be an input signal. Two filters  $\bar{h}$  and  $\bar{g}$  are applied to signal  $x$ . Filters  $\bar{h}$  and  $\bar{g}$  must satisfy the properties of wavelet transform, where  $\bar{h}$  is a low pass filter and  $\bar{g}$  is a high pass filter. The filtered result of  $x$  is downsampled by two to get  $x_a$  and  $x_d$ , where  $x_a$  (approximation coefficient) and  $x_d$  (detail coefficient) are the lower level coefficients of the higher level coefficient set  $x$ .  $X_a$  can be further decomposed to the next level to get  $x_{aa}$  and  $x_{da}$ . The reconstruction of lower coefficients  $x_{aa}$  and  $x_{da}$  can be done by upsampling by two and filtered by with  $h$  and  $g$ . The two filter  $h$

and  $g$  are reconstructed filters which are reciprocal with  $\bar{h}$  and  $\bar{g}$ . The coefficients  $x_{aa}$  and  $x_{da}$  perfectly reconstruct  $x_a$ . Using  $x_a$  and  $x_d$  can reconstruct back the original signal  $x$ . The filters  $\bar{h}$ ,  $h$  are referred as the low frequency filters and  $\bar{g}$ ,  $g$  as the high frequency filters.

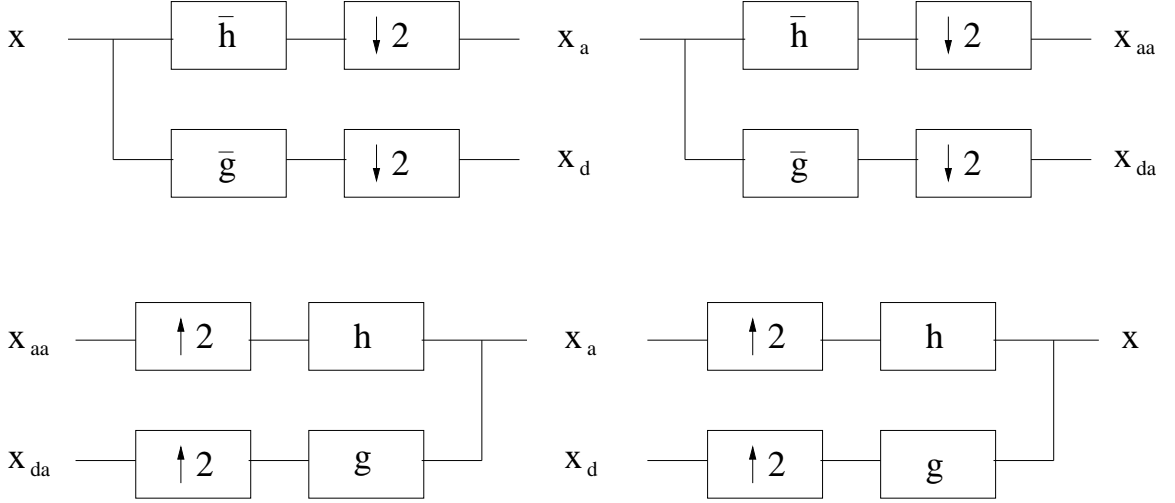


**Figure 2.9** The wavelet transform: decomposition and reconstruction

The decomposition of the wavelet transform can be implemented by two filters, the low-pass filter  $\bar{h}$  and the high-pass filter  $\bar{g}$ . The filtered results will be down-sampled by two. In reconstruction part, the low pass filter  $h$  and high pass filter  $g$  together provide a perfect reconstruction of the original signal. These four filters  $h$ ,  $g$ ,  $\bar{h}$ , and  $\bar{g}$  are called conjugate mirror filters (53). The signal analysis algorithm is as follows: Let  $x \in V_0$ , then the scaling coefficients  $x_a \in V_1$  and wavelet coefficients  $x_d \in W_1$  are defined as

$$\begin{aligned} x_a[k] &= \sum_n \bar{h}[n - 2k]x[n], \quad x_a \in V_1, \\ x_d[k] &= \sum_n \bar{g}[n - 2k]x[n], \quad x_d \in W_1. \end{aligned} \quad (2-16)$$

The scaling coefficient  $x_a$  and wavelet coefficient  $x_d$  are half resolution of the signal  $x$ . Similarly, the coefficients  $x_a$  can be further decomposed into next lower half scale

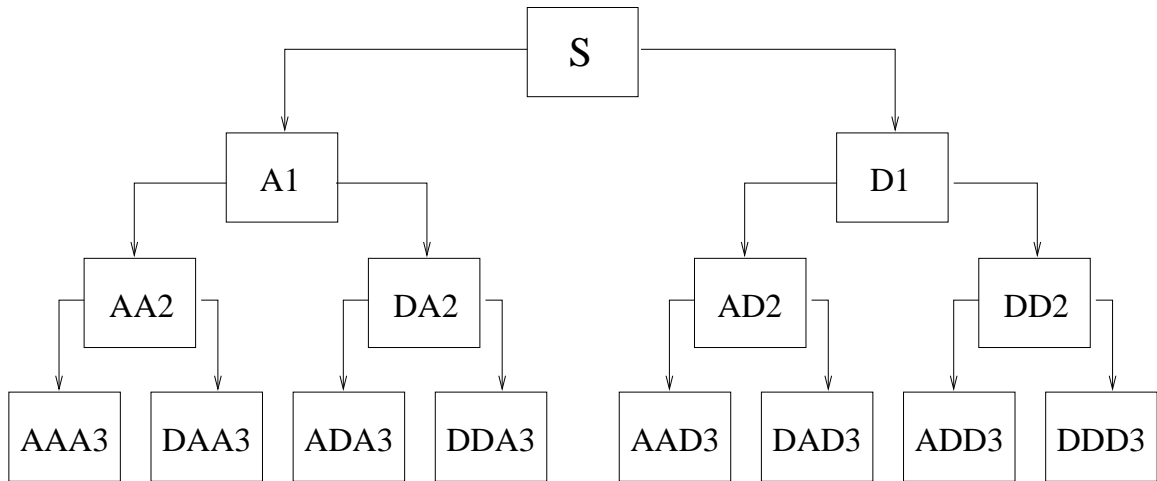


**Figure 2.10** The schematic diagram of the wavelet packet transform. The integer number  $1, 2, \dots, n$  indicates the levels of the decomposition.

coefficients  $x_{aa} \in V_2$  and  $x_{da} \in W_2$  by using same filters  $h$  and  $g$  shown as follow:

$$\begin{aligned}
 x_{aa}[k] &= \sum_n \bar{h}[n - 2k]x_a[n], \quad x_{aa} \in V_2, \\
 x_{da}[k] &= \sum_n \bar{g}[n - 2k]x_a[n], \quad x_{da} \in W_2.
 \end{aligned}
 \tag{2-17}$$

The decomposition of  $x_{aa}$  can be repeated to next lower level, and so on. The reconstruction of the input signal  $x$  from the scaling coefficients  $x_a$  and wavelet coefficients  $x_d$  is defined as

$$x[n] = \sum_k h[n - 2k]x_a[k] + \sum_k g[n - 2k]x_d[k]
 \tag{2-18}$$

Fig. 2.9 shows the schematic diagram of the decomposition and reconstruction of the multiresolution wavelet transform. It can be seen that the signal  $x$  has been convolved with the filters  $\bar{h}$  and  $\bar{g}$  respectively and then down-sampled with 2 to obtain the next level of coefficients. The new coefficients can be reconstructed by up-sampling then convoluted with two filter  $h$  and  $g$  separately. More detail explanations of wavelet transforms can be obtained from Strang (88).

The wavelet packet transform can be applied on the detail coefficient. The lower level detail coefficient is also decomposed into two subgroups by filters  $\bar{h}$  and  $\bar{g}$ . The two coefficient sets represent the low frequency and high frequency contents of the detail coefficient. This transform can be further applied on these new sets to next lower level, and so on. This process creates a binary tree structure (see Fig. 2.10). This is called the wavelet packet transform. The wavelet packet transform divides a signal into additional coefficient blocks, each block representing different frequency bands. In this paper, we have used wavelet packet transform to create the multiresolution templates for the morphological filter classification.

### 2.2.2 Lifting Scheme

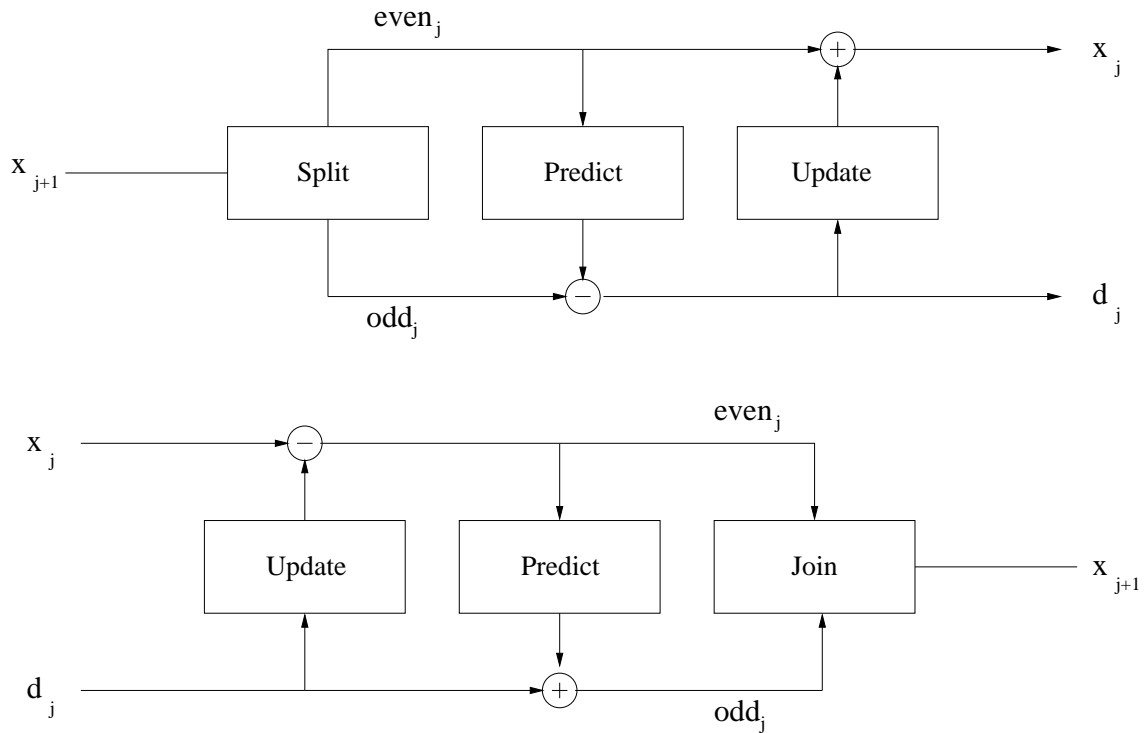
Recently a new approach to the multiresolution scheme was introduced by the so-called “Lifting Scheme”(92). The lifting scheme provides a novel mechanism of multiresolution analysis. It can be used to construct the second generation wavelets, which are not relied on one function for the translations and dilations (91).

Fig. 2.11 shows the basic structure of lifting scheme, where decomposition is shown on the top and reconstruction shown at the bottom. The basic idea about lifting scheme can be explained simply. Consider a signal  $x_{j+1}$ , the lifting scheme decomposes the signal  $x_{j+1}$  into  $x_j$  and  $d_j$ , both of which are coarser than  $x_{j+1}$ . The lifting scheme performs the decomposition in three steps: split, predict and update.

- Split: This stage splits the input signal into two subsignals: one is composed of the samples with even indexed, the other with odd indices.

$$(\text{even}_j, \text{odd}_j) = \text{Split}(x_{j+1}). \quad (2-19)$$

Both separated subsignals are half the size of the original signal.



**Figure 2.11** Lifting Scheme: decomposition and reconstruction

- **Predict:** If a sample is correlated with its neighboring samples. This sample can be predicted by a function of neighboring samples. If the odd points in the signal have strong correlations with the neighboring points, then the error of the prediction will be very small. The detail  $d_j$  coefficient is defined as the differences between the odd samples and then prediction function based on the even indexed samples:

$$d_j = \text{odd}_j - \text{Predict}(\text{even}_j) \quad (2-20)$$

The detail coefficient  $d_j$  is the error of the prediction which represents the detail information unable to be approximated by the prediction function.

- **Update:** The update stage adjusts the coarser level signal  $x_j$ , which is the scaling coefficient in the wavelet transform. The coarser signal is updated by

using the detail signal  $d_j$  and the even indexed samples.

$$x_j = \text{even}_j + \text{Update}(d_j) \quad (2-21)$$

Here the coarser level signal  $x_j$  is half the sampling scale of the finer level signal  $x_{j+1}$ . The importance of the update procedure is that it maintains the similarity between the finer and coarser level signal,  $x_{j+1}$  and  $x_j$ . The prediction stage finds the differences between the true values of the signal and their predicted values using a chosen function. But the correlation of the even indexed points are altered because of the missing the odd points. One can “lift” the correlative relationship for the even indexed points by using the detail coefficients to update their correlation. The principle of multiresolution analysis is to approximate a signal in different scales called as the scaling coefficient and this approximation is similar to the original signal at the higher levels. The detail coefficients are the errors between the approximation and the original signal. The two coefficient sets maintain the integrity of the original signal.

The idea behind the lifting scheme is to use the local correlation of the signal. If a signal has a high correlation in a local area, the prediction of the relationships between the neighboring odd and even samples can be estimated accurately. Because of the correlation in the signal, the correct prediction can be expected for this signals. Reconstruction using the lifting scheme is as simple as its decomposition. The bottom panel in Fig. 2.11 shows the reconstruction process. There are three stages in reconstruction using the lifting scheme.

- Undo Update: Using the decomposition procedure, the coarser signal  $x_j$  and detail signal  $d_j$  were obtained. To undo the update procedure, simply subtract

the update data.

$$\text{even}_j = x_j - \text{Update}(d_{j+1}) \quad (2-22)$$

The update function is the same for both analysis (decomposition) and synthesis (reconstruction) in the lifting scheme.

- Undo Predict: Using  $\text{even}_j$  and  $d_j$ , one can recover the  $\text{odd}_j$  indexed signal by adding the prediction information back.

$$\text{odd}_j = d_j + \text{Predict}(\text{even}_{j-1}) \quad (2-23)$$

The odd indexed signal can be obtained by subtracting the prediction of the even indexed points from the detail coefficients.

- Join: The join stage simply merges the even and odd indexed samples into original signal.

$$x_{j+1} = \text{Join}(\text{even}_j, \text{odd}_j) \quad (2-24)$$

The join function is the reverse function of the lazy wavelet transform.

The lifting scheme has the same properties as the wavelet transform in most cases. It replaces the low-pass and high-pass filters with predict and update process. It decomposes a signal into smaller signal with half scale of the original one and the decomposition can be repeated until running out of samples. The reconstruction then uses the scaling and detail coefficients from the lower levels to recover higher level signal perfectly. It also has one advantage in that it can map the signal from the integer domain into the integer domain (8). However, most important advantage for the lifting scheme is its flexibility in generating a multiresolution scheme matching the properties of a signal. With the newly generated predictive and updated methods, the lifting scheme can generate a new wavelet families (20).

### 2.2.3 Morphological Lifting Scheme

Heijmans and Goutisias (35, 36) proposed a morphology-based multiresolution analysis called max-lifting scheme which maps the signal into nonlinear morphological spaces where the lifting scheme may then be utilized in multiresolution mapping. Using the max-lifting scheme, we investigated a different way to execute three stages of the lifting scheme.

The lifting scheme is an implementation engine to accomplish multiresolution analysis, but its flexible structure extends beyond the wavelet transform, i.e., mixing the nonlinear functions into multiresolution transform. The proposed morphology-based multiresolution analysis max-lifting scheme maps the signal into nonlinear morphological spaces by using the operators of mathematical morphology. This new morphological function can divide a signal into two groups where one is the smoothed background activity and the other the spiky transient. This new morphological lifting scheme is briefly described as follows:

1. Separate the signal into two groups with one group containing only even indexed points and the other odd indexed point,

$$(\text{even}_j, \text{odd}_j) = \text{Split}(x_{j+1}). \quad (2-25)$$

2. Predicting the odd indexed values using morphological erosive operator with both even and odd points:

$$\begin{aligned} x_j(i) &= P(\text{even}_j(i), \text{odd}_j(i), \text{even}_j(i+1)) \\ &= (\text{even}_j(i), \text{odd}_j(i), \text{even}_j(i+1)) \ominus B, \end{aligned} \quad (2-26)$$

where  $x_j$  represents lower level scaling coefficients,  $B$  is the pre-defined circle structuring element, and  $\ominus$  denotes the morphological erosion operator. Unlike

the standard lifting scheme, the nonlinear erosion operator covers both the odd and even indexed points of the input data. To overcome the nonlinearity of morphology operation, the odd indexed signal is saved and will be used for perfect reconstruction in the reconstruction process.

3. Update the even indexed coefficients with the scaling coefficients

$$\begin{aligned} \text{even}_j(i) &= \text{even}_j(i) - \mathbf{U}(x_j(i), x_j(i+1)) \\ &= \text{even}_j(i) - \frac{1}{2}(x_j(i) + x_j(i+1)). \end{aligned} \quad (2-27)$$

The detail coefficients are then joined with the difference between even and odd indexed points and the prediction result from the above, is given by:

$$d_j = \text{Join}(\text{odd}_j - x_j, \text{even}_j). \quad (2-28)$$

This is just a short introduction about this morphological lifting scheme. In section 3.3, we will meet this method again and a more detailed description will be represented.

## 2.3 Stochastic Point Process of Spike Trains

Interictal spike is an important indicator of epileptic foci. These spikes can be identified by using spike detection algorithms, such as the method proposed in this paper. The stochastic process method investigated here is very useful many neurological applications. Our application of interest is to understand how different region of the brain interact (67,68). The recorded spike signals from the EEG/MEG data, produced from localized groups of nerve cells simultaneously firing together, are considered as a series of events in a spike train. The sequence of these spikes

are treated by stochastic point process measuring the time intervals between the occurrence of these spikes. The idea of a stochastic point process is that this process determines its statistical relationship by regarding the timing informations between when events occurred. It is a formulation for finding the correlation only related the timing information of a sequence of events. In the point process, the spike detection process is used to identify the occurrence of a spike and track the time interval between spikes. The stochastic point process may be used to model events in a single train. Relationships between multiple spike trains may be investigated by using cross statistical relationships between trains. The following is a brief description of the cross-correlogram analysis for multiple spike trains.

Assume that there exists two spike trains  $A$  and  $B$  both consisting of sequence of several spikes and each spike is treated as an event. The null hypothesis is that the occurrences of spikes in train  $A$  is independent with respect to the occurrence of spikes in train  $B$ . For an observed event in train  $A$ , two events occur in train  $B$  are before and after the event in train  $A$ . The approach is to determine the relationship between these events. The morphological characteristics of these spike events, such as duration and amplitude, are ignored in this analysis. The time interval between an event in train  $A$  and the leading and following events in train  $B$  adjacent to the event of  $A$  are denoted as  $V_{-1}$  and  $V_1$ . The  $V_{-1}$  and  $V_1$  are called the backward and forward recurrence times, respectively (see Fig. 2.12). For the same procedures, one can find other recurrence times  $V_{-2}$  and  $V_2$  by locating the second adjacent events. This procedure may be repeated to collect the  $n$ th recurrence times  $V_{-n}$  and  $V_n$ , i.e.,  $n$ th adjacent events in  $B$  with respect to an event in  $A$ .

To construct the pointed cross-interspike statistical relationship, a histogram of these observed recurrences is computed first. In train  $A$ ,  $N$  spike events are selected.

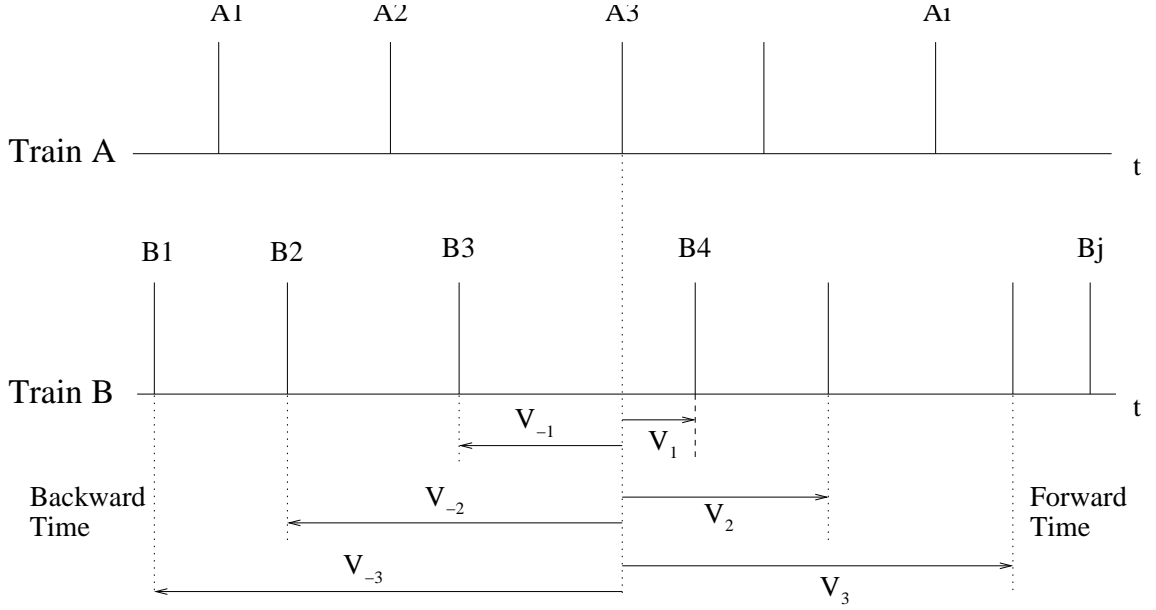


**Figure 2.12** Two Spike Trains  $A$  and  $B$  are plotted. The  $A_1$  to  $A_i$  are the spike events observed in train  $A$ . Meantime, the  $B_1$  to  $B_j$  are occurred in train  $B$ . The occurrence times of these events are appearing randomly. The event  $A_3$  has been first selected. The backward recurrence times  $V_{-1}$  to  $V_{-3}$  and the forward recurrence times  $V_1$  to  $V_3$  are collected from the adjacent spike events in train  $B$  with respect to the event  $A_3$ .

Each event has  $J$  backward and forward recurrence times observed with respect to the events in train  $B$ , denoted as  $V_{-j}$  and  $V_j, j = 1, \dots, J$ , individually. A range which is capable of covering the both  $V_{-j}$  and  $V_j$  are from  $-\infty$  to  $\infty$ , however in practical it can set to a reasonable ranges which are covering the most significant recurrence times, is chosen and divided into several intervals,  $n_k$ , with each interval equal to a width  $\Delta$ . These intervals are equivalent to the bins of a histogram. For example, the  $k$ th interspike bin in the span  $[(k-1)\Delta, k\Delta]$ . In statistical terms, the histogram is an estimator of the probability density function (pdf) of cross-interspike intervals,  $f(\tau)$ , where

$$f(\tau) = \text{Prob}\{\text{events in train } B \mid \text{the occurrence of entire in train } A\}. \quad (2-29)$$

If one utilizes enough observations, this calculation will approximate an estimator corresponding to

$$\lim_{N \rightarrow \infty} \left[ \frac{n_k}{N\Delta} \right] = \frac{1}{\Delta} \int_{(k-1)\Delta}^{k\Delta} f(u) du = \frac{F(k\Delta) - F((k-1)\Delta)}{\Delta}. \quad (2-30)$$

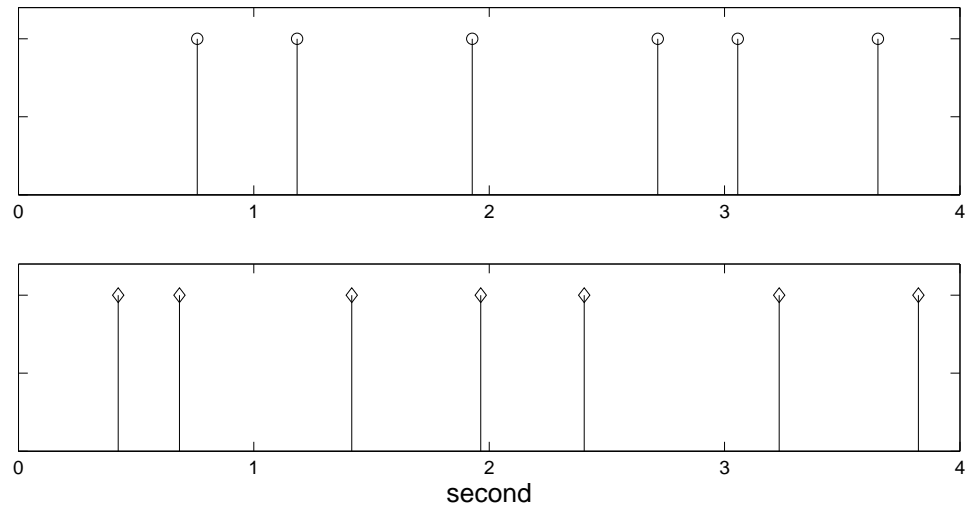
where  $F(\tau)$  is the cross-interspike interval distribution function where it satisfies  $F(\tau) = \int_0^\tau f(u) du$ .

To clarify the idea of the cross-interspike histograms (also called as the cross-correlogram) of stochastic point processes, I include two examples. The first example, define a spike train  $A$  as the master channel, where there are a total of 5000 simulated events. Spike train  $B$ , referred to as the slave channel, has been independently generated with another 5000 events having no relationship to the events in train  $A$ . The sampling rate of both simulated trains is 250Hz. Parts of these two channels are shown at the top panel of Fig. 2.13. The events in the two spike trains are uncorrelated with respect to each other. Each event in the spike train  $A$  is used to identify adjacent events in train  $B$  and find their recurrence times, denoted as  $\{V_{-J}, \dots, V_{-1}, V_1, \dots, V_J\}$ . In this example, the  $J$  is set to 25, thus there are 25 adjacent forward and backward recurrence times. These recurrence times are used to establish the histogram  $f(\tau)$  and show the pdf of the cross-interspike intervals between the two trains. The width of the bins are set to be 4 msec. Initially, the number of events in each bin is set to zero. If a recurrence time falls into the range of a bin, then the number of events at this bin is incremented. This procedure is applied every recurrence to accumulate the counts in each bin. The pdf of the cross-interspike trains is the final number of in the bins. The bottom panel of Fig. 2.13 is the cross-correlogram of two uncorrelated spike trains. It shows that the histogram of two trains is flat with no significant variation in the figure. The flat line of the histogram indicates that the events of the two trains are not correlated each other; That is the events in each train is generated

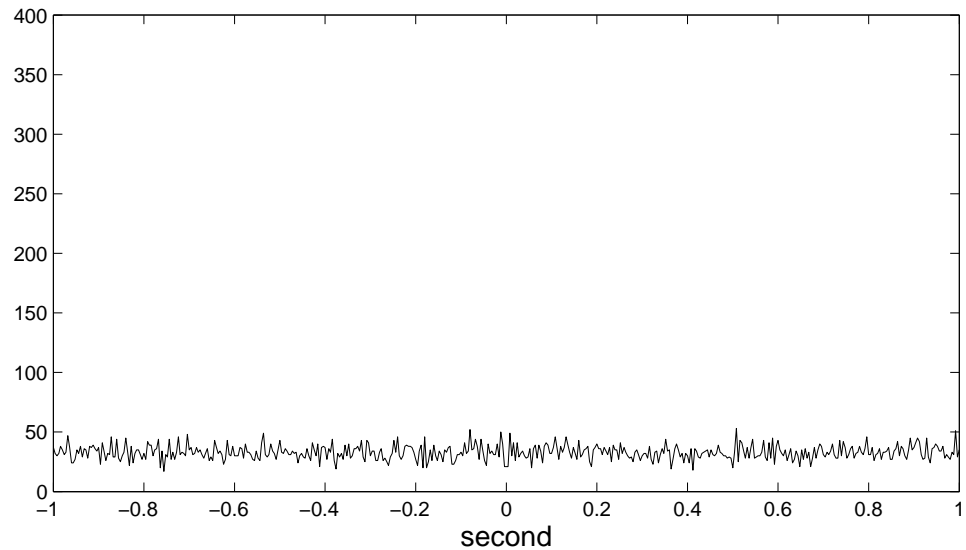
independently for each other. As expected, the stochastic point process correctly presents the statistical relationship between these trains.

In the second example, the events of the slave spike train  $B$  occur about 0.2 second latency after the adjacent events in train  $A$ . It also collected all the forward and backward recurrences between two trains and plotted the correlogram for the cross-interspike intervals. If an event occurred in the train  $A$ , there exists a latency until another event appears in the train  $B$ . This relationship between  $A$  and  $B$  can be shown by using the cross-correlogram. The top panel of Fig. 2.14 shows the simulated generated spike trains  $A$  and  $B$ . At the bottom of this figure is the cross-correlogram of the cross-interspike intervals. A marker 'x' shows that a maximum count (the most strong correlation) of the histogram is at the time 0.2 seconds. Around the time of 0.2 second, the count is still relatively large indicating that the events of in train  $B$  are mainly delayed 0.2 second, but with small variations. The flat variation area other than around 0.2 second implies that there is no statistical correlation in these areas similar to previous example. This example shows that this technique can successfully detect the physical relationship between two trains.

If the events in train  $A$  have appeared 0.2 second later than the events in train  $B$ , this histogram will be similar to example two, but the maximum count point will shift to -0.2 second. It indicates that the events in train  $B$  has a tendency to lead the events in train  $A$  0.2 second early.

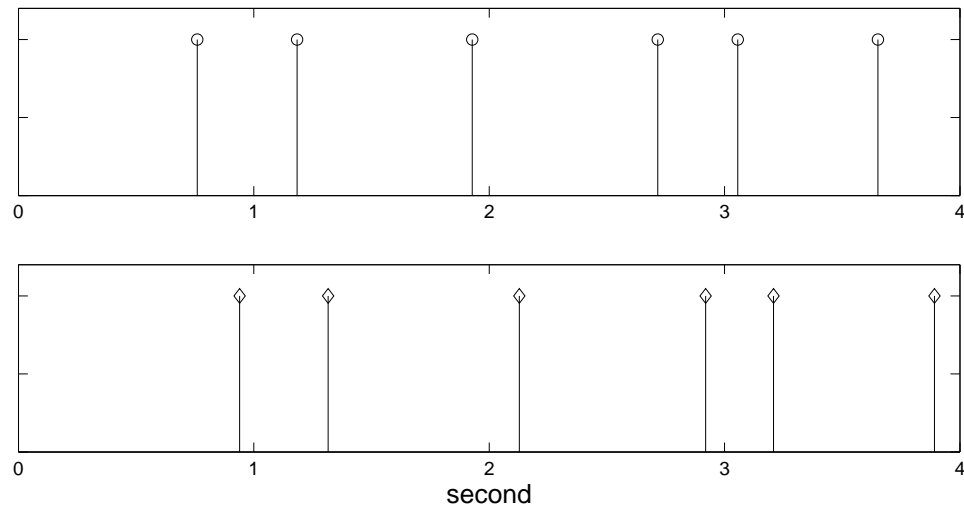


(a) Two Uncorrelated Spike Trains

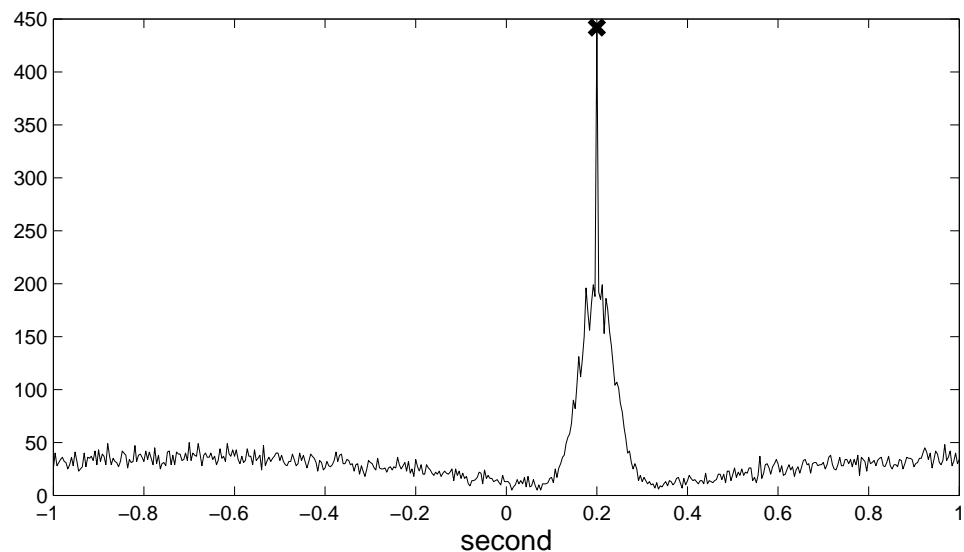


(b) Correlogram of the uncorrelated Spike Trains

**Figure 2.13** (a) Two uncorrelated spike trains, the top one is the master spike train  $A$  and bottom is slave spike train  $B$ . There are 5000 events in each train. These events are generated independently and randomly. (b) The cross-correlogram of the interspike events is the histogram of the forward and backward recurrences of the events of spike train  $B$  concluded on the occurrence of events in  $A$ . There is no indication that these two trains have any correlation. The x axis is the time, the y axis is the count number of the histogram.



(a) Two correlated Spike Trains



(b) Correlogram of the correlated Spike Trains

**Figure 2.14** (a) Two correlated spike trains, the top one is the master spike train  $A$  and bottom is slave spike train  $B$ . There are total 5000 spike events in both trains (only show partly). The events in  $A$  are created randomly. Once a event in train  $A$  has been generated, Around 0.2 second, a following event is generated in  $B$ . (b) The correlogram of the cross-interspike trains: this is the histogram of the forward and backward recurrences of the events of spike train  $B$  relating to spike train  $A$ . There exists a peak at the time 0.2 seconds and it is the maximum correlation between the two trains. The x axis is the time, the y axis is the count number of the histogram. The calculation is interpreted as the probability of one event occurring in  $B$ , given that an event has occurred in  $A$ .

### 3.0 METHODS FOR SEPARATION OF SIGNAL COMPONENTS

A new approach is developed to separate interictal spikes from the ongoing EEG, based morphological filtering of signal decomposition in multiresolutions. This new method is different from the classical parametric method or direct analysis methods because it does not rely on tedious parameter estimation or complex descriptions of transients. Instead this new approach attempts to differentiate the morphological features of the two components and extract spiky transients from the background data. Two methods have been developed as presented in this chapter.

#### 3.1 The Concept of Multi-resolution Morphological Separation Method

The process of using mathematical morphology can recognize and extract an object's shape characteristics. A signal can be separated into two different components by using an appropriate structuring element (SE) taking into account the a priori knowledge of the target component. Different structuring elements will give different separation results. In the process, considerations the "spiky" transient activity of varied triangular shape are of the features of interest. It is known that a circular disc is a smooth polygon with constant curvature along of its curvature. Using this structuring element is like using a ruler to measure an object curvature, where the background activity has constant curvature locally matched with the disc. Complex structures of target patterns may require a number of different structuring elements or circular discs with different radii to catch the patterns. Using various disc of radii may be equivalent to using a single disc of a fixed radius on signal decomposition at

different scales (resolutions): the latter is what we used to develop a morphological filter for detecting an separate various triangular-shape spikes.

### 3.1.1 Effect of Using Different Sizes of Structuring Element

The structuring element (SE) extracts morphological characteristics from the input signal. It is important to understand that this operation using different sizes of structuring elements. They identify different morphological shapes and produce different separation results. The SE plays an essential role in this application. In our case, we decided that a circular disc could be used to measure the degree of the shape variation for EEG data. This was suggested because a circle is a polygon with constant curvature which is able to detect the curvature variation of the signal. Another question raised after picking the structuring element, is what size of the structuring element can lead to best result.

Fig. 3.1 demonstrates the results applying three different structuring elements (SEs) on a triangle-shape signal, which contains a sharp peak representing a spiky signal. Three different structuring element discs are shown with different radii. For the first experiment, the radius of the disc is equal to  $r$ , the second one is  $2r$ , and the final is  $4r$ . Using the morphological opening operation, see section 2.1.2, the structuring element smooths the upward sharp peak without affecting the remainder of the triangular signal. From these experiments one can compare the differences of the smoothed signal and the sharp residue when the size of the SE changed.

On the top Fig. 3.1, the smallest structuring element circular disc with radius  $r$  was applied to smooth the sharp peak. The left of the first row shows that the SE is under the peak, the middle and right figures are the two separated components, smoothed and sharp, after the morphological operations. It is immediately seen that

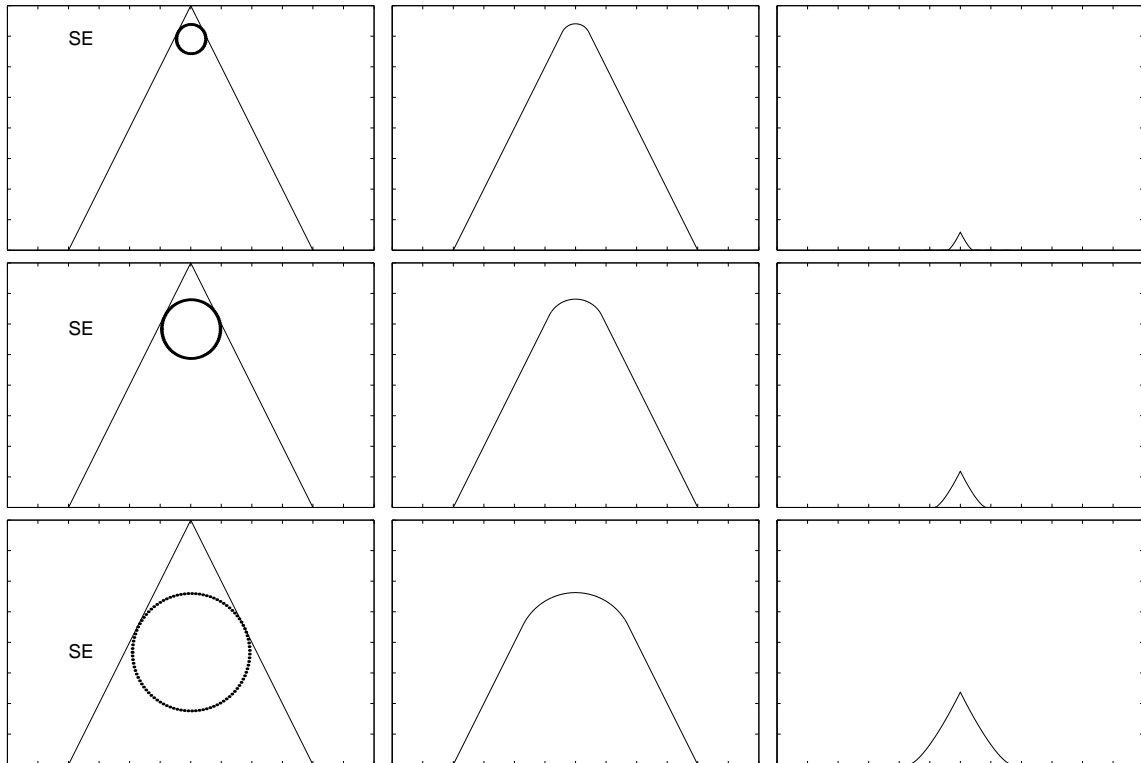


**Figure 3.1** The separation result using Different sized structuring element operated on a triangle signal. Top row shows that the radius of structuring element circular disc is  $r$ , second row is  $2r$  and the last row  $4r$ . The first column represented the input signal operated by a morphological opening operation. The middle and right columns represent the separated background activity and spiky signal, separately. It shows that the largest SE separates the biggest sharp peak from the input signal.

a small portion of the peak has been recognized and separated from the input signal. The rest of the original signal was not affected by the morphological filter. The separated peak is small because the SE is also small. In the second experiment, the SE is twice as large as the first SE and the same morphological operation is applied on the identified triangular signal. The middle row of the figure shows the morphological operation and the two separated components. This time the separated peak is larger than in the first experiment. The third experiment shows that the structuring element circular disc, with the largest radius  $4r$ , separates the largest peak from the input

data. The separated components to all experiments are shown in the middle and right of the last row in Fig. 3.1.

These three experiments show that the size of the structuring element will affect the properties of sharp peaks separated from the triangular signal. The numerical results indicate that different SEs will lead into different results. Once the geometric shape of SE has been decided, in this case a circular disc, the size of the structuring element needs to be carefully chosen in order to allow the extraction of the sharp spiky pattern from the input data. In general, a larger structuring element is able to separate a larger portion of the sharp peak signal.

### 3.1.2 Effect of Using Coarse Scale Signals

In section 3.1.1, it has shown that the bigger peak signal will be extracted by using larger circular structuring element disc. Beyond using these structuring elements of different radii, it can alter to use other approach to separate the signal into two components. The size of these SEs are enlarged by the power of two and the morphological operations are applied to the original scaling domain of the input signal. If one can alter the size of structuring element, it is also possible to obtain a similar result by changing the scale of the signal. Thus, instead of enlarging the size of structuring element, one can shrink the scaling of the input signal and keep the radius of the structuring element unchanged. Additional experiments have been conducted in order to compare the results between enlarging the structuring element and shrinking the scaling of the input signal. In these experiments, It has assumed that the radius of structuring element is  $r$  units and the scaling of the input signal is reduced by power of two at each time.

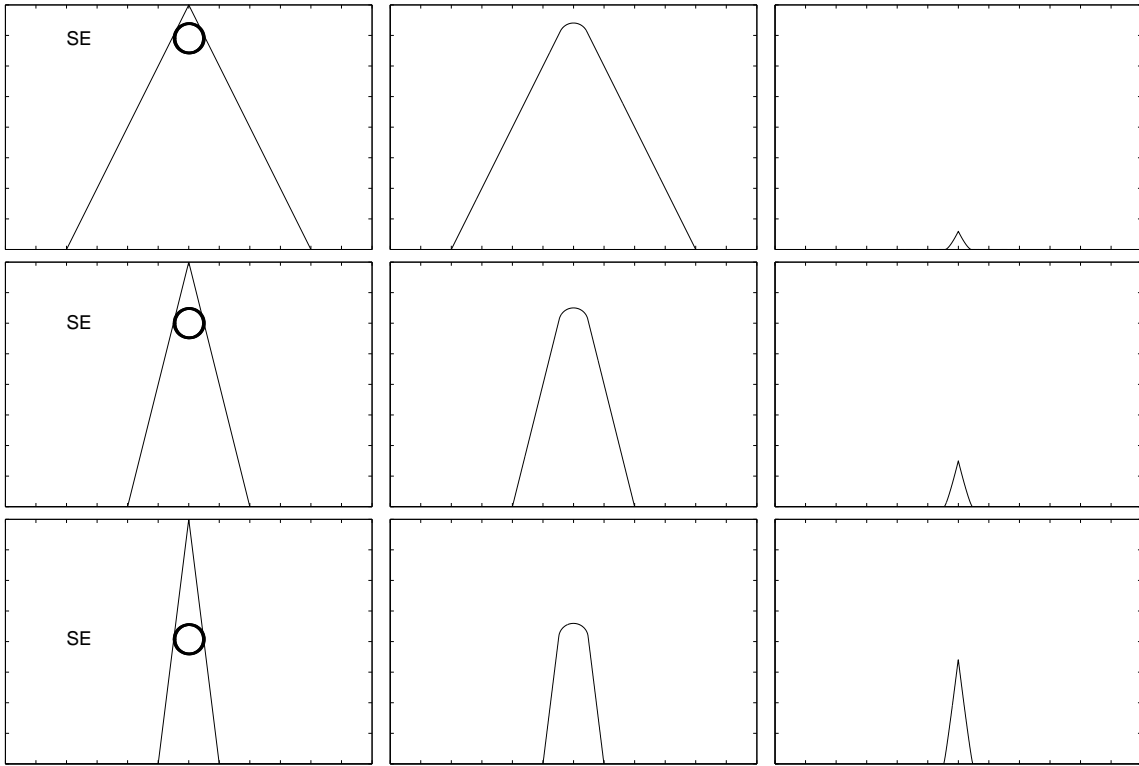


**Figure 3.2** The separation results of using coarse scale signal with a fixed sized structuring element. The resolution of the top row is equal to original one, the second row is reduced to the half and the third row is a quarter of the original resolution. The first column shows that the various scale signal operated by a morphological opening operator. The middle and right columns represent the separated background activity and “spiky” transient, respectively. The coarser of scale changed, the higher of the peak signal was.

Let the original scale be indicated as  $t$  and the alteration of scale be labeled as  $t'$ . The new scale  $t'$  is reduced by the factor of power two. The relationship between the scaled signal  $f(t')$  and  $f(t)$  is expressed as:

$$f(t') = f(2^{-n}t), \quad n \in N. \quad (3-1)$$

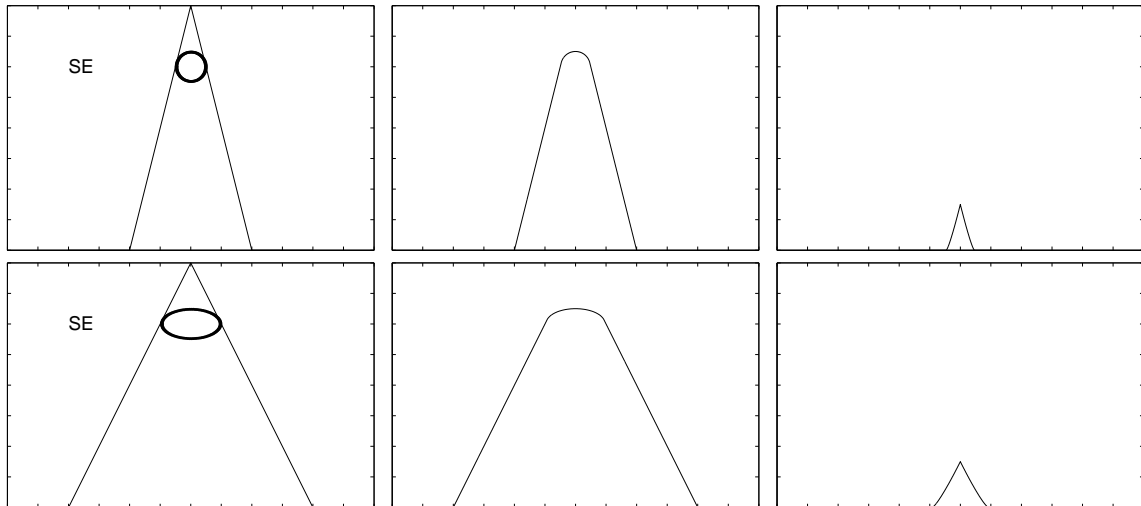
The shape of scaled signal  $f(t')$  is to the signal  $f(t)$ . The SE is defined as  $r$  unit in any scaling resolution and is fixed for any scaling transformation.

Fig. 3.2 demonstrates the results of changing the scale resolution of the input signal, with the radius of structuring element circular disc fixed. The input data is a triangular signal which is the same as in the previous section. The structuring element is a circular disc with its radius defined as  $r$  unit. The top row of Fig. 3.2 shows the operations and results, where the scale  $t'$  is equal to  $t$ . It is the same process as the top row of Fig. 3.1. In this case, the sharp shape peak is very small. In the middle row of the same figure, the signal,  $f(t') = f(2^{-1}t)$ , is presented. The radius of the SE is set to  $r$  in the scale  $t'$ . The separated peak and the smoothed background activity are shown in the right and middle of this row. The bottom row shows another example by further reducing signal's scale to a quarter of the original one. The scale of signal  $f(t')$  is equivalent to  $f(2^{-2}t)$ . The structuring element is set to a circular disc with a radius of  $r$  units. The morphological operation has divided the reduced scale signals into two groups. To convert the signal  $f(t')$  into  $f(t)$ , just reverse the equation (3-1) shown as

$$f(t) = f(2^n t'), \quad n \in N. \quad (3-2)$$

Eq. (3-2) shows that the reduced scale  $t'$  is converted back into the original resolution by increasing its scale with power of two.

The results for the varied scale  $t'$  converted back into its original one  $t$  are shown Fig. 3.3 and 3.4. Top row of each figure is the operated result applied on the  $t'$ . The bottom row shows the converted result of its original scale  $t$ . The center and right columns of these figures represent the the smoothed component and sharp peak, respectively. It can be seen that the conversion results have extracted the peak from the triangular signal. It is interesting to point out that the circular structuring element is converted into an ellipse on the original scale. This vertical height of this ellipse is the same to the radius  $r$ , but its horizontal width is twice large than vertical



**Figure 3.3** [Top] The resolution of the triangular data is reduced to half of its original resolution. The results of the smoothed background activity and peak are shown in the middle and right columns. [Bottom] The results of the top have been converted into its original resolution and shown in the bottom row. The separation process applied on different scale signals is able to divide a triangular signal into two different components.

dimension. This is because the reduced scaling has shrunk by two, but the amplitude of the signal did not change during the scale transformation. The conversion of the original scale has transformed a circular disc into an ellipse. This morphology operation is like that one has used an ellipse as the structuring element to recognize and separate the input signal into two components. Fig. 3.4 shows the separated peak and the smoothed background activity by converting to quarter of the original scale. This peak is larger than the peak in Fig. 3.3. The background activity is also smooth. For these experiments, the morphological operators were applied to the reduced scale signal and separated the peak from a triangular signal. It concludes that either changing the size of the structuring element or reducing the scale of signal are capable of separating the spiky sharp patterns from the input signal.

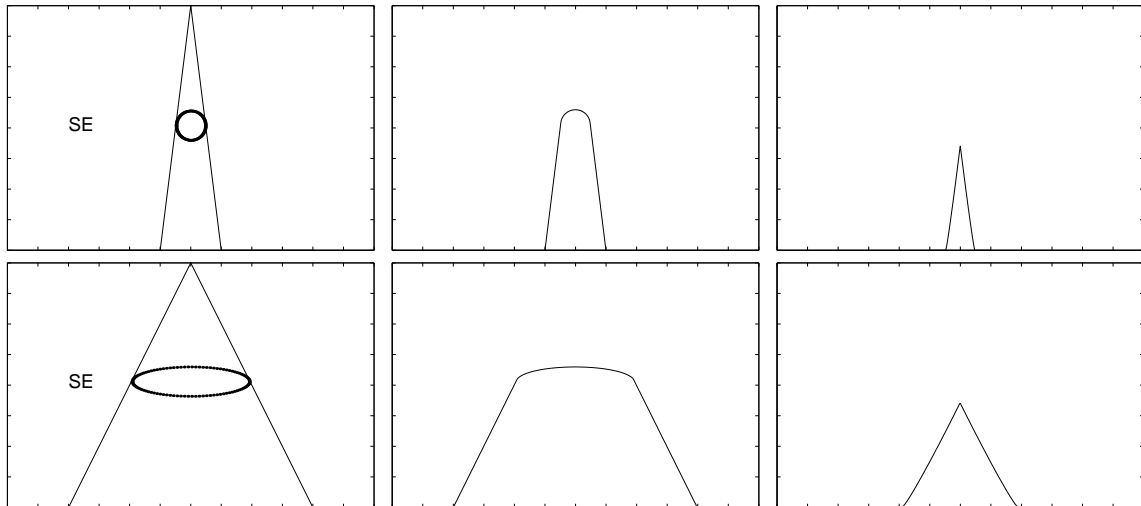


**Figure 3.4** [Top] The triangular data has been reduced into a quarter of its original resolution. The results of the separated background activity and peak are shown in the middle and right columns. [Bottom] The bottom row is the results of converting the top row into its original resolution. The separation process can divide the triangular signal into two different components by reducing its resolution and changing it back. The separated peaked transient is higher than the previous one using half-resolution and converting it back.

### 3.1.3 The Comparison Between Varying SE Size and Varying Signal Scale

It has been demonstrated that the processes of changing the size of SE and altering the signal scale are equivalent in terms of separating two components from an input signal. It is also interesting to compare the differences of these peaked spikes. Figure 3.5 shows the comparisons between the two methods. The left column of Fig. 3.5 is the original signal applied with a structuring element with a radius  $r$ . The top of middle column shows the operation of a structuring element with a  $2r$  radius. The last column of the top row shows the structuring element with a  $4r$  radius. The middle bottom figure shows that the operation applied to the half reduced scale signal transform the structuring element into an ellipse; when the original scale has been reconstructed back. While the bottom shows that the circular disc of the structuring

element has been converted into an ellipse with its horizontal radius four times than vertical one. The ellipse occurred because the input signal has being reduced to a quarter of its scale and converted back into its initial form. It is clearly seen that by using different structuring elements have been proven to separate the area of peak from the triangular signal.

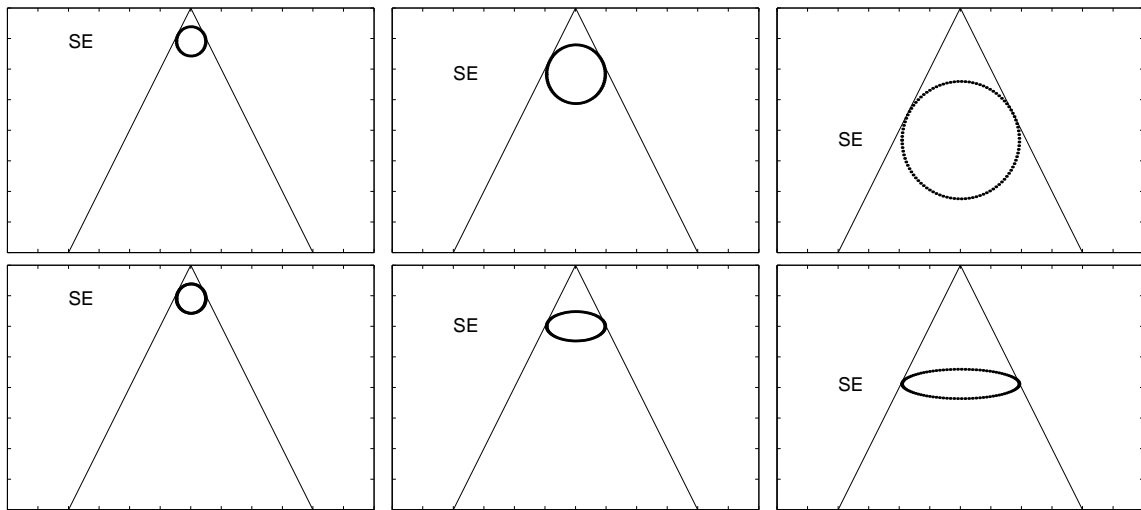


**Figure 3.5** Comparison between varying SE size [top], and varying signal scale (have been converted back into its original scale) [bottom]

The smallest structuring element can only separate a tiny portion of the peak while a morphological filter with the larger structuring element extracts a larger portion of the peaked signal from the triangle signal. The structuring element applied on a reduced scale signal and converted into the original scaling can extract a similar peak the input data. The result of the morphological operation, using the quarter scale signal, separates a largest peak. Both methods are capable of extracting the target patterns from a triangular signal. The changing of signal scale can be obtained by using wavelet transforms. A wavelet transform is known as a multiresolution transform which decomposes a signal into two coefficient sets: one is the approximated coefficient set and the other is detail coefficient set (it also widely called as wavelet

coefficient set). Each coefficient set is a half scale of the upper level coefficient. The decomposition coefficient set can then be decomposed into next level, and so on. The integrity of the signal is not changed or affected by the wavelet transform. It makes the perfect reconstruction of the decomposed signal into its original form. Our goal is to separate a signal  $z$  into the two components  $x$  and  $y$ , one of whom contains the spiky transients of various size. This can be achieved by operating a morphological filter in signal decomposition at different scales (resolutions).

### **3.2 A Separation Method Using Morphological Filtering in Wavelet Packet Transform**

Using structuring elements of different sizes, a morphological filter will extract different magnitudes of the sharp peak. Instead of using different sizes of structuring elements, the morphological operation can be used on the scaled signal to approximate similar results. The changing of the signal scale is a multiresolution analysis. The wavelet transform can decompose a signal into two coefficient sets each with half scale of the signal. Each coefficient set can be repeatedly decomposed into the next lower level with coarse scale of the previous level. A morphological filter then separates the coarser scale coefficients into two components: the background activity and the spiky transient. The sum of the two separated components is still equal to the original coefficients. A detail step-by-step descriptions about the proposed method are given in this section.

#### **3.2.1 Linear Function**

A linear transformation is given by

$$y(t) = T[x(t)] \tag{3-3}$$

where  $y(t)$  is the output signal and  $x(t)$  is input signal,  $t$  is time index, and  $T$  is a linear operator.

**Definition 9.** *Let  $V$  and  $W$  be vector spaces over the field  $F$ . A linear transformation  $T$  from  $V$  into  $W$  is a function  $T$  from  $V$  into  $W$  such that*

$$T(c\alpha + \beta) = cT(\alpha) + T(\beta) \quad (3-4)$$

*for all  $\alpha$  and  $\beta$  in  $V$  and all scalars  $c$  in  $F$ . (38)*

The extension of definition 9 shows as follows:

$$T(c\alpha + d\beta) = cT(\alpha) + dT(\beta), \quad (3-5)$$

where  $\alpha$  and  $\beta$  are in  $V$  space and  $c$  and  $d$  are scalar. In our case, we are particularly interested in the case where the scalars  $c$  and  $d$  are equal to one; i.e.

$$T(\alpha + \beta) = T(\alpha) + T(\beta) \quad (3-6)$$

### 3.2.2 Morphological Classification

Define a signal  $x$ . The wavelet transform decomposes  $x$  into two coefficient sets  $x_a$  and  $x_d$ . The first coefficient set  $x_a$  is called as approximation coefficients of  $x$  and the second set  $x_d$  is called as detail coefficients or wavelet coefficients of  $x$ . Using the opening and closing operations, it is possible to design a morphological filter (see eq. 2-9) with its structuring element as a circular disc with fixed radius set to 1. This morphological filter is able to classify the approximation coefficient  $x_a$  into two subgroups based on their morphological characteristics. One subgroup is the morphological filtered result of the coefficient  $x_a$  with only smooth variation remaining and the other subgroup is the residues of the filtering containing only rough shape

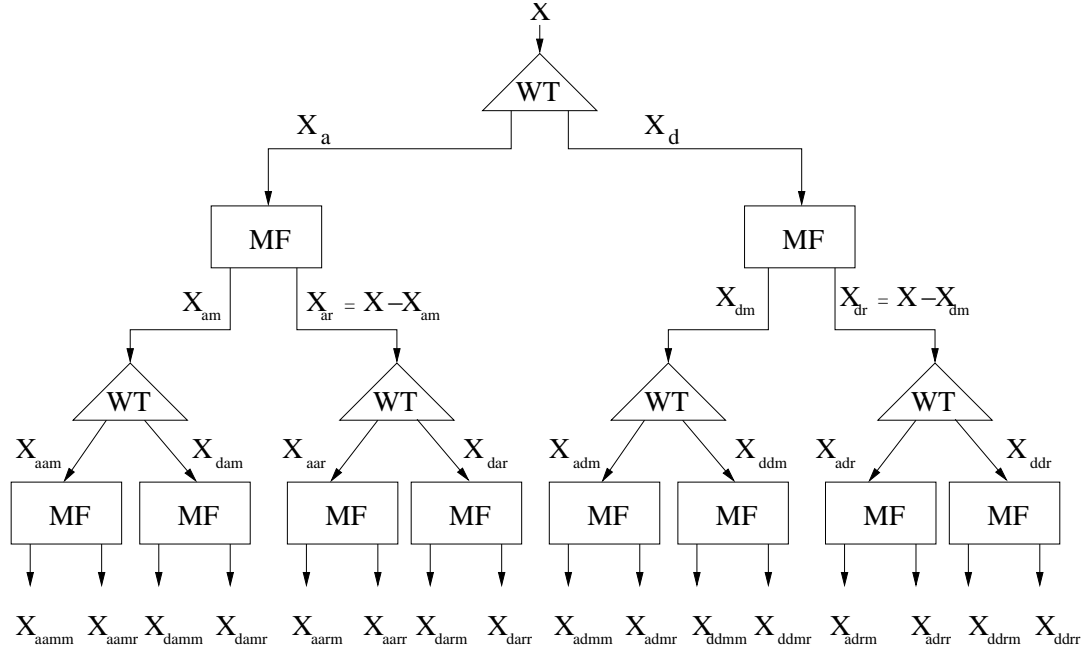


**Figure 3.6** The morphology wavelet separation method

and peaked signal of  $x_a$ . The first subgroup is labeled as  $x_{am}$  representing the background activity. The second subgroup labeled as  $x_{ar}$  containing the rough shape and peaked signal which exhibits the spiky transient. The wavelet transform provides templates equivalent to reducing the scaling of signal and the morphological operator then separate the scaled signal into two groups. The coefficient set  $x_d$  can be also classified into two subgroups by using similar procedures as the classification of  $x_a$ . The two subgroups of classification from  $x_d$  are labeled as  $x_{dm}$  and  $x_{dr}$ , which includes the morphological characteristics belonging to the background activity and transient phenomenon, separately. This morphological classification divides a coefficient set into two subgroups so that the summation of these two subgroups is same as the original coefficients. It can be shown as  $x_a = x_{am} + x_{ar}$  and  $x_d = x_{dm} + x_{dr}$ , (Fig. 3.6). The morphological operation is used as a thresholding criterion which only divides the coefficient into two components, while the properties of signal do not change.

The wavelet transform decomposes the approximate coefficient  $x_a$  into the next lower level coefficient sets  $x_{aa}$  and  $x_{da}$ .  $x_a$  has been classified into two groups  $x_{am}$  and  $x_{ar}$  by the morphological operator.  $x_{am}$  is decomposed into  $x_{aam}$  and  $x_{dam}$ , while  $x_{ar}$  is transformed into sets  $x_{aar}$  and  $x_{dar}$ . The lower level approximation coefficient,  $x_{aa}$ , is equal to the summation of the  $x_{aam}$  and  $x_{aar}$ . The lower level detail coefficient  $x_{da}$  is equal to the aggregation of  $x_{dam}$  and  $x_{dar}$ . The two small sets  $x_{dm}$  and  $x_{dr}$  of the coefficient  $x_d$  were decomposed into  $\{x_{adm}, x_{adr}\}$  and  $\{x_{dam}, x_{dar}\}$ , while the first two groups are equal to  $x_{ad}$  and the last two are corresponding to  $x_{dd}$ . These divided groups can be further decomposed and classified into the next by repeating the same morphology wavelet processes until the desired separation results have been reached. Because the wavelet transform is a linear function, each classified group can be decomposed separately.

### **3.2.2.1 Decomposition.**

Let  $x$  be the signal to be processed,  $\bar{h}$  represent a low-pass wavelet filter and  $\bar{g}$  a high-pass wavelet filter. The first level wavelet decomposition derives an approximation coefficients  $x_a$  and detail coefficients  $x_d$  using the filters  $\bar{h}$  and  $\bar{g}$ , respectively:

$$\begin{aligned} x_a[p] &= \sum_n \bar{h}(n-2p)x[n] \\ x_d[p] &= \sum_n \bar{g}(n-2p)x[n]. \end{aligned} \quad (3-7)$$

The decomposed coefficients  $x_a$  and  $x_d$  can be further decomposed by the wavelet transform to derive second level coefficients:

$$\begin{aligned} x_{aa}[p] &= \sum_n \bar{h}(n-2p)x_a[n], \\ x_{da}[p] &= \sum_n \bar{g}(n-2p)x_a[n] \end{aligned} \quad (3-8)$$

and

$$\begin{aligned} x_{ad}[p] &= \sum_n \bar{h}(n-2p)x_d[n], \\ x_{dd}[p] &= \sum_n \bar{g}(n-2p)x_d[n]. \end{aligned} \quad (3-9)$$

The  $x_{aa}$  and  $x_{da}$  are the approximate coefficients and detail coefficients of the upper level coefficient  $x_a$ . Similarly,  $x_{da}$  and  $x_{dd}$  are the coefficients obtained from  $x_d$ .

Using the mathematical morphology filter  $M_f^B$  (see eq. 2-9),  $x_a$  is divided into two subgroups  $x_{am}$  and  $x_{ar}$ . Similarly,  $x_d$  is divided into  $x_{dm}$  and  $x_{dr}$ . Thus

$$\begin{aligned} x_a &\xleftrightarrow{M_f^B} M_f^B(x_a) = x_{am} + x_{ar} \\ x_d &\xleftrightarrow{M_f^B} M_f^B(x_d) = x_{dm} + x_{dr}. \end{aligned} \quad (3-10)$$

Eq. (3-10) shows that the separated subgroup of the morphological classification are still equal to the coefficients  $x_a$  and  $x_d$ , it divides them into two parts by morphological thresholding. It can plug  $x_a = x_{am} + x_{ar}$  into  $x_{aa}[p] = \sum_n \bar{h}(n-2p)x_a[n]$  and  $x_{da}[p] = \sum_n \bar{g}(n-2p)x_a[n]$  (eq. 3-8), one obtains

$$\begin{aligned} x_{aa}[p] &= \sum_n \bar{h}(n-2p)x_a[n] \\ &= \sum_n \bar{h}(n-2p)(x_{am} + x_{ar})[n] \\ &= x_{aam}[p] + x_{aar}[p] \\ &= x_{aam} + x_{aar}, \end{aligned} \quad (3-11)$$

And  $x_{da}$  will obtain

$$x_{da}[p] = x_{dam} + x_{dar}. \quad (3-12)$$

Using similar procedures, the coefficients  $x_{ad}$  and  $x_{dd}$  from the upper level coefficient  $x_d$  are derived as follows:

$$x_{ad}[p] = x_{adm} + x_{adr}, \quad (3-13)$$

and

$$x_{dd}[p] = x_{ddm} + x_{ddr}. \quad (3-14)$$

The two coefficients of first level,  $x_a$  and  $x_d$ , are classified into two subgroups by using the morphological filter. The second level coefficient  $x_{aa}$  is divided into two categories by the same morphological classification filter, see eq. (2-9). This filter operation applied to the eq. (3-11) is derived as follow:

$$\begin{aligned} x_{aa} &\stackrel{M_f^B}{\longleftrightarrow} M_f^B(x_{aa}) & (3-15) \\ &= (x_{aa})_m + (x_{aa})_r, \\ &= (x_{aam} + x_{aar})_m + (x_{aam} + x_{aar})_r \\ &= (x_{aam})_m + (x_{aar})_m + (x_{aam})_r + (x_{aar})_r \\ &= x_{aamm} + x_{aarm} + x_{aamr} + x_{aarr} \end{aligned}$$

Eq. (3-15) shows the result for the second level coefficients  $x_{aa}$ . where this coefficient has been derived into four subgroups  $x_{aamm}$ ,  $x_{aarm}$ ,  $x_{aamr}$  and  $x_{aarr}$ . With similar classification procedures, the remaining of coefficient sets  $x_{da}$ ,  $x_{ad}$  and  $x_{dd}$  are derived into four subgroups. The classification results of all the second level coefficients are listed as follows:

$$x_{aa} \stackrel{M_f^B}{\longleftrightarrow} M_f^B(x_{aa}) = (x_{aa})_m + (x_{aa})_r = x_{aamm} + x_{aarm} + x_{aamr} + x_{aarr} \quad (3-16)$$

$$x_{da} \stackrel{M_f^B}{\longleftrightarrow} M_f^B(x_{da}) = (x_{da})_m + (x_{da})_r = x_{damm} + x_{darm} + x_{damr} + x_{darr} \quad (3-17)$$

$$x_{ad} \stackrel{M_f^B}{\longleftrightarrow} M_f^B(x_{ad}) = (d_{ad})_m + (d_{ad})_r = x_{admm} + x_{adrm} + x_{admr} + x_{adrr} \quad (3-18)$$

$$x_{dd} \stackrel{M_f^B}{\longleftrightarrow} M_f^B(x_{dd}) = (d_{dd})_m + (d_{dd})_r = x_{ddmm} + x_{ddrm} + x_{ddmr} + x_{ddrr}. \quad (3-19)$$

The wavelet decomposition and morphological operations are not limited into the second level only. These operations can be further applied to the third level, and so

on. The multiresolution property of wavelet transform provides the templates for the morphology classification. The decomposed coefficient is equivalent to changing the scaling of the signal and the structuring element size of the morphological operator is fixed, at one unit for each different level.

### **3.2.2.2 Reconstruction.**

The reconstruction of wavelet transform also used two different filters  $h$  and  $g$  to rebuild the original signal from the decomposed coefficients. These two filters  $h$  and  $g$  are the synthesis filters related to analysis filters  $\bar{h}$  and  $\bar{g}$ . The reconstruction from the second level coefficients is shown as follows:

$$\begin{aligned} x_a[p] &= \sum_n h(p-2n)x_{aa}[n] + \sum_n g(p-2n)x_{da}[n] \\ x_d[p] &= \sum_n h(p-2n)x_{ad}[n] + \sum_n g(p-2n)x_{dd}[n]. \end{aligned} \quad (3-20)$$

The reconstruction of the first level coefficients is

$$x[p] = \sum_n h(p-2n)x_a[n] + \sum_n g(p-2n)x_d[n]. \quad (3-21)$$

From the eq. (3-16) - (3-19) and (3-20), one can rewrite the second level wavelet reconstruction of  $x_a$  and  $x_d$  shown as

$$\begin{aligned} x_a[p] &= \sum_n h(p-2n)x_{aa}[n] + \sum_n g(p-2n)x_{da}[n] \\ &= \sum_n h(p-2n)[x_{aamm} + x_{aarm} + x_{aamr} + x_{aarr}] + \\ &\quad \sum_n g(p-2n)[x_{dammm} + x_{darm} + x_{damr} + x_{darr}] \\ &= [\check{x}_{aamm} + \check{x}_{aarm} + \check{x}_{aamr} + \check{x}_{aarr}] + [\check{x}_{dammm} + \check{x}_{darm} + \check{x}_{damr} + \check{x}_{darr}], \end{aligned} \quad (3-22)$$

$$\begin{aligned}
x_d[p] &= \sum_n h(p-2n)x_{ad}[n] + \sum_n g(p-2n)x_{dd}[n] \\
&= \sum_n h(p-2n)[x_{admm} + x_{adrm} + x_{admr} + x_{adrr}] + \\
&\quad \sum_n g(p-2n)[x_{ddmm} + x_{ddrm} + x_{ddmr} + x_{ddrr}] \\
&= [\check{x}_{dammm} + \check{x}_{darm} + \check{x}_{damr} + \check{x}_{darr}] + [\check{x}_{ddmm} + \check{x}_{ddrm} + \check{x}_{ddmr} + \check{x}_{ddrr}].
\end{aligned} \tag{3-23}$$

The reconstruction of the first level coefficients (initial signal level) is derived from eq. (3-21)

$$\begin{aligned}
x[p] &= \sum_n h(p-2n)x_a[n] + \sum_n g(p-2n)x_d[n] \\
&= \sum_n h(p-2n)[\check{x}_{aamm} + \check{x}_{aarm} + \check{x}_{aamr} + \check{x}_{aarr}] + \\
&\quad \sum_n h(p-2n)[\check{x}_{aamm} + \check{x}_{darm} + \check{x}_{damr} + \check{x}_{darr}] + \\
&\quad \sum_n g(p-2n)[\check{x}_{admm} + \check{x}_{adrm} + \check{x}_{admr} + \check{x}_{adrr}] + \\
&\quad \sum_n g(p-2n)[\check{x}_{ddmm} + \check{x}_{ddrm} + \check{x}_{ddmr} + \check{x}_{ddrr}] \\
&= [\check{x}_{aamm} + \check{x}_{aarm} + \check{x}_{aamr} + \check{x}_{aarr}] + \\
&\quad [\check{x}_{dammm} + \check{x}_{darm} + \check{x}_{damr} + \check{x}_{darr}] + \\
&\quad [\check{x}_{admm} + \check{x}_{adrm} + \check{x}_{admr} + \check{x}_{adrr}] + \\
&\quad [\check{x}_{ddmm} + \check{x}_{ddrm} + \check{x}_{ddmr} + \check{x}_{ddrr}]
\end{aligned} \tag{3-24}$$

where the check sign  $\check{\cdot}$  and double check sign  $\check{\check{\cdot}}$  represent the second level reconstructed signal and first level reconstructed signal, respectively. The linearity of the morphological operator does not affect the perfect reconstruction of this process because it merely divides a signal into two groups.

Equation (3-24) shows the reconstruction from the classified coefficients. The morphological filters are considered as the classification operators which separate the decomposed coefficients into two different sub-coefficients at each levels. The

reconstructed signal can be regrouped by its morphological characteristics to reach the final separation by the nonlinear morphology classification method.

$$\begin{aligned}
x[p] &= \{\check{\check{x}}_{aamm} + \check{\check{x}}_{damm} + \check{\check{d}}_{admm} + \check{\check{x}}_{ddmm}\} + \\
&\quad \{\check{\check{x}}_{aarm} + \check{\check{x}}_{aamr} + \check{\check{x}}_{aarr} + \check{\check{x}}_{darm} + \check{\check{x}}_{damr} + \check{\check{x}}_{darr} + \\
&\quad \check{\check{x}}_{adrm} + \check{\check{x}}_{admr} + \check{\check{x}}_{adrr} + \check{\check{x}}_{ddrm} + \check{\check{x}}_{ddmr} + \check{\check{x}}_{ddrr}\} \\
&= x_{background} + x_{transient}
\end{aligned} \tag{3-25}$$

Equation (3-25) shows that the signal  $x$  is separated into two components: one is the background activity which is filtered by the morphological filter. The other is the transient phenomenon which is the residue between the morphological filtered signal and the original signal. The background activity has been smoothed by the morphological filter and the remaining contains sharp signal. The morphological filter classifies the input signal by its morphological characteristics at different scaling coefficient sets. After the classification, a portion of a signal has the same morphological properties with respect to a priori known structuring element. The similarly classified signals all put together to form a bigger signal. For the second level decomposition and classification, the signal  $\check{\check{x}}_{aamm}$ ,  $\check{\check{x}}_{damm}$ ,  $\check{\check{d}}_{admm}$  and  $\check{\check{x}}_{ddmm}$  all have similar morphological shape but different sharpness; the rest of the signal sets belongs to the residues. This proposed method separates an input signal  $z$  into two components  $x$  and  $y$  by their morphology properties. It has been shown that a linear wavelet transform with a morphological classification method can separate a signal into two different components, which are background activity and transient signal.

### 3.2.3 Synthetic Spike Signal Using Morphological Wavelet Packet Transform

A signal  $z$ , shown at Fig. 3.7, containing both background activity and a sharp transient, is used to demonstrate this signal separation process. The structuring element disc, with its radius equal to one, is used for the morphological operations to detect the geometrical differences of two components.

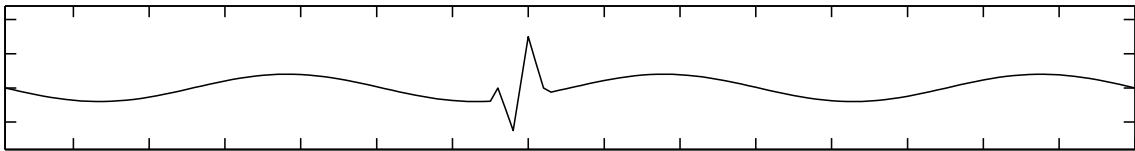


**Figure 3.7** A synthetic signal composes with a background activity and spiky transient pattern. In the middle region, the sharp peaked pattern is embedded in the smooth background activity (the rest areas).

The first level of wavelet packet transformation decomposes the simulated signal  $z$  into two coefficient blocks: one is the approximation coefficient and the other is detail coefficient. Applying the morphological filter (eq. 2-9) to these coefficient sets with a circular structuring element, each coefficient is classified into two subgroups. Fig. 3.8 shows the simulated signal and the two first level decomposition coefficients. The thick line is indicated as  $x_{am}$  and  $x_{dm}$  which are the morphological filtered result. The residue  $x_{ar}$  is the differences between approximation coefficients  $x_a$  and the classified signal  $x_{am}$ ; the residue  $x_{dr}$  is the differences between  $x_d$  and  $x_{dm}$ . The  $x_{am}$  and  $x_{dm}$  represent the smoothed part of the input signal, where the  $x_{ar}$  and  $x_{dr}$  are the “spiky” part of the signal. Morphological filter works as a classification process to separate a set into two groups. To this point, we have successfully divided a signal on its reduced scaling into two subsets by their geometrical shape. The subsets  $x_{am}$  and  $x_{dm}$  are reconstructed back into their original scale. The  $x_{ar}$  and  $x_{dr}$  are reconstructed into their original scale. The reconstructed signal is equal to the original signal.

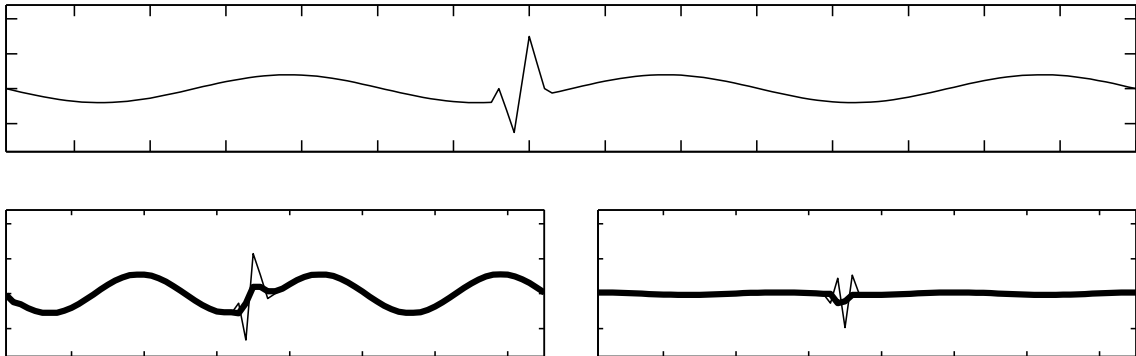


**Figure 3.8** [top] The input signal. [bottom, left] The thin line is the approximated coefficients and the thick line is  $x_{am}$ , [bottom, right] The thin line is the detail coefficients and the thick line is  $x_{dm}$ . Note that the difference between  $x_a$  and  $x_{am}$  is the residue  $x_{ar}$ , while the difference between  $x_d$  and  $x_{dm}$  is  $x_{dr}$ .

Fig. 3.9 shows the reconstruction of the original signal from the two classified sets. The top of the figure is the demonstration signal. The middle is the reconstruction from  $x_{am}$  and  $x_{dm}$ , indicating the background activity. The bottom is the reconstruction result of  $x_{ar}$  and  $x_{dr}$  which is the transient component. It can be clearly seen that the separated background activity is a smoothed signal with some distortions at the range of the spike. The transient contains the sharp spike. Visual inspection shows that the morphological filter applied on decomposed coefficients can be used to separate the demonstration signal into two different components. However, there are still some rough shape variations in the middle of background activity. There are due to the structuring element not being big enough to completely cover the sharp signal. The separation of the “sharp” transient can be improved by decomposing first level coefficients into second level coefficients by repeating this process.

Thus the classified sub-coefficients  $x_{am}$  and  $x_{ar}$  are decomposed into the second levels. The signal  $x_{dm}$  and  $x_{dr}$  are decomposed to the other sub-coefficients, too. Figure 3.10 shows that the effort of the second level decomposition with the wavelet

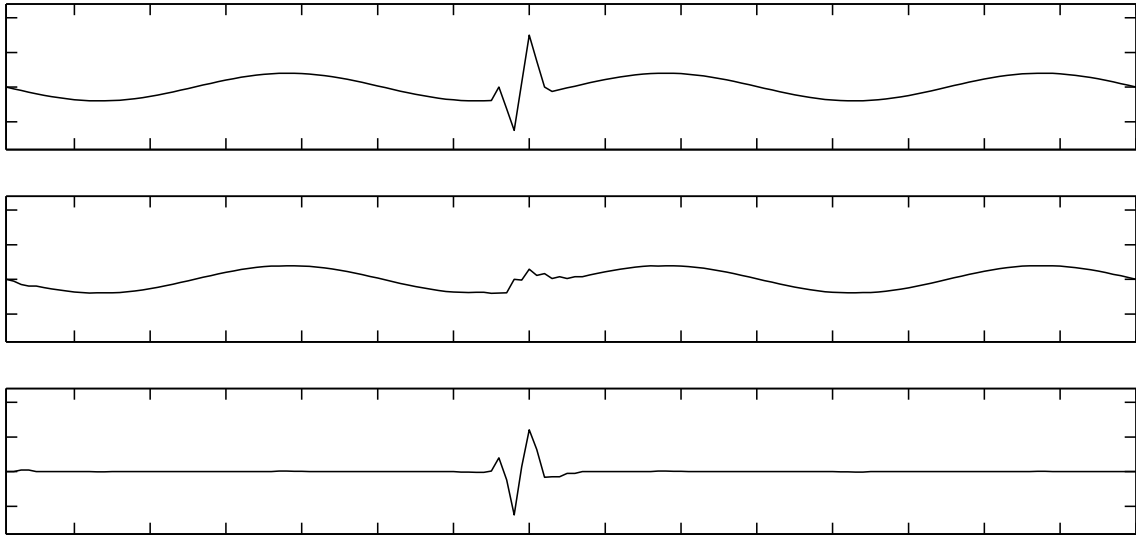


**Figure 3.9** [top] A demo signal, [middle] The background activity reconstructed from  $x_{am}$  and  $x_{dm}$ , [bottom] The transient reconstructed from  $x_{ar}$  and  $x_{dr}$ . The reconstructed background activity looks smoother except some ripples in the middle. The transient contains the sharp peak signal extracted from input data.

transform and the classification operations of the morphological filter. The top of this figure is the demonstration signal. The first level decomposition of the input signal is shown in the middle. The bottom figure shows the second level decomposition of the new signal  $x_{am}$  and  $x_{dm}$  from the first-level coefficients. The thick lines of the bottom of Figure 3.10 are  $x_{aamm}$ ,  $x_{dammm}$ ,  $x_{admm}$  and  $x_{ddmm}$  which are the decomposed coefficients classified by the morphological operation.

The reconstructed signal from the separated the second level classified coefficients  $x_{aamm}$ ,  $x_{dammm}$ ,  $x_{admm}$  and  $x_{ddmm}$  represents the final background activity. The differences between the original signal and separated background activity are the transients. The sum of the two separated components are equal to the original signal. Fig. 3.11 shows the final result of the morphology wavelet separation method. It can be clearly seen that the background activity is a smoothed and the transient is a sharp spike

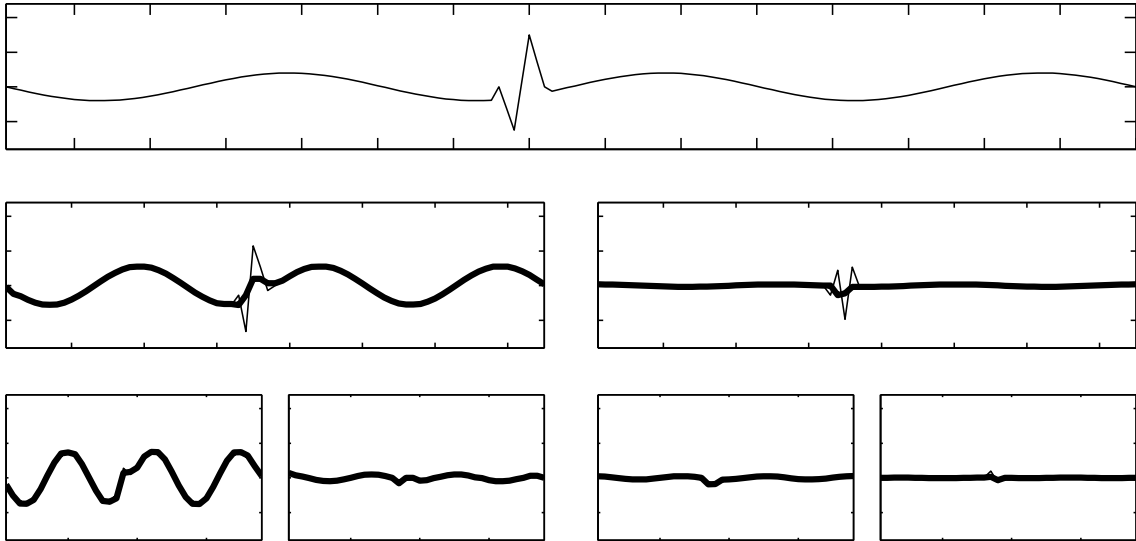


**Figure 3.10** The demonstrative signal [top] has been decomposed and classified by the proposed morphological filter to level two. [middle] First level wavelet packet decomposition coefficient and classified morphology subgroups. The thin line is the decomposed coefficient from the wavelet transform and the thick line is the filtered morphological coefficients  $x_{am}$  and  $x_{dm}$ . The  $x_{ar}$  and  $x_{dr}$  are the differences between  $x_{am}$  and  $x_{dm}$  and the decomposed coefficients. [bottom] The second level wavelet packet decomposition. It only shows that the second level decomposition of  $x_{am}$  and  $x_{dm}$  and the morphological classification of their decomposition coefficients.

located in the middle.

From the separation process using the demo signal, it is clearly shown that the developed separation method divides this synthetic signal into two components. We found that the reconstruction from the second level is necessary because the spiky signal can be best recognized by the structuring element at this level. The second level decomposition has reduced the scale into a quarter of the original scale. The peaked pattern is covered by the unit length structuring element. The structuring element has the best aspect to determine the morphological differences. It can be concluded that this signal must be processed on the level two of wavelet packet transform. If the separation using the second level transform does not give a satisfied separation result,

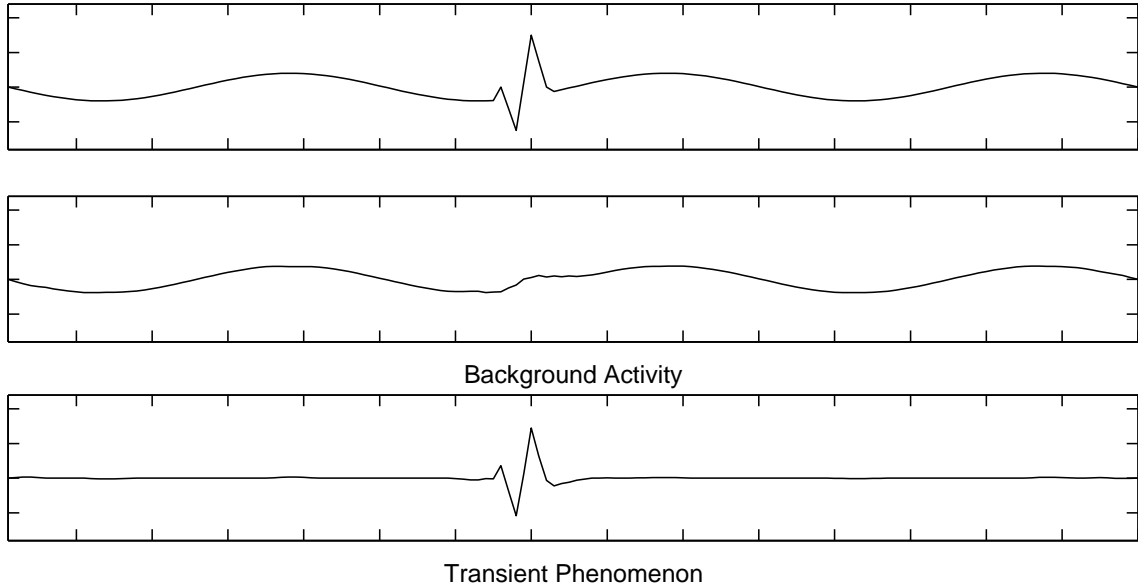


**Figure 3.11** [top] Demonstration signal; [middle] Separated Background Activity; [bottom] Transient Phenomenon. The background activity contains only smooth morphological characteristics and the transient is rough morphological shape. The small ripples, see Fig. 3.9, exist in the first level reconstruction have been eliminated on the second level reconstruction. The summation of two components is equal to the demo signal.

one can continuously decompose signal the  $n$ -th level until the optimized separation results have been reached.

The procedures of morphology wavelet classification method are summarized as follows:

1. Decompose an input signal  $x$  into two lower level coefficient sets by using the low-pass filter  $\bar{h}$  and high-pass filter  $\bar{g}$ . The two coefficient sets are the approximated coefficient  $x_a$  and detail coefficient  $x_d$ , where each one is a half of the scale of signal  $x$ .

$$x_a = \bar{h} * x, x_a \in V_1$$

$$x_d = \bar{g} * x, x_d \in W_1,$$

where symbol  $*$  denotes the discrete-time wavelet convolution and the  $V_1$  and  $W_1$  indicate the first-level spaces for two coefficient sets.

2. Apply the morphological classification filter,  $M_f^B$ , on both coefficients  $x_a$  and  $x_d$  and partition each of them into two groups:

$$\begin{aligned} M_f^B(x_a) &= x_{am} + x_{ar} \\ M_f^B(x_d) &= x_{dm} + x_{dr}, \end{aligned}$$

where  $\{x_{am}, x_{dm}\}$  are the sub-signals containing the smooth morphological shapes and  $\{x_{ar}, x_{dr}\}$  are the sub-signals containing rough variation.

3. Repeat the decomposition process (step 1) and morphological classification (step 2) until reaching level  $n$ .
4. Reconstruct the signal using the sub-signal having similar morphological characteristics. For example, if the final level is 2, then the reconstruct will be as follows: The first group of the smoothed coefficient is  $x_{aamm}, x_{damm}, x_{admm}$  and  $x_{ddmm}$ . The second group is the remaining subgroups which are the residues of the morphological classification. The reconstruction is equal to eq. (3-25).

### 3.3 A Separation Method Using Morphological Lifting Scheme

Heijmans and Goutsias (31) (37) have implemented a non-linear morphological wavelet transform by using the lifting scheme. Section 2.2.3 has introduced the basic concept of the morphological lifting scheme. A detail description to explain the separation of background and transient subsignal is included in this section. The “lifting scheme” is used to do the wavelet transform. The mechanism of the lifting

scheme keeps the multiresolution property of the wavelet transform and its structure is very flexible which makes the embedding of other linear and nonlinear operators into the lifting scheme easier. For example, the lifting scheme can include a non-linear rounding operator which makes all the coefficient integers (8). The mathematical descriptions and the numerical results of a demonstration signal using the lifting scheme will also be presented at this section.

### 3.3.1 Decomposition and Reconstruction Processes of the Morphological Lifting Scheme

The lifting scheme is an implemented method accomplishing multiresolution analysis similar to the wavelet transform, but its flexible structure extends its ability beyond the wavelet transform, i.e., allowing the mixing of nonlinear operator into the multiresolution transform. Heijmans and Goutsias proposed a morphology-based multiresolution analysis called max-lifting scheme (35) which maps the signal into nonlinear morphological spaces. Altering the max-lifting scheme, we proposed different morphological operators to build the three stage lifting scheme (see section 2.2.2). The procedures of these three stages are listed as follows:

1. The first stage is to split a signal into two groups by labeling the even and odd indexed sampling points of the signal.

$$(\text{even}_j, \text{odd}_j) = \text{Split}(x_{j+1}). \quad (3-26)$$

This split process is called the lazy wavelet which simply splits the signal into two small group according to the indices without any further operations.

2. Predict the odd indexed values by using the morphological erosion operator on the even indexed points and the odd indexed point in between two even points.

$$\begin{aligned} x_j(i) &= \text{P}(\text{even}_j(i), \text{odd}_j(i), \text{even}_j(i+1)) \\ &= (\text{even}_j(i), \text{odd}_j(i), \text{even}_j(i+1)) \ominus B \end{aligned} \quad (3-27)$$

where  $x_j$  represents lower level scaling coefficients,  $B$  is a pre-defined structuring element (circular disc), and  $\ominus$  denotes the morphological erosion operator. Unlike the max-lift scheme, the erosion operator uses both odd and even indexed data points. Thus, this process needs to remember the odd indexed points in order to perfectly reconstructed the signal. The reason for using both even and odd indexed points to support the morphological erosion operator is that the erosive operation detects the downward peaks and smooths them with the structuring element. In our case, the epileptic spike is a sharp signal with a peaked point. In order for the morphology operation to find this characteristic and separate it from the background activity, the centered peak information must be included to catch this particular morphological shape. The drawback of this process is that it requires an extra memory to record the values of the sequential odd points which are critical for the perfect reconstruction process.

3. Update the coefficients amplitude at the even indexed points by finding the differences between the coefficients of even indexed points and the the average of the two adjacent even scaling coefficients points.

$$\begin{aligned} \text{even}_j(i) &= \text{even}_j(i) - \mathbf{U}(x_j(i), x_j(i+1)) \\ &= \text{even}_j(i) - \frac{1}{2}(x_j(i) + x_j(i+1)). \end{aligned} \quad (3-28)$$

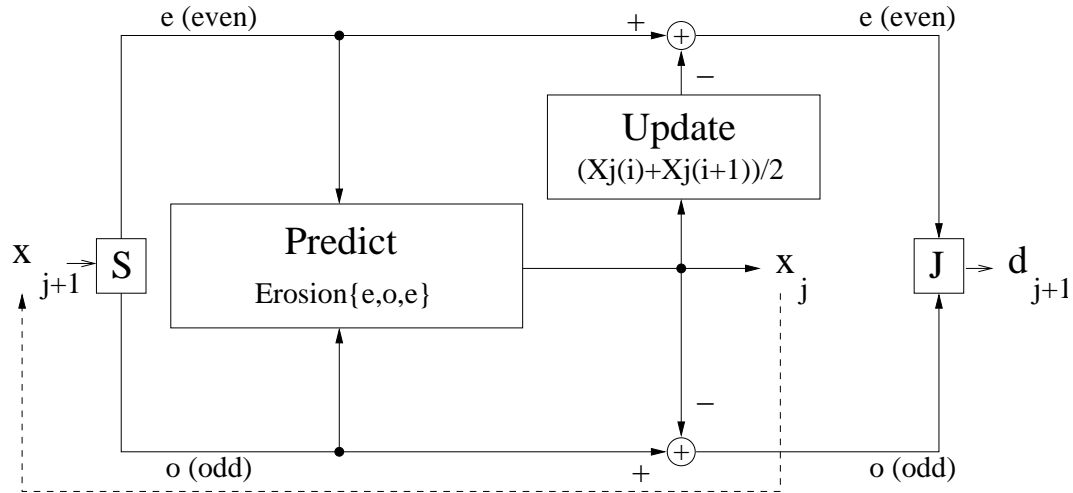


**Figure 3.12** Morphological Lifting Scheme: Decomposition. The  $x_j$  and  $d_j$  represent the lower level approximation and detail coefficients. The block contains “S” means the split process and “J” is the join process.

The detail coefficients,  $d_j$ , are defined as the joining of the updated even indexed (as eq. (3-28) and odd indexed point together:

$$d_j = \text{Join}(\text{odd}_j - x_j, \text{even}_j). \quad (3-29)$$

The points of the detail coefficient is still same as the higher coefficient  $x_{j+1}$ . This is because the non-linear morphological operation does not have inverse operation to reconstruct the signal. In order to perfectly reconstruct the original signal, the system needs to remember additional information. Additional memory space is required compared to the standard lifting scheme. The update procedure tries to correct the prediction errors in the detail coefficient. The average of two even points is a smoothing operation so that the difference of the centered even point is the sharp variation. If the neighboring points are a slowly varying signal, the differences will be small. If the region has a sharp amplitude change, the differences indicate that they belong to a “spiky” signal.

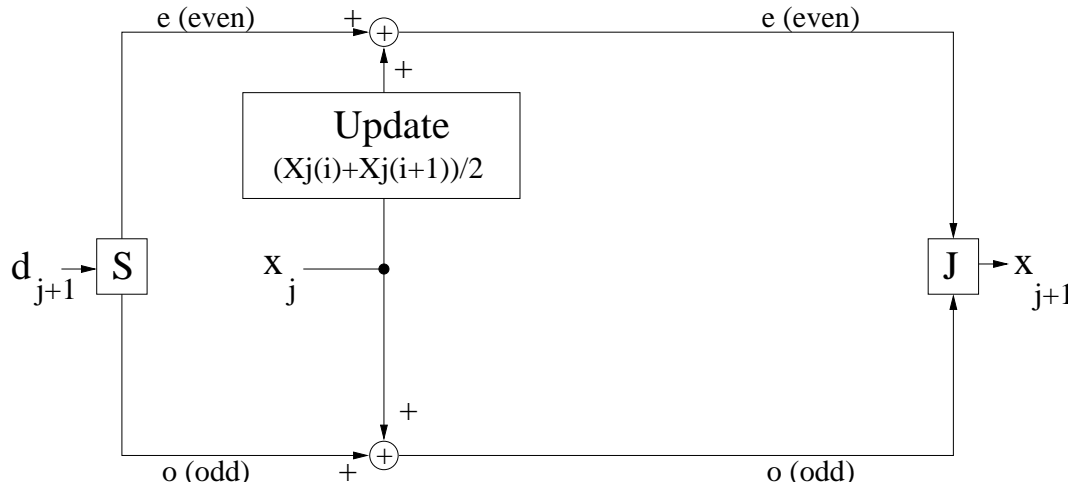


**Figure 3.13** Morphological Lifting Scheme: Reconstruction. The lower level coefficients  $x_j$  and  $d_j$  are perfectly reconstructed into the higher level coefficient  $x_{j+1}$ . The block containing a alphabet “S” is the split process, and “J” means join process.

Fig. 3.12 shows the schematic diagram of the decomposition process. The input signal  $x_{j+1}$  is the higher level coefficient set and  $j + 1$  indicates finer resolution. The decomposition produces the two coefficient set, where  $x_j$  is approximation coefficient set with coarser resolution and  $d_{j+1}$  is detail coefficient with the same resolution of  $x_{j+1}$ . The coefficient  $x_j$  can be further decomposed into next level, and so on.

The reconstruction of this morphological lifting scheme can be performed by changing the signs of update function with the scaling coefficients  $x_j$  and  $d_j$ , Figure 3.13. The decomposition subtracts the the average of even indexed points and the reconstruction simply adds the values back. The join function is to regroup the even and odd indexed points into a larger set  $x_{j+1}$  (the higher level coefficient set). The reconstruction process will perfectly recovered the original signal  $x_{j+1}$ . The reconstruction procedure does not require a prediction stage. This is because the decomposition procedure remembers the odd indexed points and the reconstruction procedure joins the previously recorded information to perfectly reconstruct the

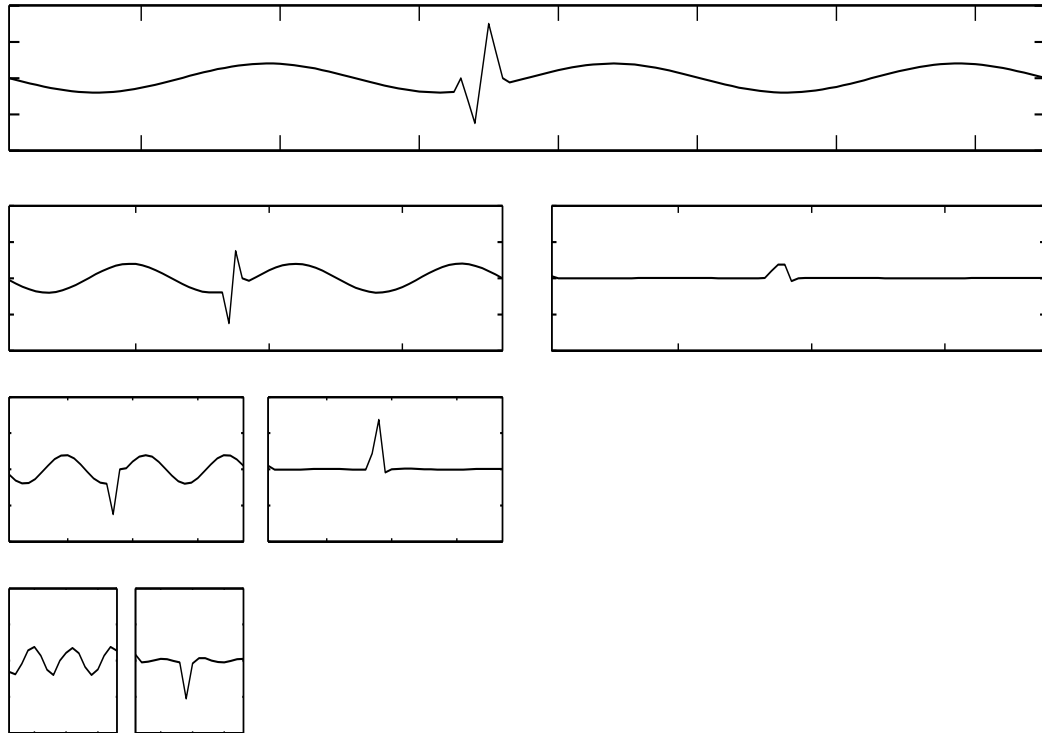


**Figure 3.14** Results of separation: background activity reconstructed from scaling coefficients  $x_3$  only and spiky transients from wavelet coefficients  $d_1, d_2$  and  $d_3$

signal.

### 3.3.2 Synthetic Spike Signal Using Morphological Lifting Scheme

This example demonstrates the representation of two components by the morphological lifting scheme. The demonstration signal is the same as in the morphology wavelet separation method in section 3.2.3 (see Fig. 3.7). Each level of decomposition creates two coefficient sets: one set is approximation coefficients and the other set is detail coefficients. The approximation coefficients are decomposed to the next level.

Fig. 3.14 shows three level decompositions of the demonstrative signal using the morphological lifting scheme. At the top of the figure is the original input signal. The

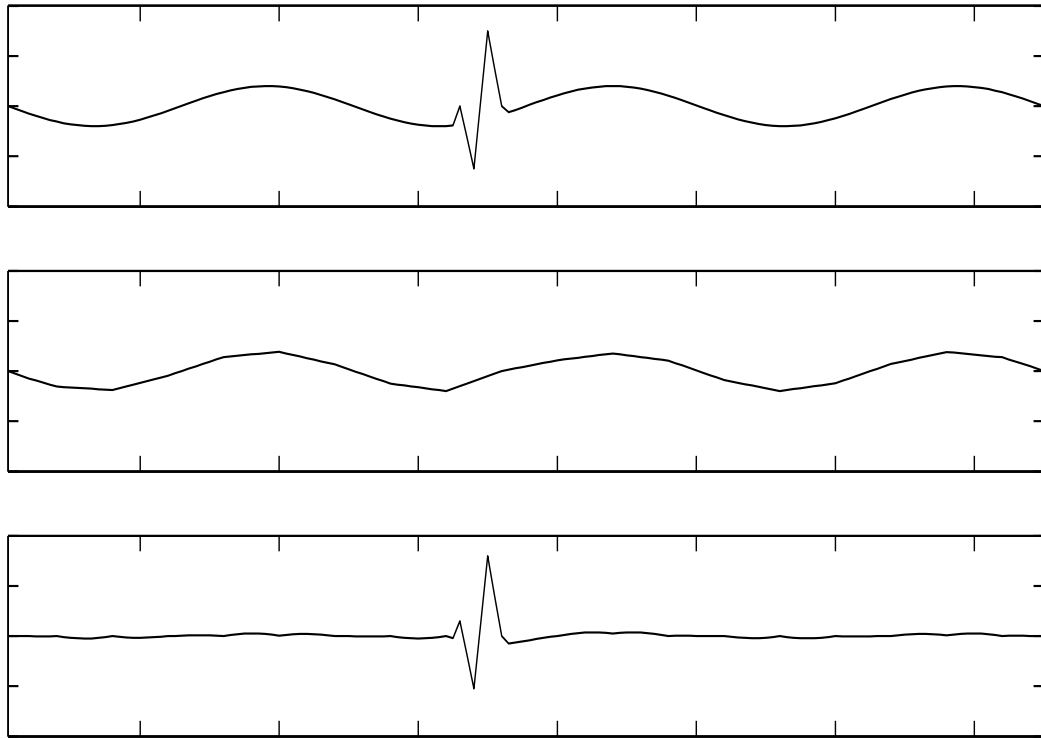


**Figure 3.15** Separation Result by Using Lifting Scheme [top] A Demo Signal [middle] Separated Background Activity [bottom] Transient Phenomenon

left and right sides of the second row are the first level decomposed approximation coefficient  $x_1$  and detail coefficient  $d_1$ . The third row contains the second level decomposed coefficient sets obtained from the coefficients  $x_1$ . The bottom row contains the level three coefficients derived from  $x_2$ . These coefficients were obtained by using split, prediction and update stages introduced in section 3.3.1.

Figure 3.15 shows the separation result. The top of this figure is the demonstration signal. The middle panel of Fig. 3.15 is the separated background activity which is the reconstruction from the approximation coefficient of the lowest level only. The bottom of figure is the transient which is reconstructed from all the detail coefficients. The sum of the two separated subsignals are equal to the input signal. It

can be clearly seen that the spiky signal has been extracted from the input signal. The background activity is a smooth signal without any sharp amplitude variation and “peaked” points. This demonstration illustrated that the proposed morphological lifting scheme can divide a signal into two components by differentiating their morphological characteristics.

## 4.0 EXPERIMENTAL RESULTS ON EEG/MEG DATA

The empirical results using both simulated data and real epileptic EEG/MEG data are provided in this section. The simulated EEG data, composed of two components background and transient activity, is first used to test the developed methods. The real EEG/MEG signal, collected from an epilepsy patient, is applied later. The epileptic EEG data is all assumed to have two components: one is the background activity and the other is “spiky” transient. The separated transient signal is then analyzed by using stochastic point analysis to indirectly verify these abnormal activities.

### 4.1 Experiment of Simulation Data

The simulated EEG data was manually generated and then applied by both the morphology wavelet separation method and the morphological lifting scheme method to test the performance of the separation. The simulated data is similar to real EEG signal.

#### 4.1.1 Results of Simulated Data Using Morphological Filtering in Wavelet Packet Transform

The simulated EEG data was generated to test the performances of the proposed separation methods. This simulated EEG data is trying to mimic the real epileptic EEG data composed two components: the background activity and the transient phenomenon. The transient part of this simulated EEG data is actually extracted from real EEG “spiky” data. We extracted several segments of spikes from real subdural epileptic EEG data (see appendix A). The simulated background activity is manually generated “by hand” with slow amplitude variations. The background and

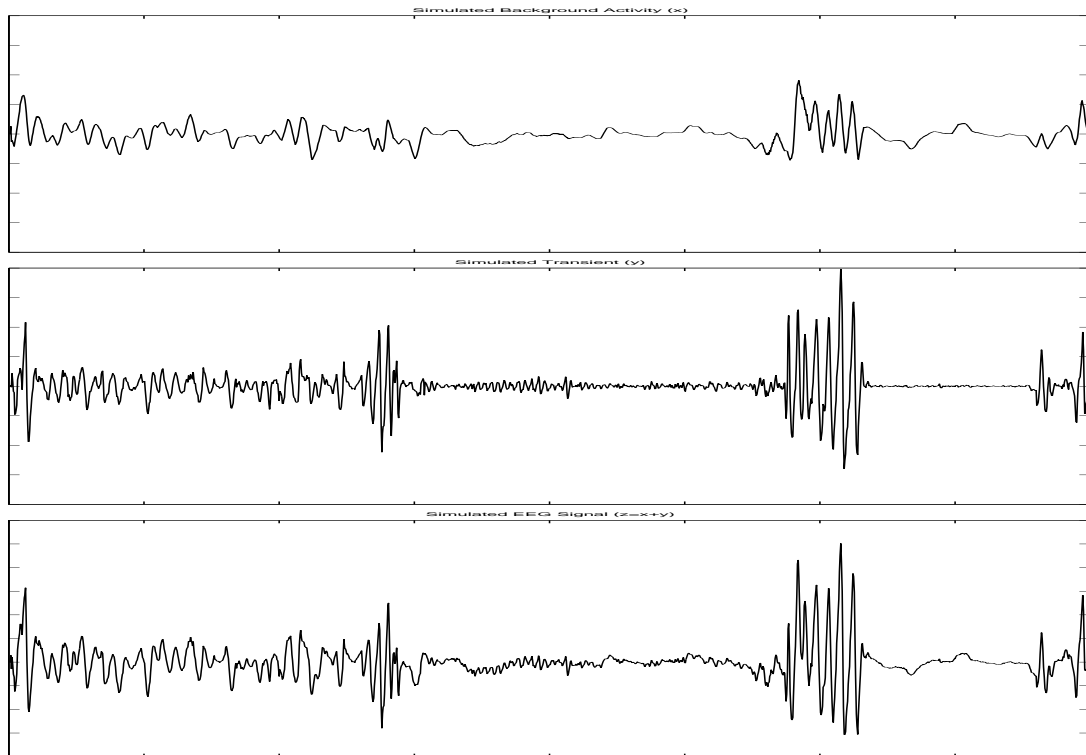


**Figure 4.1** [top] The simulated EEG background activity, [middle] The simulated EEG transient signal, [bottom] The simulated EEG data which is the summation of two simulated components. The simulated transient has rough shape variation than the background activity and these two signals are non-stationary with different morphology characteristics.

transient activities are assumed non-stationary. Fig. 4.1 shows the simulated EEG signal. The top and middle are the simulated background and “spiky” transients, respectively. The bottom is the simulated data which is the summation of the two simulated components.

Visual inspection the simulated EEG data, one can find the simulated transient signal looks sharp and its amplitude variation is faster than the imitative background activity. The sharp signals represents the abnormal activity which is widely seen in the EEG data when a seizures occurred. The shape of the background activity is smoother

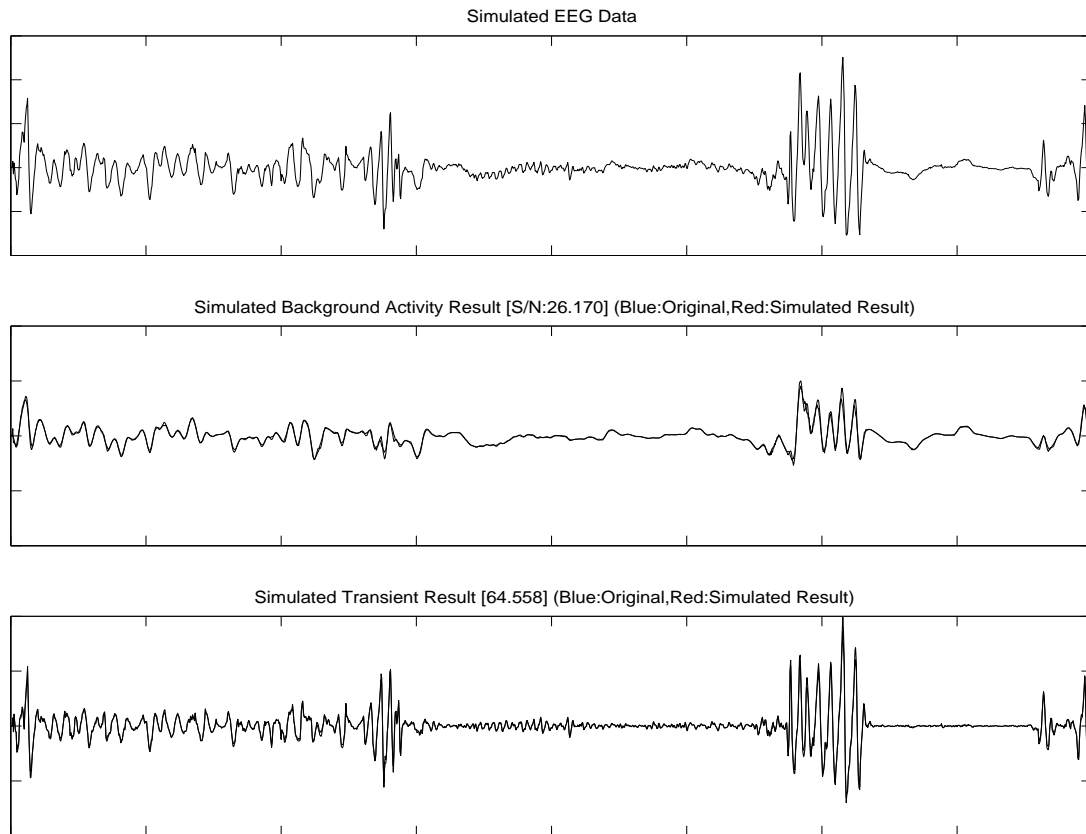


**Figure 4.2** A simulated EEG data is divided into two components by using the morphology wavelet thresholding method, where the top is the simulated EEG data, the middle shows the separated background activity and the bottom is the separated transient. The two separated components visually look very similar to the original simulated components in Fig. 4.1. The signal noise ratio (the higher is the better) is 26.17 and 64.56 for each components with respect to the original input signals.

than the transient signal. The morphological characteristics of two components are different to each other: one is smooth and other is rough.

The morphology wavelet separation method, see section 3.2, is applied to the simulated EEG data. The wavelet packet transform has decomposed the simulated signal at levels three. The decomposed coefficients of each level are classified into two components by using the morphological filter. The structuring element is set to a circular disc with radius equal to one. Fig. 4.2 shows the separated results. The top

panel of figure is the simulated EEG signal, the middle and bottom panels are the separated background activity and the transient signal, respectively. The separated components by using this method are similar to the original ones.

The numerical results demonstrate that the morphological filter is able to extract the transient signal from the background activity. In order to measure the performance, a signal-to-noise ratio (S/N) is provided to give the numerical comparisons. Let  $S$  be the simulated data and  $\hat{S}$  be the separated result. The S/N is defined as:

$$S/N = \frac{\sum |S|^2}{\sum |S - \hat{S}|^2}. \quad (4-1)$$

The higher value of the signal noise ratio, the better quality of the separated result is. The S/N ratio of this simulated background activity and the separated result is 26.17. The s/n ratio for simulated transient and the separated result is 64.56.

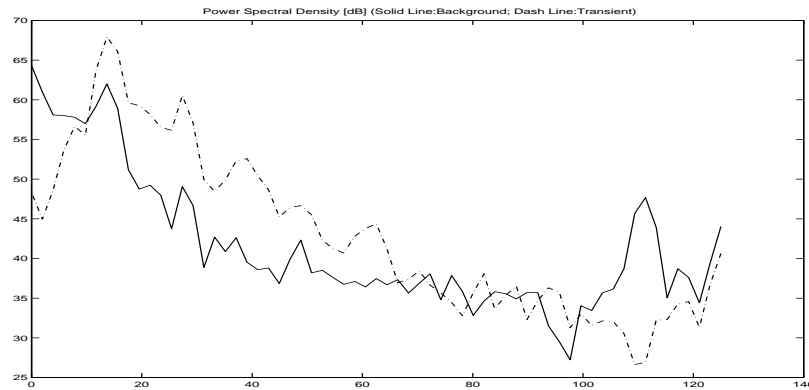


**Figure 4.3** Power spectrum (dB) of two simulated EEG background activity and transient. The solid line is the simulated background activity and dash line is the transient.

The spectral method is also used to divide the simulated signal into two components. The spectral method used the a cut-off filter to separate two subsignals. It has assumed that two components have different frequency ingredients. Fig. 4.3 shows the power spectrum of two components. The background activity shows that the

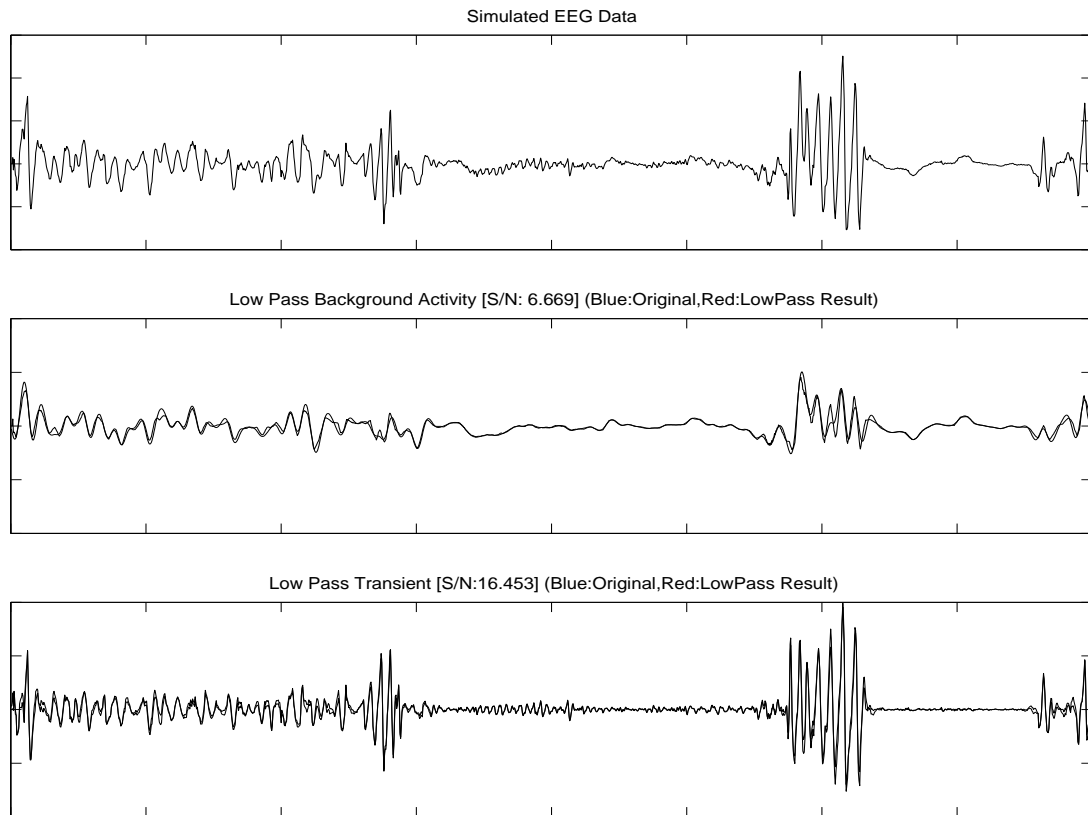


**Figure 4.4** The Separated Result of Simulated EEG Using Low Pass Filter

major energy is on the low frequency domain and the transient has high frequency ingredients. However, it can be seen that the two components have overlapped in the frequency domain. The frequency ingredients lower than the cut-off frequency is the background activity and the higher ones are belongs to transient signal. A low-pass filter has been applied to the simulated data. The cut-off frequency of this filter is set to 11 Hz, where two simulated signals are starting to divert. The results by using this low-pass filter is shown on Fig. 4.4. The S/N ratio of background activity using low-pass filter is 6.67 and is 16.17 for transient signal. The numbers show that the the morphology wavelet separation method has a better performance than the cut-off method.

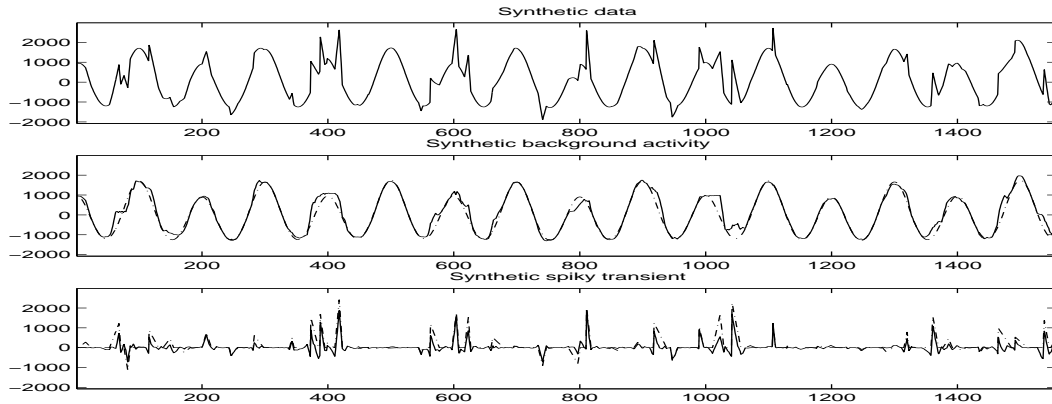


**Figure 4.5** The experimental result of synthetic data using morphological filtering of the wavelet packet transform is shown in this figure. The top panel is the synthetic signal, the middle panel is background activity, where the dash-dot line is original form and solid line is the separated component. The bottom panel is spiky transient, where the dash-dot line the original one and solid line is separated result.

Another experiments using different synthetic signal have been performed to compare the results between the morphological filtering method with other approaches. The synthetic signal contains the background activity ( $x$ ) and transient ( $y$ ). The summation of  $x$  and  $y$  will be the simulated data. Two different approaches are used to separate the spiky transient signal from the background signal. The first one is using a median filtering to separate a input signal into two components and the second one is using developed morphological filter but not using wavelet transform to change signal scale. The second approach is to decimate the input signal into its half resolution, which the morphological filter is applied to these decimated coefficient. The filtered result is decimated and the morphological filter is applied again until reaching levels three. The reconstruction is repeatedly interpolating the last level results by two by two until the signal has been reconstructed into original scale. The median method is using a one-dimensional median filter with its length equal to 17 points, which are the maximum duration of a spiky transient.

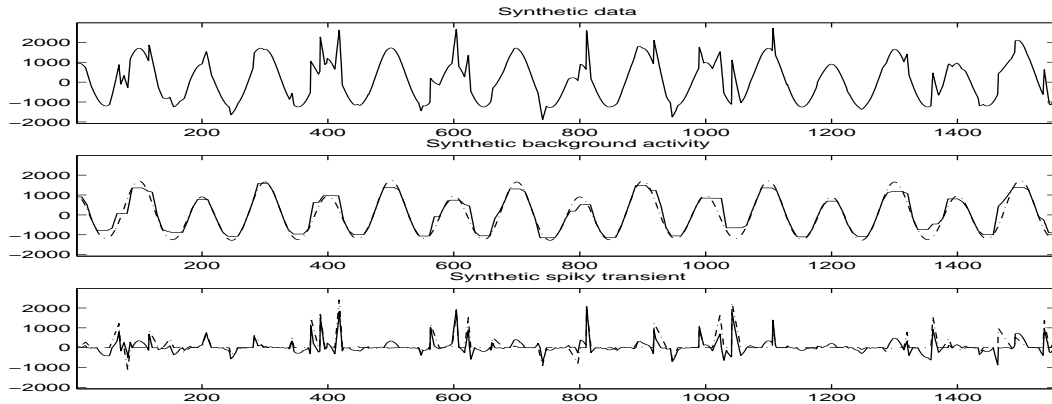


**Figure 4.6** The experimental result of synthetic data using morphological filter applied on down-sampled signal (without using wavelet transform to do multiresolution decomposition) is shown in this figure. The top panel is the synthetic signal, the middle panel is background activity, where the dash-dot line is original form and solid line is the separated component. The bottom panel is spiky transient, where the dash-dot line the original one and solid line is separated result.

The synthetic transient signals are generated by randomly selecting the duration of spikes between 5 points to 17 points. The amplitudes of the peak points are randomly set between -2048 to 2048 and can be located at any points inside the duration of these spikes (between 5 to 17 points). Each trail has generated 50 spikes to test the performance for each method. The background activity is a composition from four sinusoidal waves with different frequencies. These frequency are selected as 5 Hz, 2.5 Hz, 1.25 Hz and 0.5 Hz. The scalar amplitude for each sinusoidal signal are randomly selected between the -1024 and 1024, where the strength of 2.5 Hz is set slightly larger than other frequency components. The synthetic signal is the summation of these two randomly generated components. These two methods have divided the synthetic signal into two components: one is background activity ( $x'$ ) and the other is spiky transient ( $y'$ ). To compare the results, a signal-to-noise ratio for

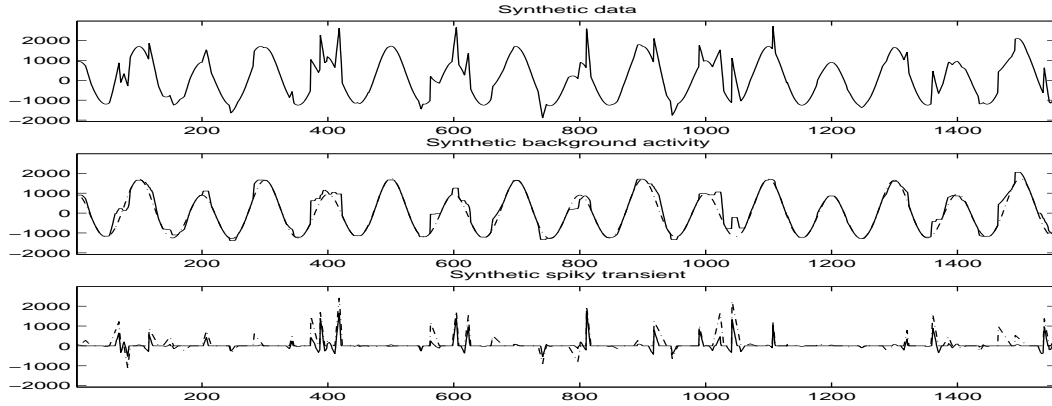


**Figure 4.7** The experimental result of synthetic data using a one dimensional median filter with support length 17 points is shown in this figure. The top panel is the synthetic signal, the middle panel is background activity, where the dash-dot line is original form and solid line is the separated component. The bottom panel is spiky transient, where the dash-dot line the original one and solid line is separated result.

both synthetic background and transients are defined as follows:

$$SN_x = \frac{\sum x^2}{\sum (x - x')^2} \quad (4-2)$$

$$SN_y = \frac{\sum y^2}{\sum (y - y')^2} \quad (4-3)$$

The larger number of the signal-to-noise ratio, the better separation results are given.

Figure 4.5 shows a synthetic data is separated into two components by using the developed morphological filtering with wavelet packet transform. The top is the synthetic data composed with spiky transient and background activity. The middle panel of same figure shows the original background activity (as the dash-dot line) and the separated background (solid line). On the bottom panel, the separated transient (shown as solid line) and the original one are shown here.

Figure 4.6 and 4.7 are the the separation results using the down-sampling and median filter, respectively. The top panels of these figures are the synthetic data composed with spiky transient and background activity. The middle panels show

**Table 4.1** The Signal-to-Noise Ratio of Synthetic Transient Data for a Single Trial

Morphological Filter on Wavelet Transform Method	2.7208
Morphological Filter on Decimated Data	2.2097
Median Filter	2.2424

**Table 4.2** The Signal-to-Noise Ratio of Synthetic Background Data for a Single Trial

Morphological Filter on Wavelet Transform Method	18.2335
Morphological Filter on Decimated Data	14.8086
Median Filter	15.0272

the original background activity (as the dash-dot line) and the separated background (solid line). The original transient (dash-dot line) and separated transient (solid line). The table 4.1 and 4.2 are the numerical result of the signal-to-noise ratio using this synthetic data shown in the figure. For the background activity, the morphology wavelet separation method scores 2.72, the decimation method is 2.20 and the median separation method is 2.24. As the results of of the spiky transients, the first method scores 18.23, the second is 14.80 and the last is 15.02. Our developed method has a better separation result than using other approaches.

Similar experiments have been performed 500 times and the average results of the signal-to-noise ratio are listed on table 4.3 and 4.4. These average numbers show similar performance as the single trial.

**Table 4.3** The Average Signal-to-Noise Ratio of 500 Trials for Synthetic Transient Data

Morphological Filter on Wavelet Transform Method	2.7118
Morphological Filter on Decimated Data	2.6687
Median Filter	2.1113

**Table 4.4** The Average Signal-to-Noise Ratio of 500 Trials for Synthetic Background Data

Morphological Filter on Wavelet Transform Method	16.3575
Morphological Filter on Decimated Data	13.8351
Median Filter	13.2639

#### 4.1.2 Results of Simulated Data Using Morphological Lifting Scheme

The morphological lifting scheme, see section 3.3, is applied to same simulated EEG data to divide the input signal into two components. The simulated data has been decomposed at levels three and each level created two coefficient sets. One set is belonging to the background activity, which has slower amplitude variations, and the other is the spiky transient containing rough shape and fast amplitude variation. This methods judges the morphological characteristics to separate two components. The separation results are shown in Fig. 4.8. Top is the simulated EEG data, middle and bottom of same Figure are the separated background activity and transients. In visual inspection, the separated spiky transient has fast amplitude variation and contains a lot sharp peaked spiky pattern. The background activity has slow amplitude changes, but it contains some small sharp peaked patterns. It is because that the morphological erosive operator operates only covers three sampling points (center and two adjacent points) and the update procedure may need more sampling points in order to give a better estimation to smooth these peaks. The results show that the morphological lifting method is capable of separating these transient signals from the simulated signal.

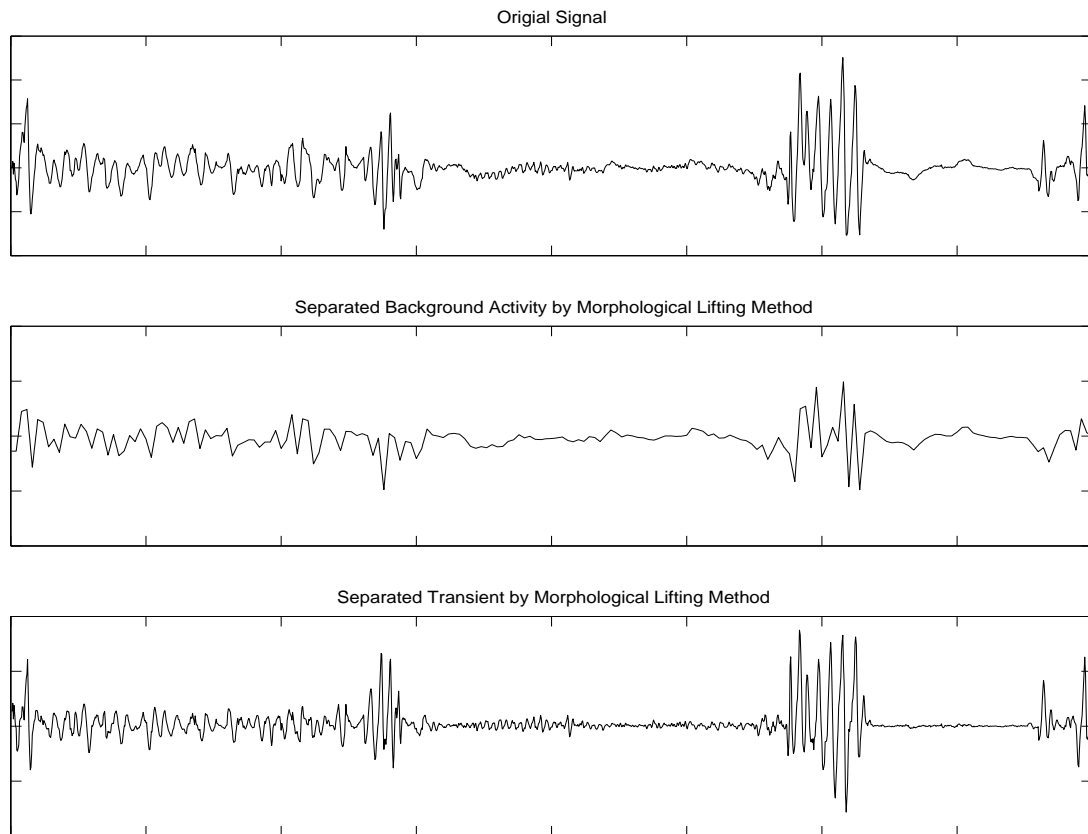


**Figure 4.8** [top] The simulated data [middle] The separated background activity by using morphological lifting method [bottom] The separated transient by using morphological lifting method

## 4.2 Separation Results Using Real EEG Data

After the experiments of using simulated EEG data for both morphology wavelet separation method and the morphological lifting scheme modeling, the real EEG data were tested in this section. The real EEG data used is a subdural EEG collected from an epilepsy patient and a segment of EEG data containing real epileptic spikes.

#### 4.2.1 Results of Real EEG Data Using Morphological Filter in Wavelet Packet Transform

A segment of a subdural EEG data from a young epilepsy patient, has been divided into two components by using the developed morphology wavelet separation method. This segment EEG data contains 2000 samples (8 second data with the sampling rate 250 Hz). The input signal has been decomposed on levels three by using biorthogonal wavelet. The biorthogonal wavelet filter is a FIR filter with compact support, where this filter is symmetry and can perfectly reconstructs the original signal back. Each decomposed coefficient is classified by a morphological filter. The filtered result is the smoothed subcomponents and the residues have fast amplitude variations. Each filtered signals are repeatedly decomposed by the wavelet transform and classified into another two subcomponents. The detail algorithm has been discussed on section 3.2.

The stopping level is depended on the durations of the target signal and has been set to three in this experiment. It is because the span of a spike is about 5 to 17 sampling points and the levels three decomposition reduce the signal scale of one-eighth of its of original one. At level three, the structuring element (a disc with its radius equal to one) will cover the span of a reduced spike. Figure 4.9 shows that the subdural EEG signal has been decomposed at level three by the biorthogonal wavelet transform. The decomposed coefficient is separated into two smaller subcomponents by using developed morphological filter (see eq. 2-9). This morphological process divides the decomposed coefficient sets into two categorized signals by judging their morphological features. One category contains smooth shape signal and the other is rough variation pattern. However, the integrity of these divided signals is not affected by the nonlinear morphological process. The summation of these two classified signals is the same as the original one. These classified coefficient sets are regroup by their

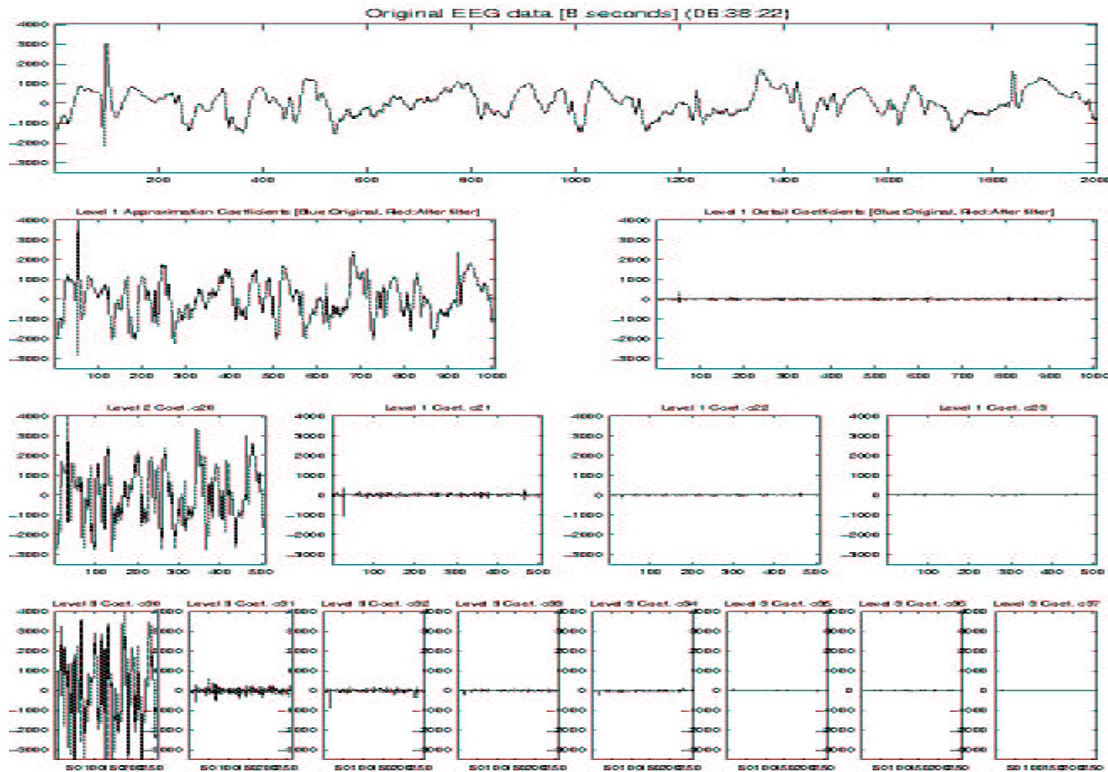


**Figure 4.9** The three level decomposition of the wavelet packet transform. Top is the input Subdural EEG data and the following are the decomposed coefficient sets. Each coefficient set is divided by a morphological classification filter.

category and reconstructed by the inverse wavelet transform. The reconstructed signal will be the final background activity and “spiky” transients.

Figure 4.10 shows the two separated components. Top panel of this figure is the subdural EEG data. The middle is background activity, where its shape looks smoother than the original EEG data. Most of the sharp peaks are eliminated. Small ripples and overshots can be seen on some areas where the large spikes originally locates in there. The bottom panel is the separated transient. The shape of the transient looks rough with fast amplitude variation. It can be seen that the locations of these spiky patterns are consistent with its original positions. It suggested that the non-linear morphological filter does not have the phase shifting of this input signal.

The two separated components are equal to the original EEG signal. The morphology wavelet separation method is a classification process which separates a signal into two subcomponents using their morphological characteristics.

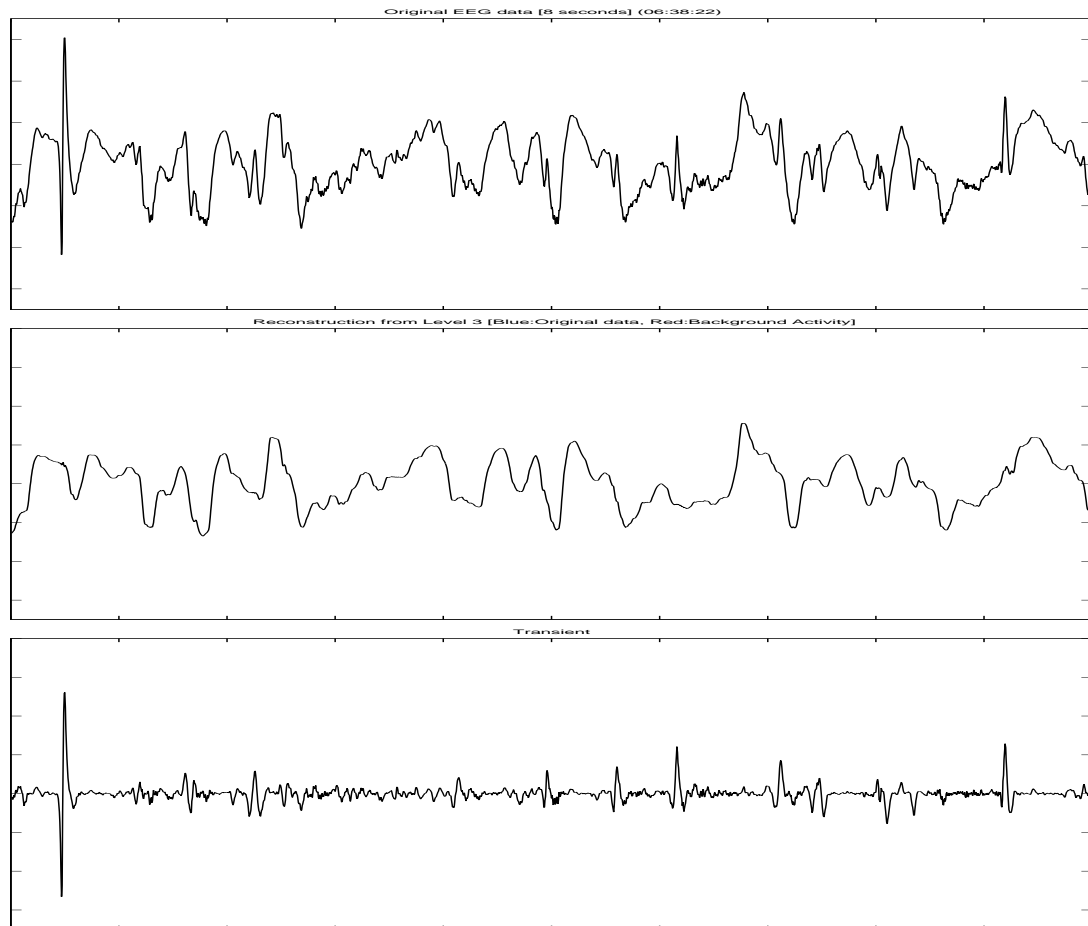


**Figure 4.10** [top] The subdural EEG data [middle] The separated background activity [bottom] The separated transient phenomenon. The EEG data is decomposed and classified by the proposed morphology wavelet thresholding method. Each classified group signals are reconstructed into two components. The separated background activity looks smoother than the original EEG. The extracted transient signal contains the spiky pattern, small artifacts. The summation of two components are equal to original signal.

### 4.2.2 Results of Real EEG Data Using Morphological Lifting Scheme

An epileptic EEG data is separated into two components by using morphological lifting scheme method. The three stages of this method are split, predict and update stages have been introduced in section 3.3. The input data is decomposed into several coefficient sets. Figure 4.11 shows the decomposed coefficient sets generated from the morphological lifting scheme. Top panel of this figure is the subdural EEG data which is the same as one used in morphological filter in the wavelet packet transform. The middle panel is the first level decomposed coefficient sets: approximation coefficient and detail coefficient. The approximation coefficients are further decomposed to the next scale level to generate another two coefficient sets, shown on third row of this figure. The decomposition has stopped at levels three, shown on the bottom of Fig. 4.11.

These decomposed coefficient are reconstructed back into its original domain. The approximation coefficient at levels three are recovered as the background activity. The three detail coefficient sets are formed to be the transient phenomenon. Figure 4.12 shows the two separated components from a EEG data. Top of figure is the EEG signal. The middle is the background activity which is reconstructed from the approximation coefficient of levels three. The bottom is the “spiky” transient reconstructed from all three detail coefficient sets. The background activity visually looks smooth, but containing some peak points. It is because that the short supports of the predict and update filters are lacking the information of neighboring points, which can provide more information to smooth these peaks. The spiky transients have rough shape. The summation of these two separated components are equal to the original EEG signal.

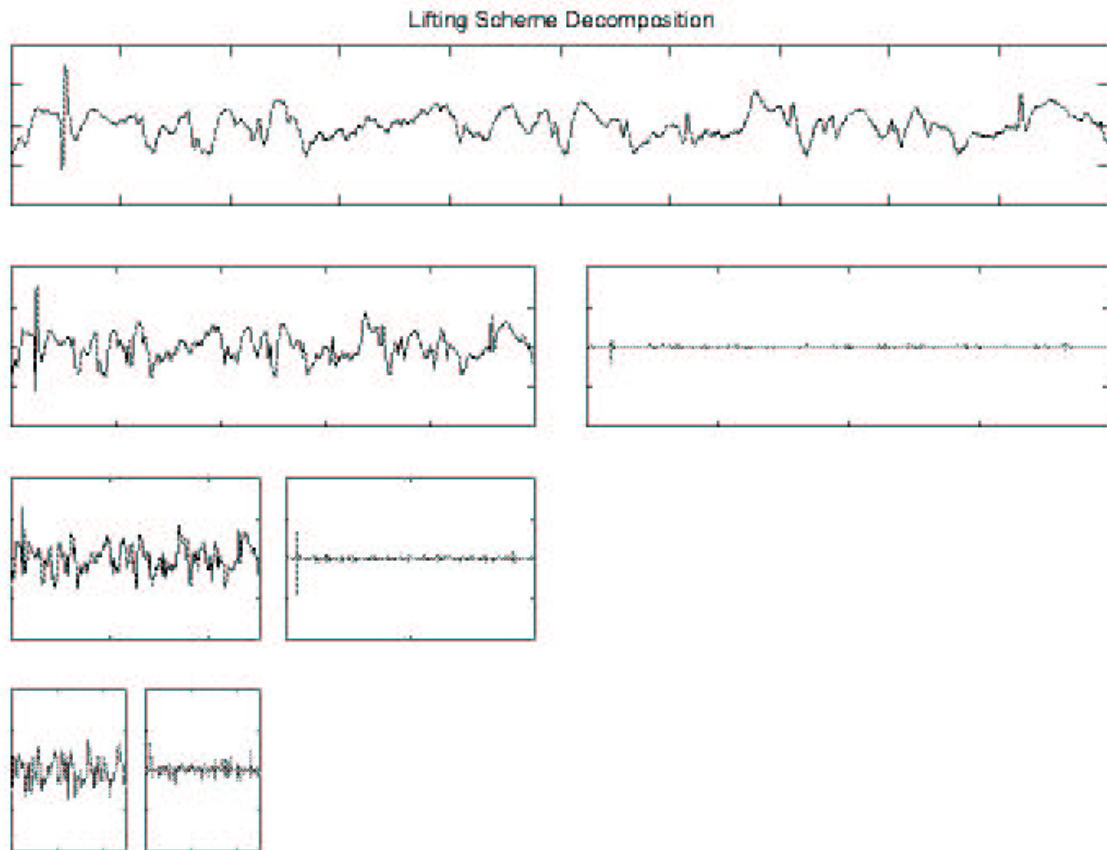


**Figure 4.11** Three levels Decomposition of a subdural EEG data using morphological lifting scheme. The top is the original subdural EEG data. The following rows are the decomposed approximation and detail coefficients for the first to third levels. The approximation coefficient of level three are reconstructed into the background activity. The detail coefficient of all three levels are reformed into the transient pattern.

### 4.3 Results of Spike Train Analysis

The epileptic spikes are important information for the epilepsy diagnose. In this section, it has investigated three different EEG data sets: subdural EEG, scalp EEG and MEG. The spiky signal is first extracted from the EEG/MEG data and these abnormal activities are further analyzed by spike train analysis.

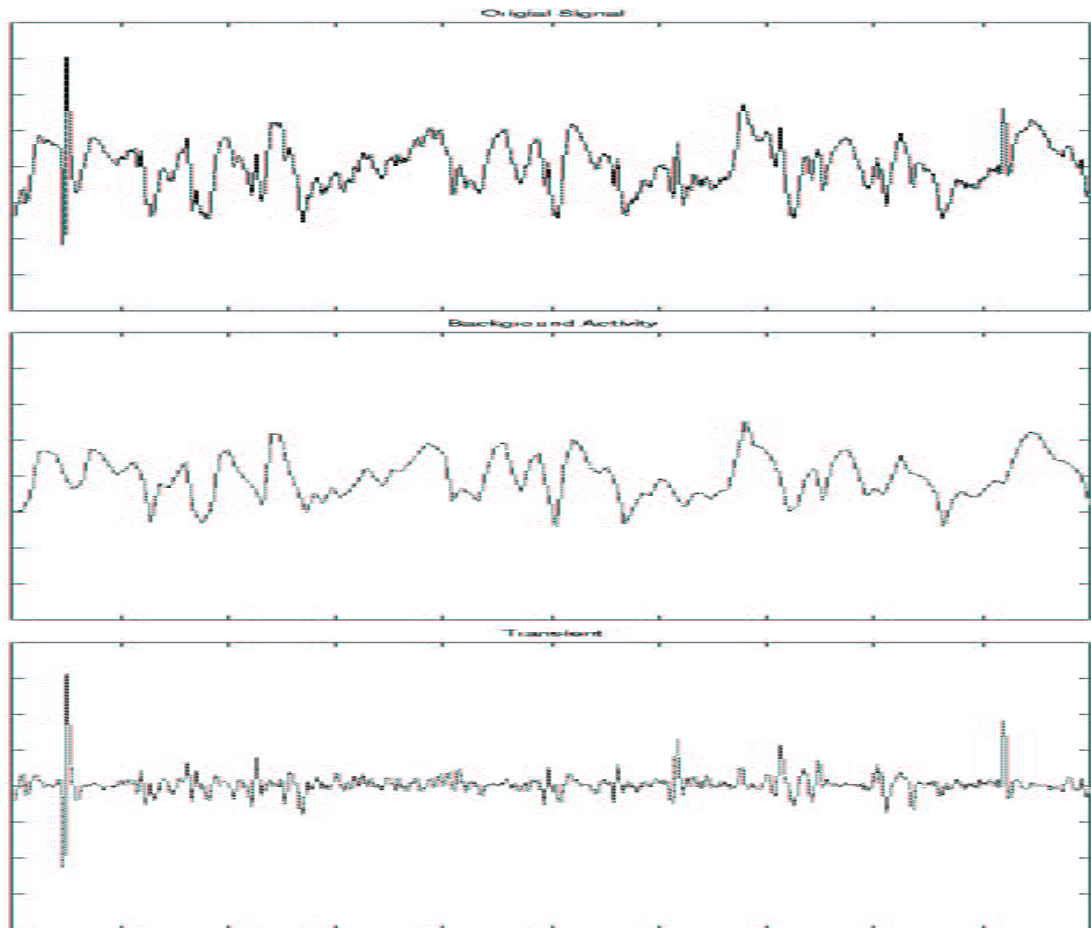


**Figure 4.12** A result of using real EEG data using morphological lifting transform: [top] A EEG data [middle] Separated background activity [bottom] separated transient phenomenon

#### 4.3.1 Spike Train Analysis Using Subdural EEG Data

The first data is a subdural EEG. This subdural EEG described in appendix A, is recorded at Children hospital, University of Pittsburgh, Pittsburgh, PA. This data has used 102 electrodes to collect the information from the brain. The epileptic spikes are commonly being seen in this EEG data. The developed method using morphological filter in wavelet packet transform has extracted these spikes from the background EEG. Their statistical relationships was derived by using the A stochastic

point process, introduced in section 2.3, is used to analyze the correlation of the spikes (events) between two electrodes.

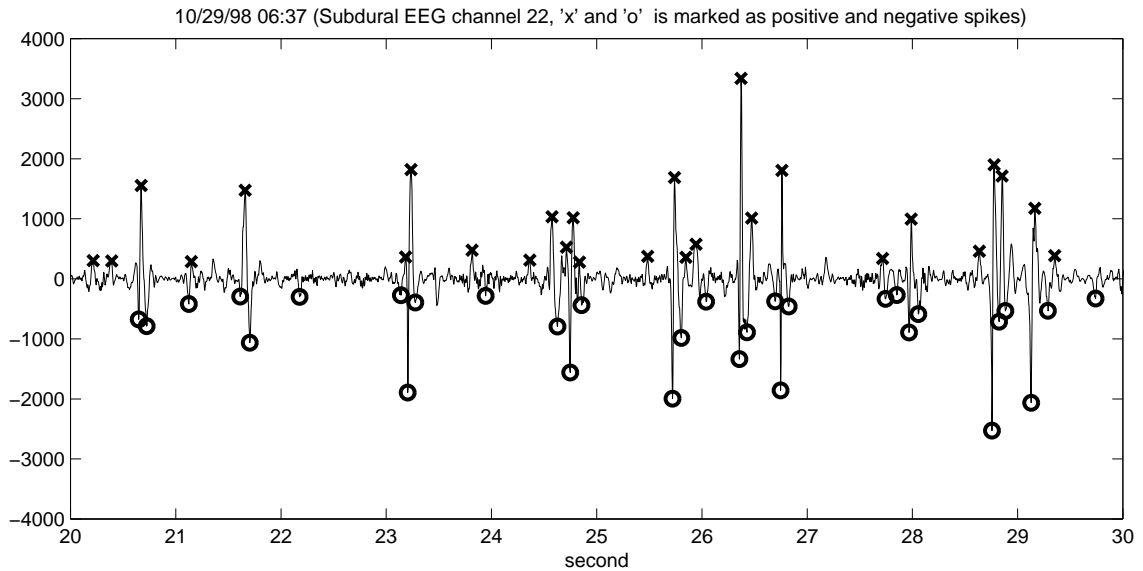


**Figure 4.13** The epileptic spikes are marked for representing the incidents of brain activities. The 'x' indicates the positive amplitude spikes and 'o' as the negative amplitude spikes. The absolute amplitude of selected peaks are larger than 300.

The first step of the spike train analysis is to find the timing informations of spiky transients. The peak of a triangular spike is used to represent the appearing time of this spike. Meanwhile, these spiky patterns can be classified into two types. One has positive peaks and the other has negative peaks. In some cases, the neurologists are mainly concentrated in negative spikes only. These spikes can also be classified by the amplitude at the peaked point. The larger amplitude spikes are easily recognized by the human eyes; but smaller spikes still reflect the functionality of the brain. The spikes with different amplitudes can be analyzed independently to represent the various status of the brain activities. Fig. 4.13 demonstrates a series of spiky transients after the separation using morphology wavelet thresholding algorithm. These spikes are divided into two groups: the 'x' marker represents the positive amplitude and 'o'

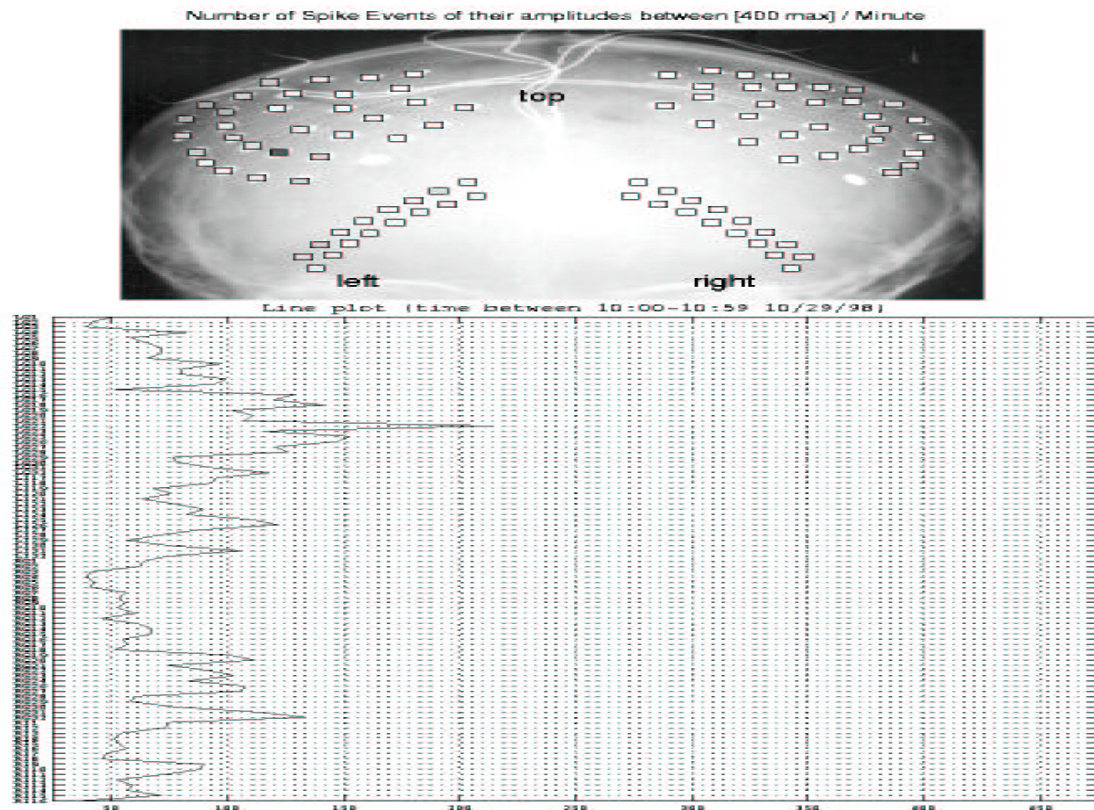


**Figure 4.14** The average number of spikes with amplitude between [400 maximum amplitude] appearing in each electrodes. Bottom of figure is the line plot which horizontal axis is average number of spikes appearing in one minute and vertical is the electrode name. Top of figure is the spatial head plot, each square box represents an electrode and its color are plotted according the average number of spike appearance. The darker of color represents the higher number, the lighter is the lower number.

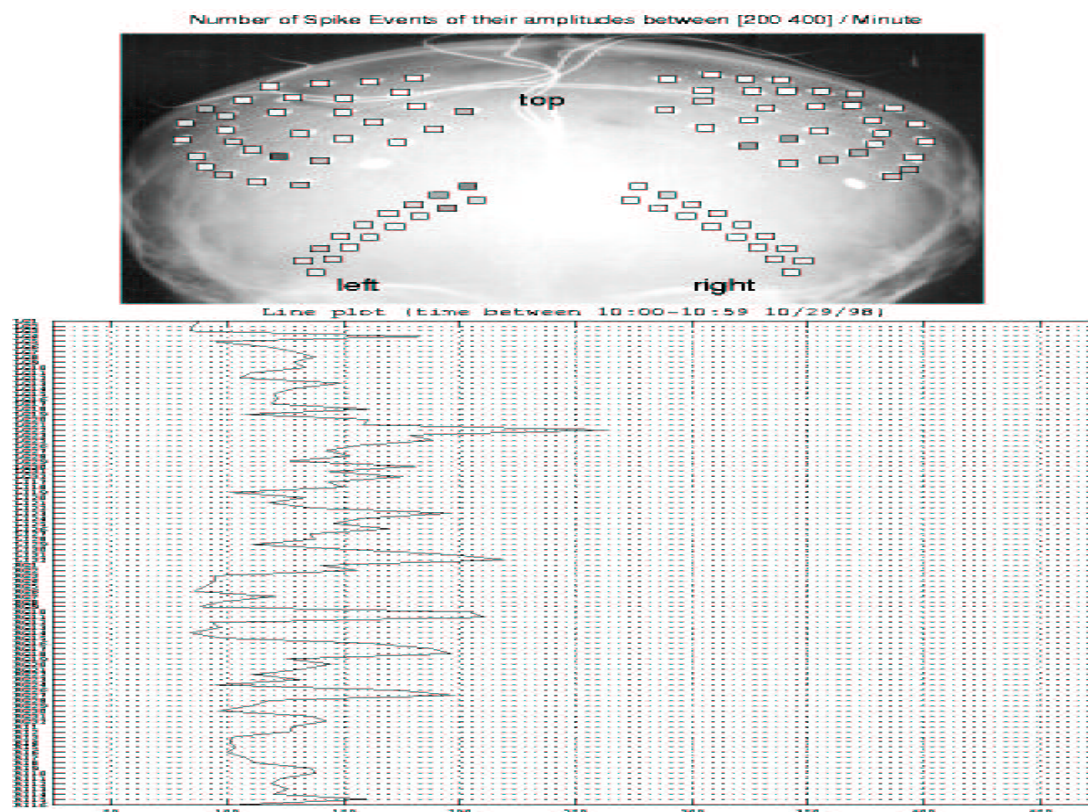
is the negative one. In this figure, only the peaked amplitudes larger than 300 (or less than -300) are selected. The range of peaked amplitude is manually selected here and can be changed for different investigations by the experts.

Once the sharp spiky signals spotted, the average number of the spikes appearing in one electrode is inquired. The EEG signal collects neurons' activities around the electrodes. The stronger abnormal signal generated by the neurons in one area, the sharper of peak point will be recorded in the electrode near the area. If the

neurons produce weaker abnormal activity, the electrode will not record any larger transients. The amplitude of these abnormal spikes can indicate the status of neurons' activities. In order to observe the wide variety of EEG spikes properly, we have divided these spikes into different groups by their peaked amplitudes. The range of different amplitude groups are selected as the amplitudes between  $\{[50\ 100],[100\ 200],[200\ 400],[400\ \text{maximum}]\}$ . For each hour long data, the average of spikes appeared in one electrode for different groups are evaluated. The results are plotted in Fig. 4.14 to 4.16. The bottom of these figures are the line plot for the average spike appearing on each electrode. The x-axis is the average appearances in minute and y-axis is electrode name. The title of line plot indicates the period of subdural EEG data processed. The top of figures are the graphical spatial plot of the head. From the subdural montage, each electrode is represented with one square box and the gray level of the box manifests the average appearing number of spikes at the electrode. The dark dots indicate higher average number and light dots have lower value. The electrodes having higher appearing number are located on left side of brain. Observing these plots, it can find that the average number for the small spikes is higher because the low amplitude spikes appeared more often. The high amplitude spikes are major occurred in the left area of the brain. Hour by hour data has been processed in the same way, it found that each hour data set shows similar average results. The consistence of long term spike analysis shows the neurons in left area of the brain having more abnormal activities.

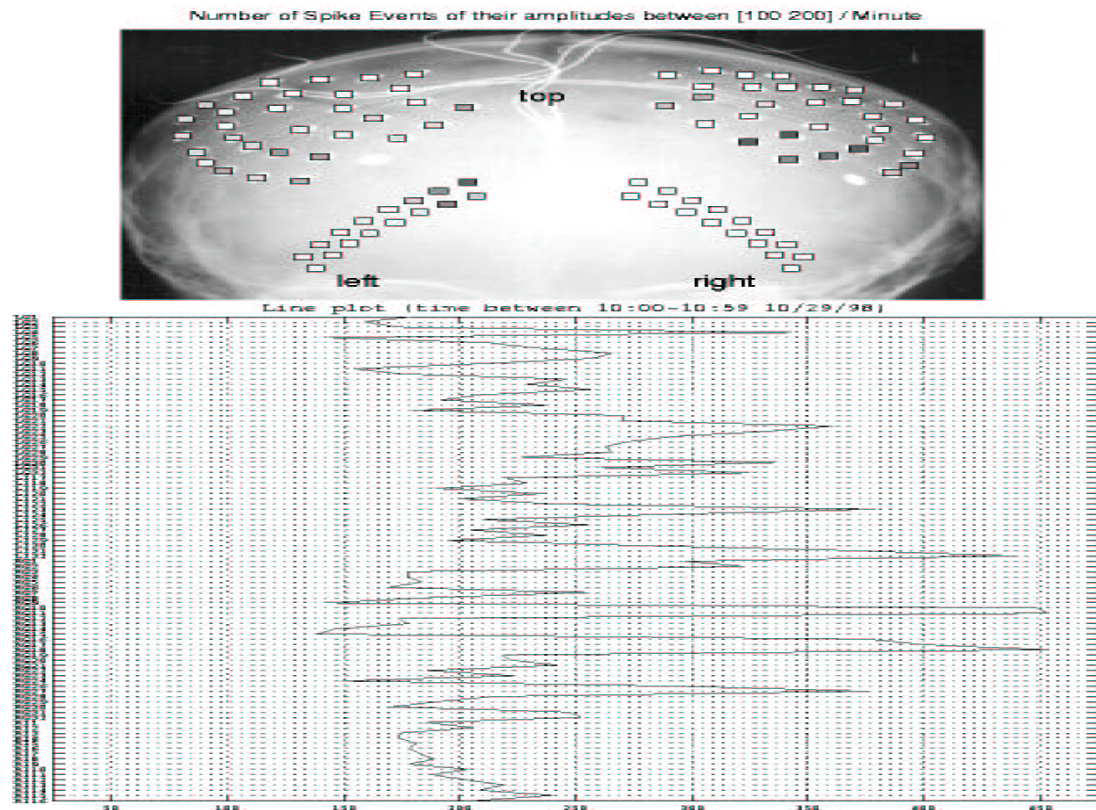
### 4.3.2 Spike Train Analysis Using Scalp EEG Data

Another analysis is using scalp EEG, which is recorded from the same epilepsy patient as previous section at the Children Hospital, University of Pittsburgh, Pittsburgh, PA, USA. The patient had stayed in the hospital for five days and EEG signal



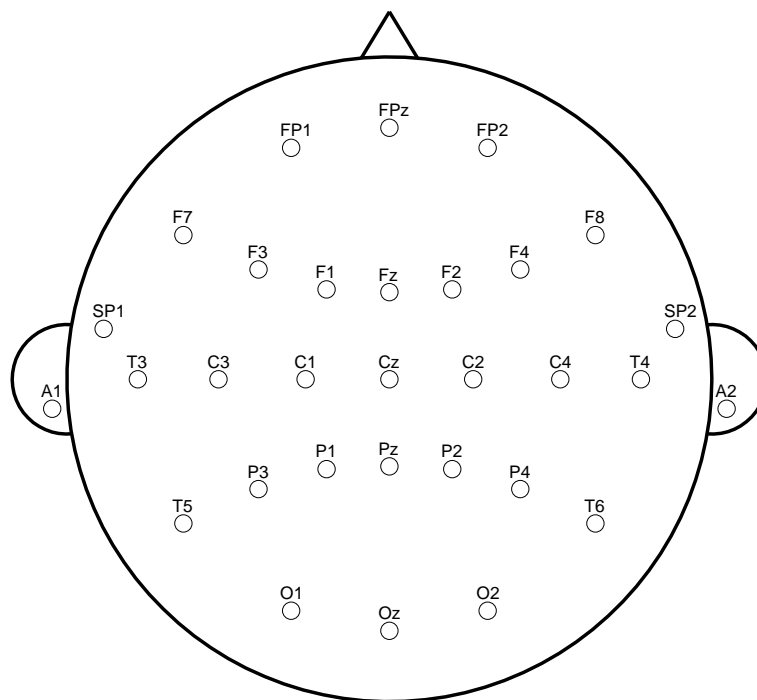
**Figure 4.15** The average number of spikes with amplitude between [200 400] appearing in each electrodes. Bottom of figure is the line plot which horizontal axis is average number of spikes appearing in one minute and vertical is the electrode name. Top of figure is the spatial head plot, each square box represents an electrode and its color are plotted according the average number of spike appearance. The darker of color represents the higher number, the lighter is the lower number.

is collected 24 hours continuously. While EEG data being recorded, the patient's condition has been close watched by nurses. Any possible seizures or abnormal symptoms are reported for further analysis. The first one and half day, there are total 35 channels EEG used to collected and the rest days has expanded to 37 channels to collect more information of the brain. The montage covered on the brain is an extended 10-20 system (see appendix D) shown at Fig. 4.17. The referential electrode (ground point) for EEG recording is located between electrode 'Cz' and 'Pz'. The sampling



**Figure 4.16** The average number of spikes with amplitude between [100 200] appearing in each electrodes. Bottom of figure is the line plot which horizontal axis is average number of spikes appearing in one minute and vertical is the electrode name. Top of figure is the spatial head plot, each square box represents an electrode and its color are plotted according the average number of spike appearance. The darker of color represents the higher number, the lighter is the lower number.

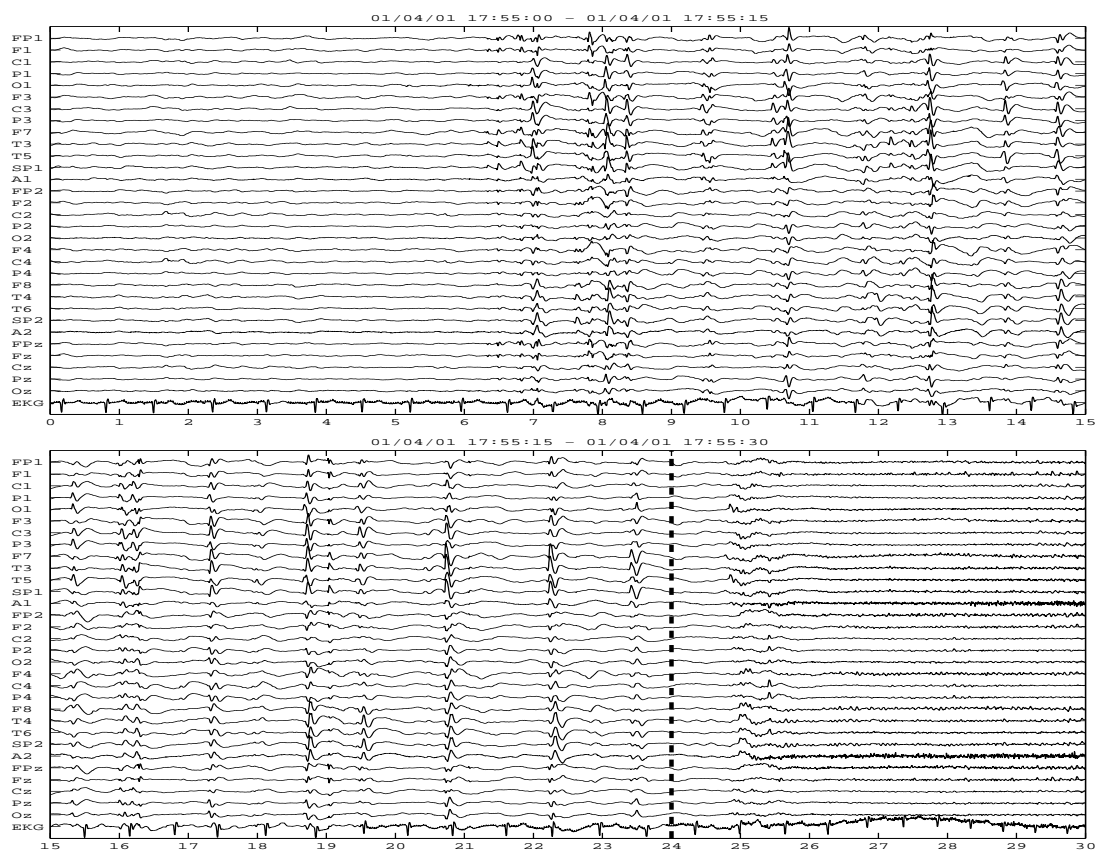
rate of scalp EEG data is 250 Hz and the cutoff low pass frequency and high pass frequency is set to 100 and 3 Hz. The gain of the amplifier is  $600 \mu V$  and A/D is set to 12 bits which the number of raw EEG is between -2048 and 2047 and actual potential range is between  $-625$  and  $625 \mu V$ . Unless specified, it has used the digital number to indicate the amplitude of EEG data than using real voltage amplitude. Total scalp EEG data is stored in 9 CDROM disks. It is pretty normal to have a huge size data collection when physician examines the epilepsy disease. One can see



**Figure 4.17** This montage is extended 10-20 system from a young life-long epilepsy patient, right of graph is right of human brain, left side is left of brain, top indicates the nose.

why the automatic computer aided recognition processes of spikes are highly needed because the size of tasks can not be accomplished only by human effort.

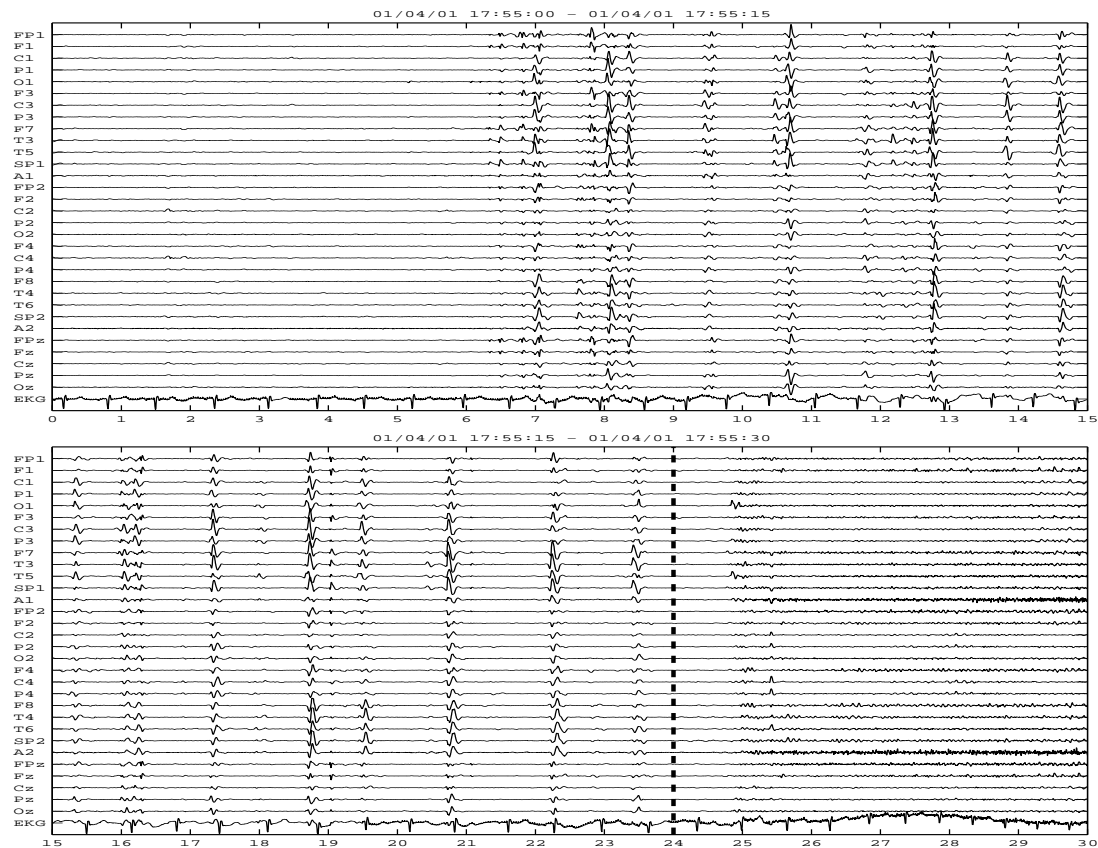
This data has been pre-processed by using the common reference method to eliminate the reference errors (see appendix C). Fig. 4.18 shows the processed EEG data. This segment of EEG data is 30 second long. The vertical axis indicates the electrode names of the electrodes and the horizontal axis is time (second), where top of figure is first 15 second and bottom is the next 15 second. The title of the figure is the date to record EEG. The last channel is EKG signal which is collected with EEG data simultaneously to monitor patient's heart condition. From the nurse's log, we have the exact information when a seizure happened. On the bottom of figure, a marked thick dash line is the time reported that the patient having a seizure activity. It



**Figure 4.18** This Scalp EEG data is recorded from the Children Hospital, Pittsburgh, PA. There are total 32 channels and the montage is shown in Fig. 4.17. This EEG data has been pre-processed by cutting the common reference. The vertical axis is the channel names and horizontal axis is time. Top shows the first 15 second long data and bottom is the next 15 seconds. The thick dash line on the bottom of figure is a seizure activity being reported by the attendant.

is very important to know when a patient had some abnormal symptoms in clinical diagnosis because physician will investigate the EEG around this region extensively.

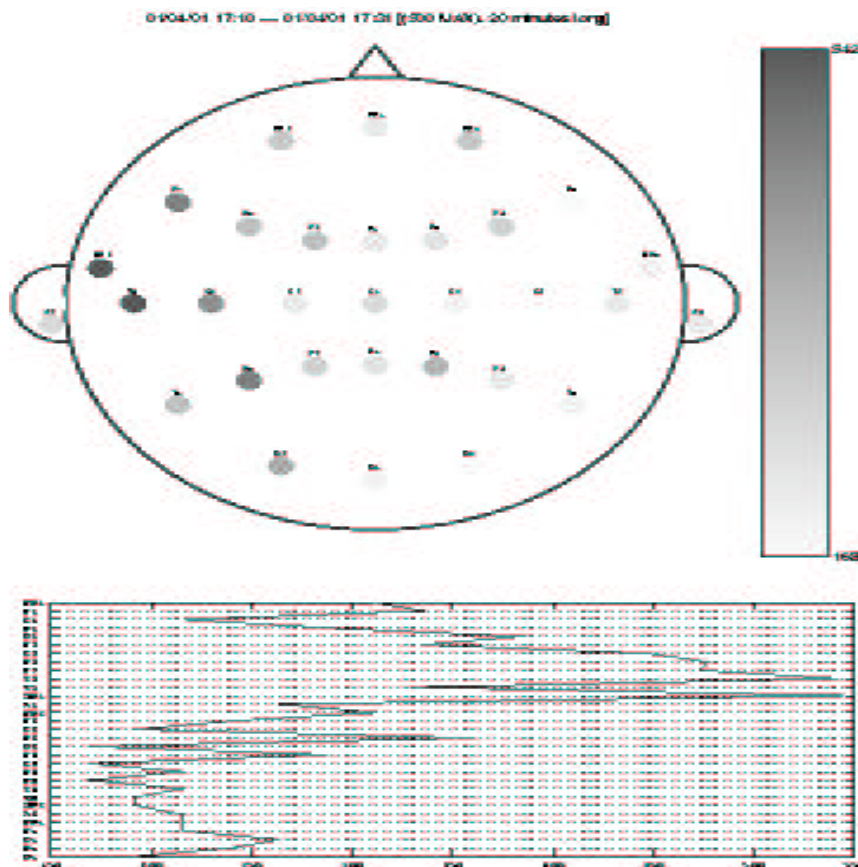
The scalp EEG is segmented into several pieces with each one minutes long. Each segment is applied with morphological filter in wavelet packet transform to extract the spiky transients from this EEG data. The wavelet transform filter has chosen the biorthogonal wavelet basis (6,8) because this wavelet basis is symmetrical having compact support. Fig. 4.19 shows the separated spiky transients. It can be seen



**Figure 4.19** The spiky transients from the scalp EEG data are extracted from EEG data, in Fig. 4.18. The vertical axis is the channel names and horizontal axis is time. Top shows the first 15 second long data and bottom is the next 15 seconds. The thick dash line on the bottom of figure is a seizure activity being reported by the attendant.

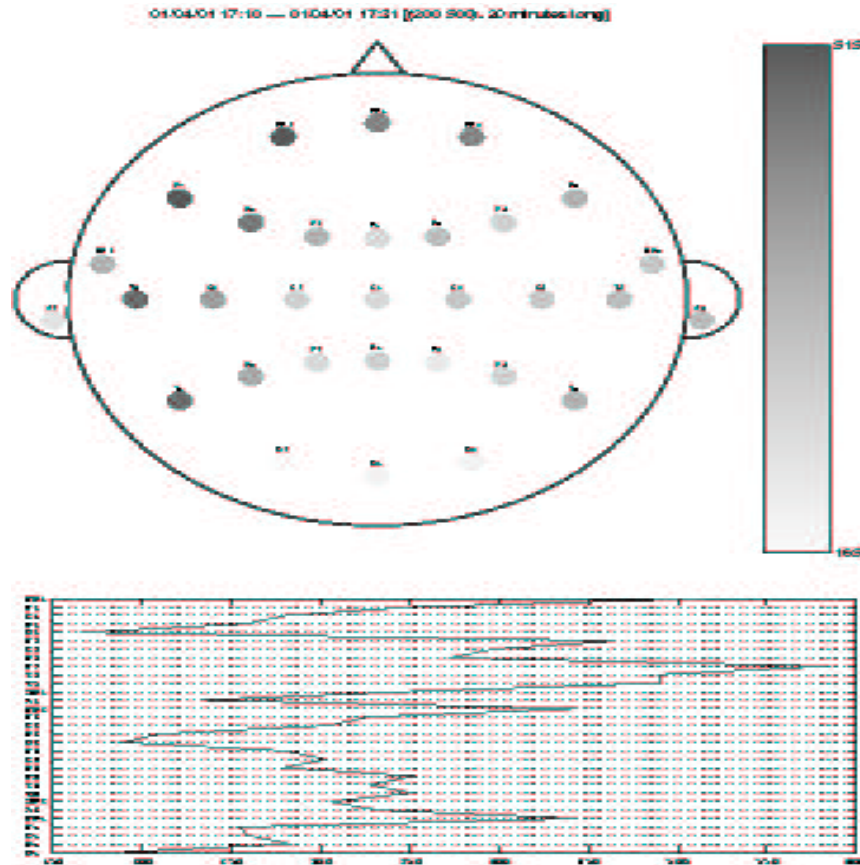
that the triangular spikes are extracted from scalp EEG data. The peak point of these separated transient has been located to represent these triangular spikes. The average appearance of spikes of each electrode is investigated to show where the area of the brain may have the most abnormal activity.

Fig. 4.20 to 4.21 shows the results that average appearing of epileptic spikes on each electrode. The left side of the figure represents the the left hemisphere of the brain and right side is right hemisphere of the brain. The top of the figure is toward to the nose. These spikes are divided into two groups: one group contains the spikes



**Figure 4.20** The separated sharp transients from the scalp EEG data (Fig. 4.18) The vertical axis is the channel names and horizontal axis is time. Top shows the first 15 second long data and bottom is the next 15 seconds. The thick dash line on the bottom of figure is a seizure activity being reported by the attendant.

with peaked amplitudes between 500 to maximum and other is between 200 to 500. Each electrode is represented with a round circle with gray color face. The dark one indicates high average number and light is low value. The map on the right side of the spatial plot is the indication of the value for each gray level. The amplitude of scalp EEG is normally smaller than subdural EEG data. It is because the skull of the head will attenuate the strength of neuron's activity. These figures show that the electrodes with higher average appearance of spikes are located at the frontal left area of the brain, such "F7", "T3" and "C3", etc. The group containing higher peaks



**Figure 4.21** The separated spiky pattern signals from the scalp EEG data (Fig. 4.18) The vertical axis is the channel names and horizontal axis is time. Top shows the first 15 second long data and bottom is the next 15 seconds. The thick dash line on the bottom of figure is a seizure activity being reported by the attendant.

amplitude spikes having dark dots is limited in less electrodes. On the bottom of figures are the line plot for the average appearance number, where x axis is average number and y axis indicated the name of electrodes. This results are consistent with the experiments using subdural EEG, which shows the left and frontal area have noticeable abnormal activity.

The stochastic point process has been used to analyze the spike trains of two different electrodes. The hypothesis of point process is the timing of an event occurred is a random process. The stochastic point process generates a cross-correlogram,

## 18:29 – 19:28 1/4/1, Correlogram of the Negative Spikes from the master channel F7

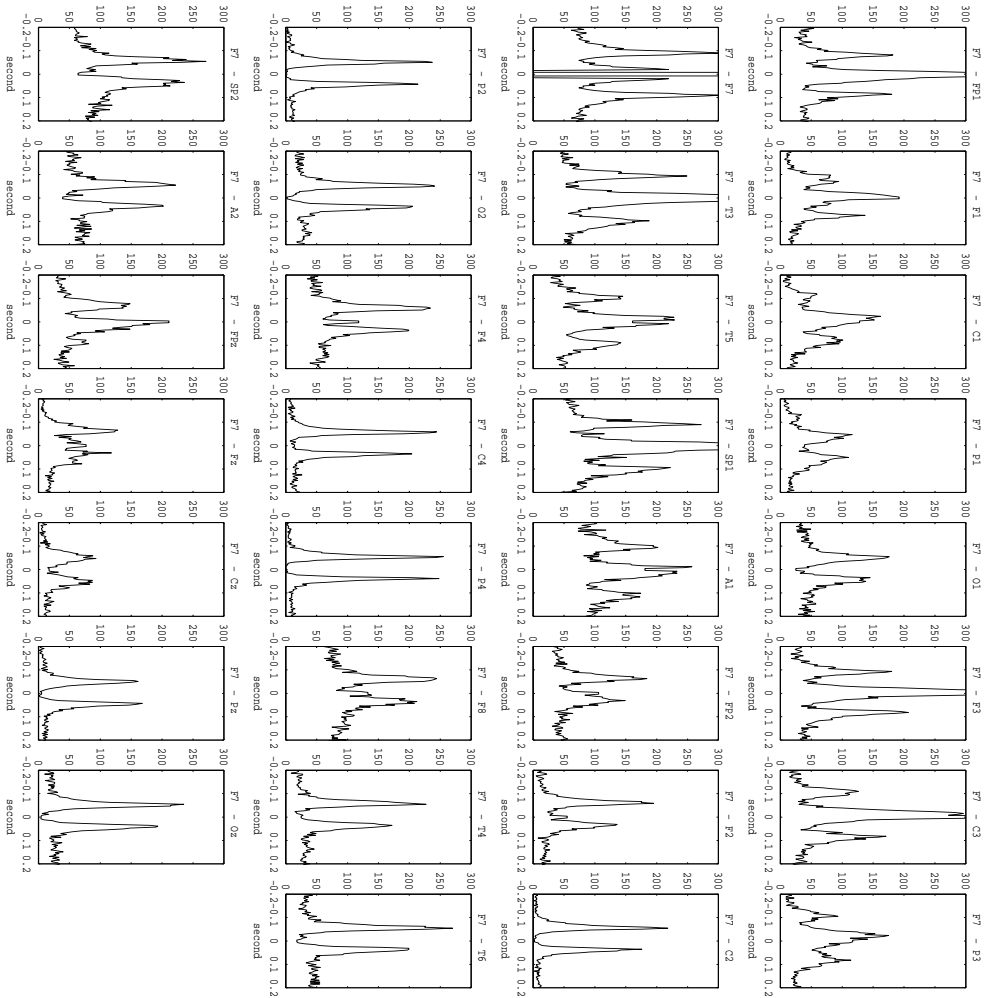


**Figure 4.22** The cross-correlogram of paired spike train from Scalp EEG Data introduced in section 2.3, to find the timing relationships of spiky events between two electrodes. If a spike occurred in one electrode, in a moment there will observe another spike appeared in the second electrodes. The cross-correlogram caught the timing correlation of the events (spikes) from different electrodes. The number of how often one observed this relationship repeatedly happened can quantify the strength of the correlation. Using the located peaked point of the triangular shape spike, it represents as the appearance time of this event.

Fig. 4.22 shows the correlograms generated by stochastic point process between electrode “F7” and the rest electrodes using the spikes with negative peak amplitude. The title of each sub-figure shows the name of two channels: the first one is the master channel “F7” and the second is the slave channel. For example, the title “F7-Fp1” indicates the cross-correlogram of the electrode “F7” and “P1”. The x axis is time (in second), where the positive time means that the spiky events occurred in the master electrode before than the events in the slave electrode, and the negative time means the events in the master electrode happened after the events in the slave electrodes. The y axis is the count of the histogram indicating how many time one have observed this relationship. The higher number indicates a strong relationship between the events of the two trains. After observing these cross-correlograms, it found that some electrodes, such as “F7-FP1”, “F7-F3”, “F7-T3”, “F7-F7”, etc., have similar correlation with respect to correlogram “F7-F7”, Those channels have highest count number in the zero on the x-axis. Cross examining the locations of these channels, it found that they are very near the electrode “F7”. This phenomenon can be explained as follows: when the neurons in one area were excited by some an abnormal activity, it immediately travels and affects the neurons near this area. The speed of the abnormal activities traveling may be very fast. Currently the sampling rate of EEG recording may not have enough resolution to reveal the fine detail of these information. Other cross-correlograms, such as “F7-P4” and “F7-C4”, have two highest counts located evenly between the center (zero delay) on the x axis. The locations of these channels are far away from the electrode “F7”. When a abnormal seizure signal occurred at channel “F7” and traveled into the area of these electrodes, the neurons of these regions were triggered and generated an abnormal activity, too. These internal activities eventually travel back into the neurons located at channel “F7” and affect them again. These reciprocal responses of the connected circuit in the

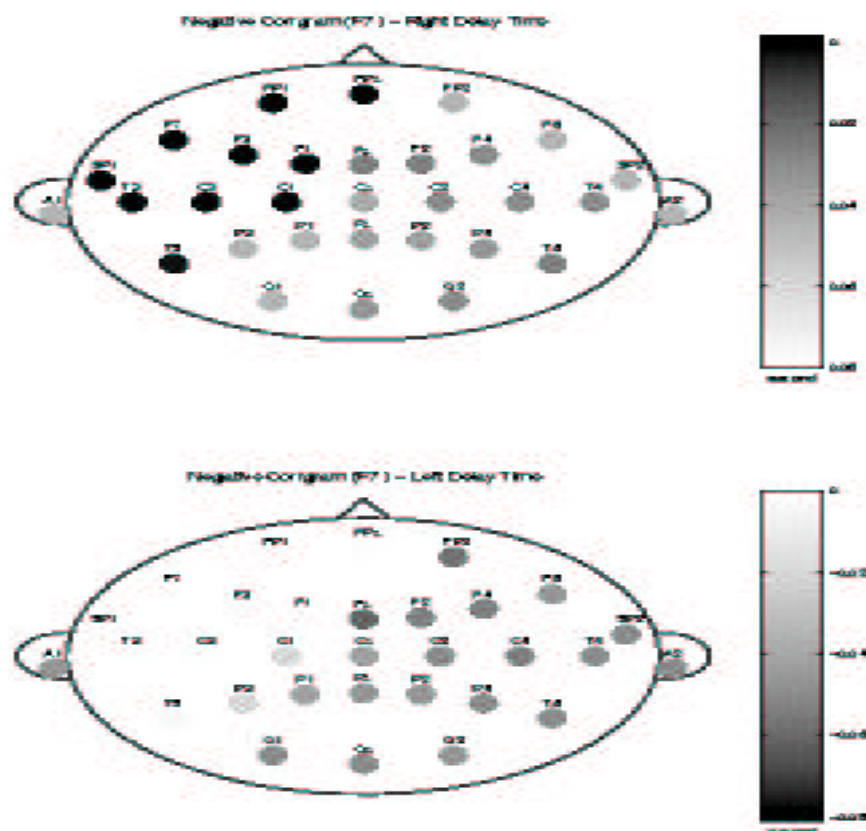


**Figure 4.23** Spatial plot of the maximum correlation from the cross-correlograms using scalp EEG Data

brain make the seizure activity can be revealed by using cross-correlogram analysis.

The stochastic point process can show the interactions between neurons in different area of brain. By selecting the highest count of the correlogram, the spatial relationship of the strongest correlation between the master electrode, in this case it is “F7”, and other electrodes can be analyzed. The cross-correlograms contain two maximum correlation information. One is how early of the events of a master electrode occurred before to the spike events in the slave electrode, shown as the maximum correlation in the positive side of the correlogram. The second maximum

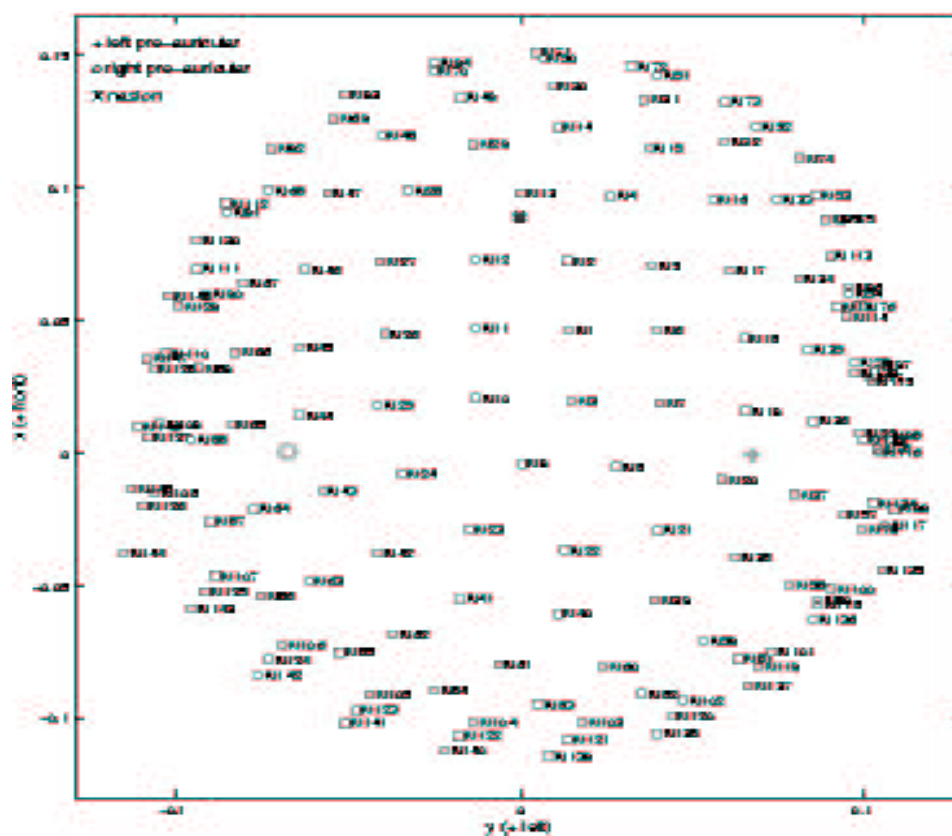


**Figure 4.24** Montage of MEG Signal, the marker '+' is left pre-auricular, marker 'o' is right pre-auricular and 'x' sign is the nasion

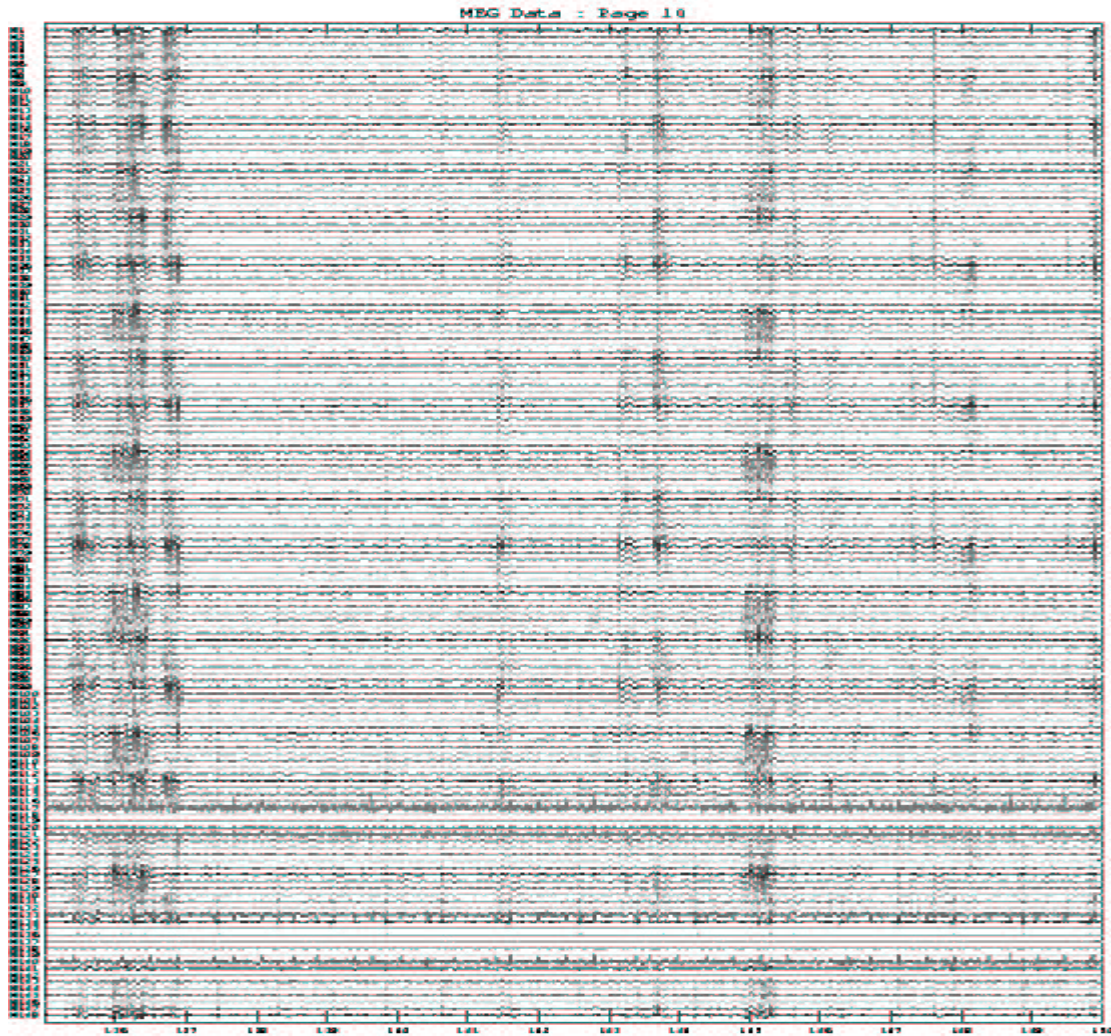
correlation is how late the events in master electrode behind the events in slave electrode, indicated at the highest correlation in the negative side of the correlogram. In order to show both maximum correlation, we show two spatial plots to observe the correlation graphically. The first one shows the positive maximum correlation (early appearance) and the second shows the negative maximum correlation (late appearance). Fig. 4.23 shows both spatial plot by analyzing the the maximum correlation of all the cross-correlograms with respect to master electrode "F7". The top of figure is the events in electrode "F7" having early appearances than the rest electrodes. The bottom is showing that the events having late appearance than the slave electrodes.

Each circle represents the location of a electrode on the surface of skull. The up direction indicates the direction of the nose. The left side of figure is pointed to left ear and right side is to right ear. The face color (gray scales) indicated the magnitude that the time of delay. The dark color indicates that this electrode has occurred early and the light one happened after. It can be seen that these spikes traveling between the up-left and the bottom-right area of the brain. The epileptic signal has been traveling between the left and right side. By analyzing the maximum correlation of the cross-correlograms, the trajectory of these extract spikes can be investigated. Hour long EEG has been used to produce this plot. The amount of data shows the relationships between the neurons in long period. It may increase the reliability than only analyzing short range EEG data.

### 4.3.3 Spike Train Analysis Using MEG Data

The third example for spike train analysis is using MEG signal recorded from the same patient in the previous examples. The MEG data is collected at Henry Ford Hospital, Detroit, Michigan, USA. The sampling rate of MEG data is 508.63 Hz and its sample period is 1.96607 ms. The cutoff low and high pass frequency is 100 Hz and 3 Hz, separately. The notch frequency is 58.3975 Hz. There are total 148 electrodes used to collect MEG data. The montage of MEG is shown in Fig. 4.24. The name of electrodes begins with letter “m” following digital number, where “m” indicates MEG and sequential number is from 1 to 148. In the figure, the ‘+’ sign indicates the position of the left pre-auricular, ‘o’ sign is the position of right pre-auricular and ‘x’ sign locates at the position of nasion. The vertical axis ( $x$  axis) indicates the front or rear of the head, where the plus indicates the front area of head and the rear side head has minus value. The horizontal ( $y$ ) axis represents the left and right side of face, where plus of  $y$  axis is left side and minus indicates the right side of the head.

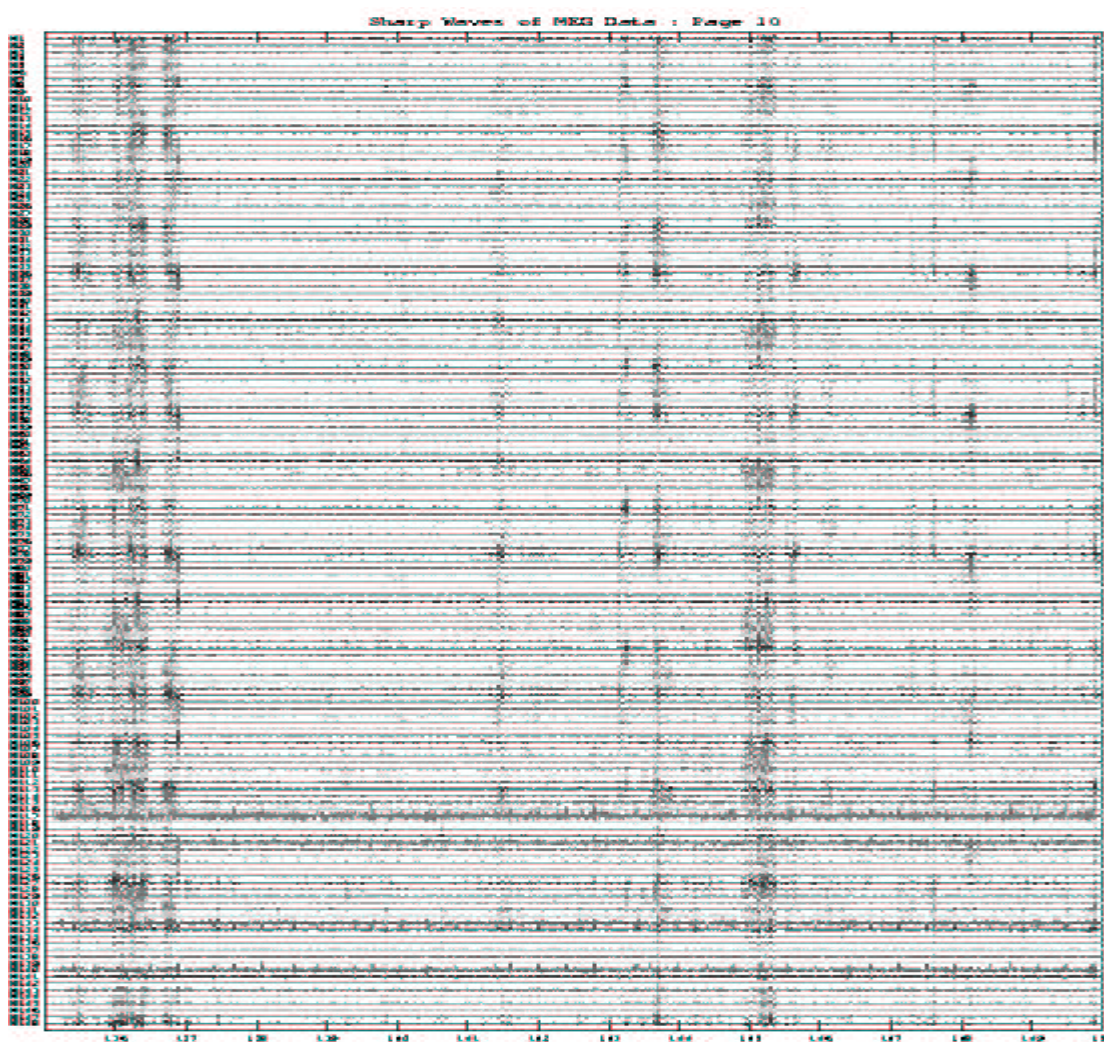
The montage is viewed from the top of head which the height of electrodes do not plotted in here.



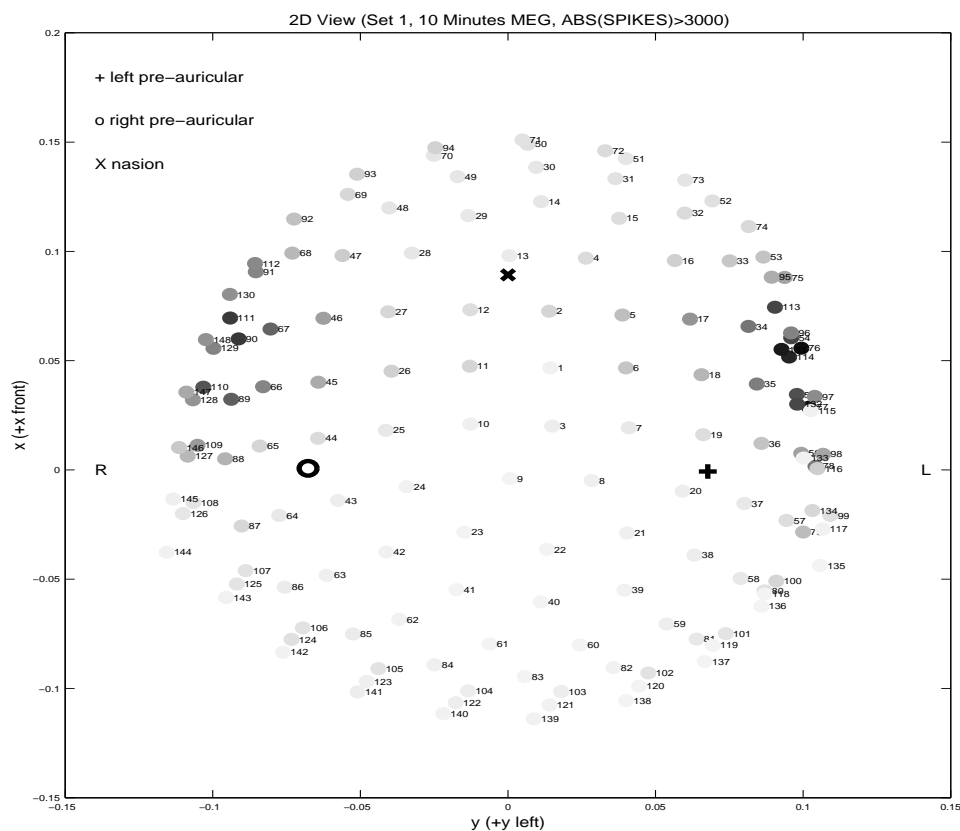
**Figure 4.25** MEG data: the horizontal axis is the time and vertical axis indicates the electrode names.

Fig. 4.25 is the MEG data, where the horizontal axis is the time and y axis indicates the name of electrodes. This segment of MEG data is 15 second long. This “spiky” transients were extracted by using the morphological filter in the wavelet

transform. It has used the biorthogonal wavelet basis to decompose signal into levels three. The extract spikes are shown in Fig. 4.26. The x axis and y axis are corresponding with raw MEG data. The transient signal has fast amplitude variation and its shape looks sharp. Visually inspection the rough shape signal, It can see that most of the sharp triangle spikes are successfully separated from the MEG signal.



**Figure 4.26** The separated spike signal from the MEG signal. The horizontal axis is the time and vertical axis indicates the electrode names.



**Figure 4.27** The result of counting spikes with their amplitude larger than 3000 in the MEG data. The dark color has higher number and the light color means lower number.

The average number of epileptic spikes appearing in each electrode is inquired. The first group analyzed is for those spikes having their peak amplitude larger than 3000 (in the digital conversion number), the second group is for the amplitudes between 2000 and 3000, and the last one is for the amplitudes between 1000 and 2000. The investigation of three groups of different amplitude spikes shows the abnormal activity of neurons in different area of brain. The average numbers for all electrodes are plotted to show the spatial relationship in the head. A circle, representing an electrode, with its face displayed with gray color is representing an electrode. The dark color indicates higher number and the light color has lower number. Fig. 4.27 is the spatial plot

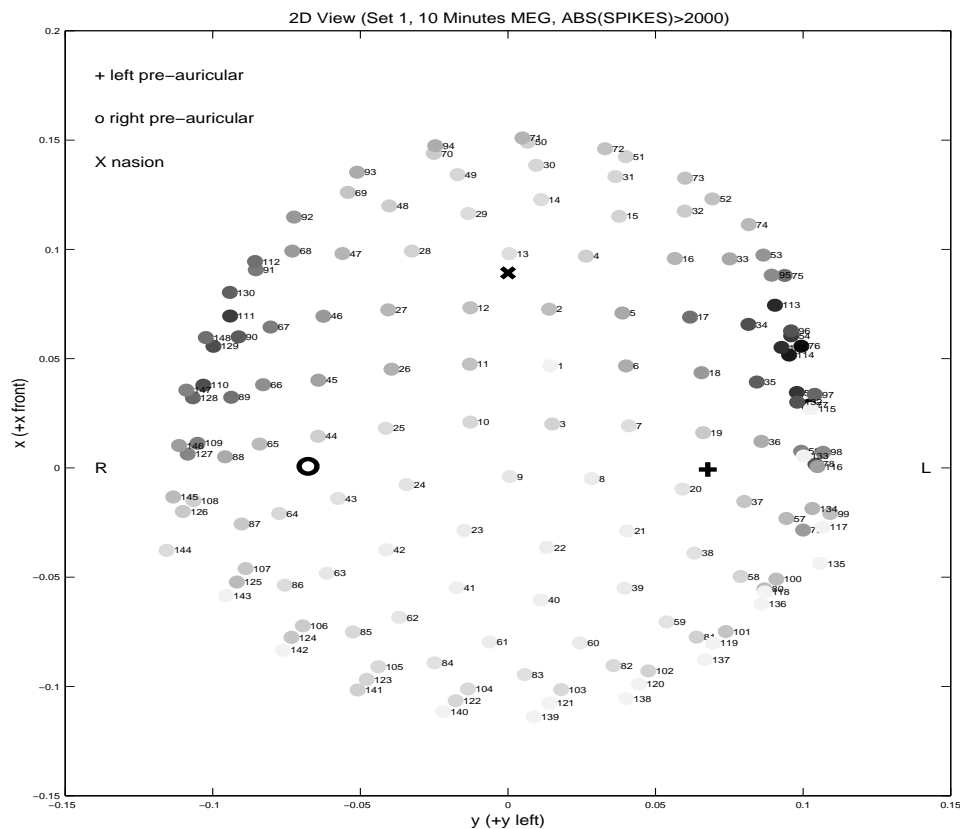


**Figure 4.28** The result of counting spikes with their amplitude larger than 2000 in the MEG data. The dark color has higher number and the light color means lower number.

for the first group. Fig. 4.27 and 4.29 are the spatial plot for the second and third groups, respectively. The markers of “+” and “o” are indicating left and right side of the brain. The “x” sign is the location of the nose. It can clearly be seen that the electrodes located at frontal left area of the brain have higher average appearance number. It is more significant when the amplitudes are larger. The electrodes located frontal right area also have large average number. But in the right side, these number is not as significant as left side and it seems that these electrodes have spread in a larger area at the right side of the brain.

The cross-correlograms generated by stochastic point process between electrode

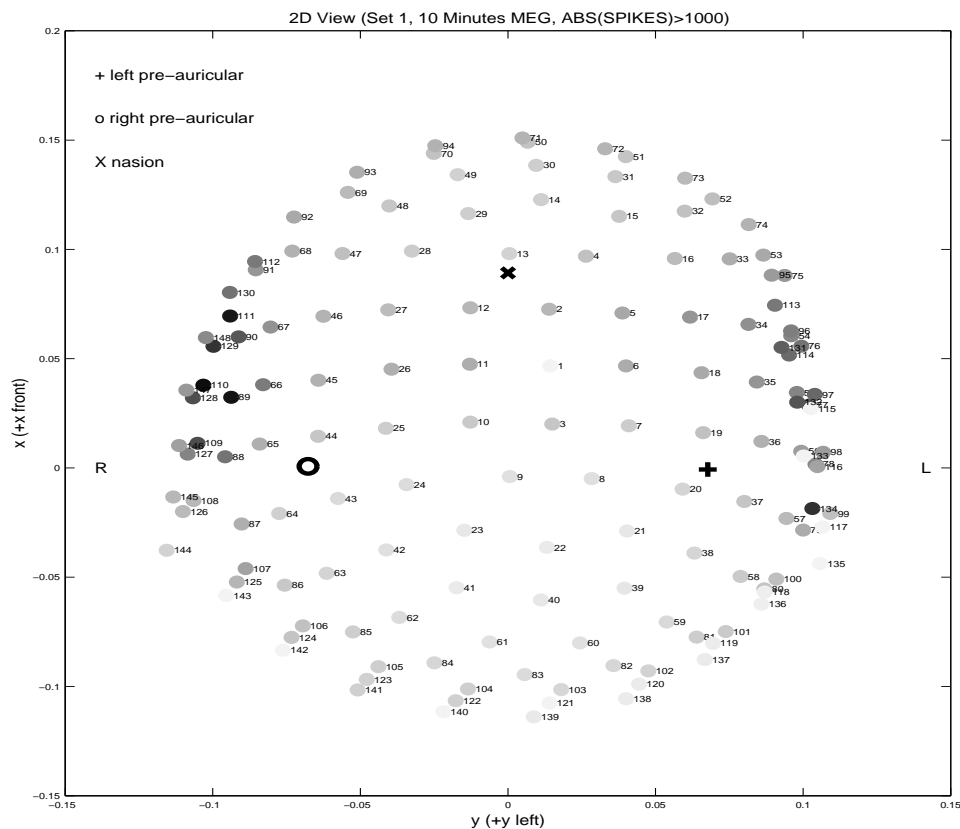


**Figure 4.29** The result of counting spikes with their amplitude larger than 1000 in the MEG data. The dark color has higher number and the light color means lower number.

“M96”, located at the frontal left area of the brain, are shown on Fig. 4.30. The maximum correlation points on both right and left side of the correlogram show the time relationships between the events of two electrodes. The maximum correlation on the right side indicates how early of the events in the master electrode appear than the events in slave electrode. The left side shows how late that the events in the master electrode showed after the events of the slave electrode. The timing shifting of the maximum correlation point are plotted on Fig. 4.31 to graphically show the relationships of the spike events between master electrode “M96” and the rest electrodes.

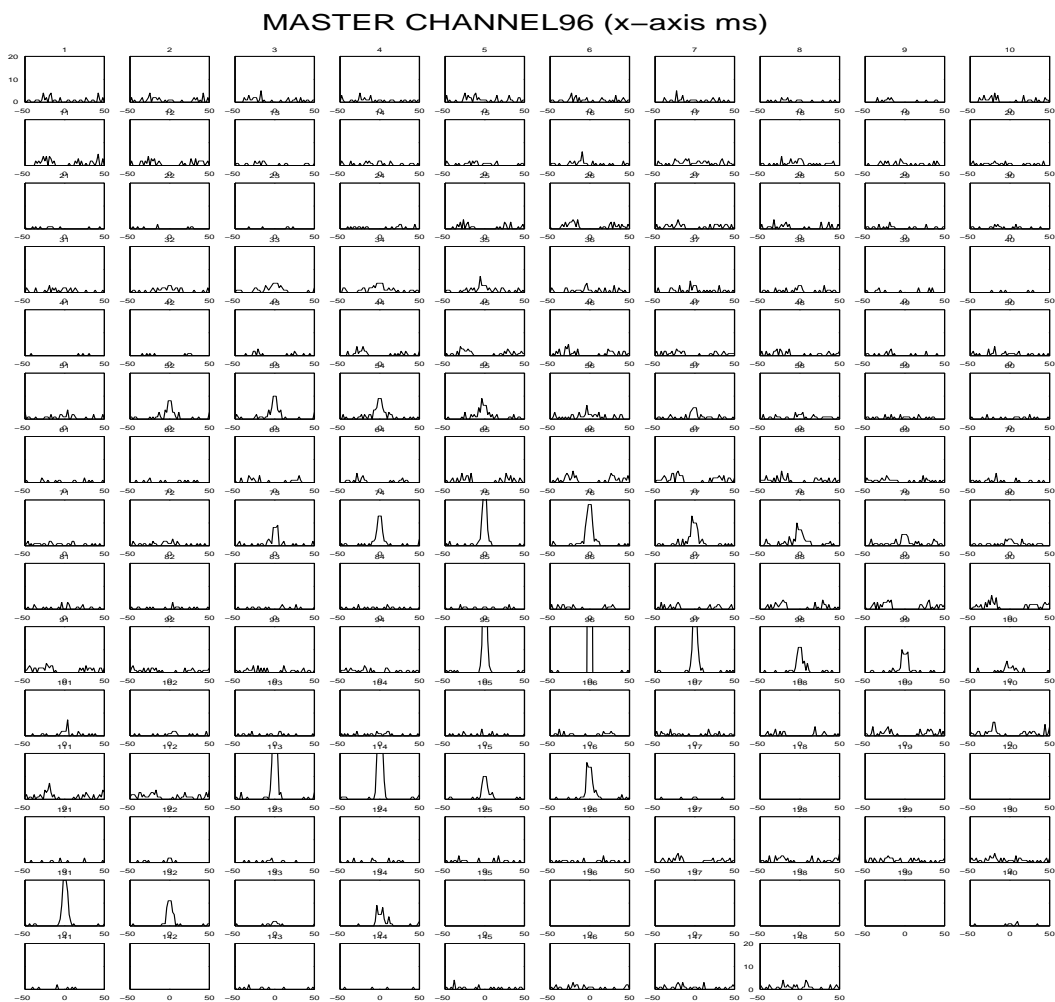


**Figure 4.30** The correlogram of MEG data

The left side of Fig. 4.31 is the left maximum correlation of the cross-correlograms and right side of this figure is right maximum correlation. The gray level indicates the time differences with respect to the center of the correlogram (the center point means no time difference). If the number of the maximum correlation is too small, which indicates that as the correlation between the events in two electrodes is not significant, is plotted as small dot. On the right column of this figure, the dark circle means the events in the master channel are leading the events in slave one, which the

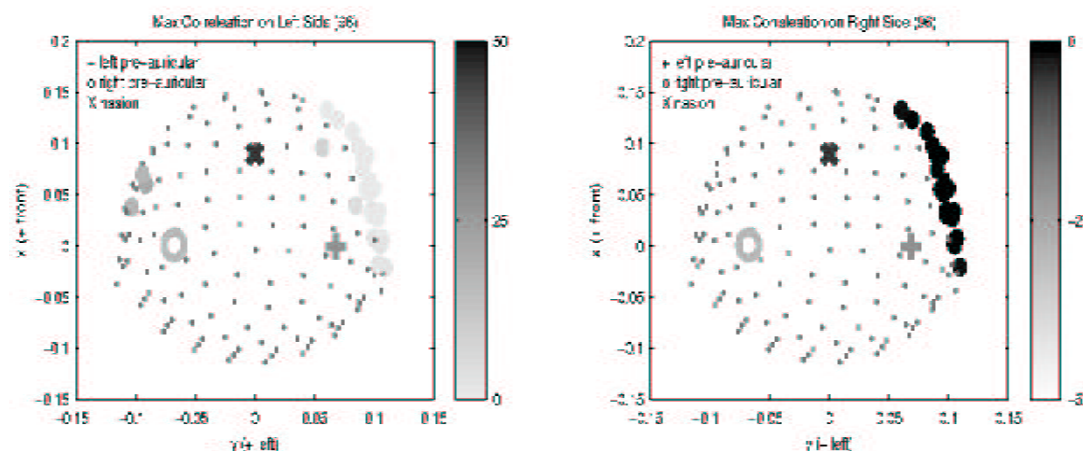


**Figure 4.31** The spatial plot indicating the time delaying of maximum peak from the correlogram

spikes generated near the master electrode appeared early than other area. It can be seen that the the the circle plate near the master one has on the left side brain have the abnormal spike events leading other electrodes. This left-frontal area of the brain has most abnormal activities consistent to the results investigated in other different EEG data.

At the left side of the this figure shows the maximum correlation on the left side of the cross-correlograms. The point of the maximum correlation shows the major leading time of events in the slave electrode occurred before the events in master. The light circle plates represent the left maximum correlation time is close to zero. It found that some electrodes on the right hemisphere (located on left of the head model) of the brain have strong correlations to the electrode “M96”, shown as some dark plated of the left column of Fig. 4.31. The correlations between these electrodes and the master electrode caught from the correlogram suggest that there is interactions at the left and right hemisphere of the brain. In our analysis, all cross-correlograms between each two electrodes are inspected. Analysis of the correlations of these spike events, separated by using our developed method, is found that the neurons near the

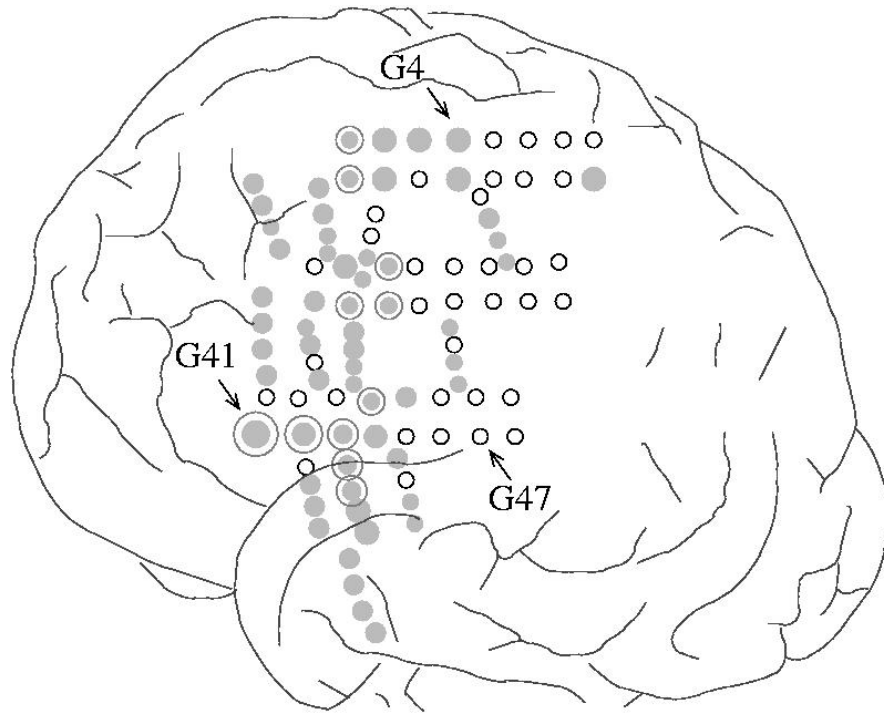


**Figure 4.32** The Spatial Plot of Cross-correlogram

left-frontal and right-frontal area have generated the major seizure activities. The correlogram suggests that the left side has more dominant influences. The rest area of the brain have less or no significant symptoms related to epileptic spikes.

In the end, another subdural EEG, recorded from the same patient, has separated into spiky transients and background activity by using morphology wavelet separation method. These spikes of every paired electrodes generated a cross-correlogram by using stochastic point process. These cross-correlograms have been analyzed by neurologist. According to the point (timing information) at the maximum correlation of each correlograms, it has analyzed their interactions depending on the spatial location of these electrodes. Figure 4.32 shows this spatial plot of this analyzed results. Each circle represents an electrode. If the amplitude of the point at maximum correlation in the cross-correlograms between two electrodes is lower than a threshold, the

experts decide there is no significant relationship between these two electrodes. If this amplitude is larger than the threshold, it will conclude there is a significant relationship between two electrodes. The empty circle indicates that there is no significant relationships between one electrode with respect to all other electrodes. The circular plate indicates that this electrode has significant relationships between the electrodes near to this electrode. This size of plate indicates the strength of significance, while the larger one has stronger relationship. The circular plate covered by a circle outside shows this electrode has significant relationship between most electrodes. The trajectories of abnormal activities generated from the brain cells are mainly on the up-and down in the front area of the brain. It can be seen that the electrodes at the front and middle area of the brain have the most strongest interactions. This area is at the temporal and frontal lobes on the left sphere of the brain. This result has been compared with an neurologist independently inspecting this data with other medical approaches. Both conclusions are consistent to each other.

## 5.0 DISCUSSIONS

This chapter discusses performances of the developed signal separation method of using morphological filter in wavelet packet decomposition and of using morphological lifting scheme as well as the application of the stochastic point process analysis to epileptic EEG signals. Their advantages and limitations are examined.

### 5.1 Summary

In this study, we have address an important problem in basic and clinical neuro science, automatic EEG spike separation and have presented a novel approach to give an improved solution to this problem. The problem has inspired us to theoretically analyze a morphological filter with a multiresolution representation. We first described the problems of automatic spike separation and limitations of current approaches. We then proposed our approach to solve this problem. This approach involved the use of the mathematical morphology, wavelet transform and the lifting scheme. The latter, the interictal spike activity has been analyzed by the stochastic point process using these separated transients to reveal the dynamic relationship of neurons.

The automatic spike separation has two parts: one is morphological wavelet separation method and the other is morphological lifting scheme. The targeted spiky transients have sharp peaks randomly appearing in the epileptic EEG signal. The rest of EEG signal is considered as a background activity. This thesis has separated these transients from the background activity. The stochastic point process is a tool for analyzing the interictal activity. Using the extracted transient, it generates a cross-correlogram to find the correlation between two sequences of spiky events. The

correlation shows the interactions between neurons in the brain. The most interactive area will be a possible focus generating the seizure.

The whole interictal spike analysis includes automatic spike separation methods and the followed stochastic point process is trying to find the possible foci of epilepsy. These methods have applied to the subdural EEG, scalp EEG and MEG data. An outline of this thesis of automatic spike separation and stochastic point process is shown in Figure 5.1.

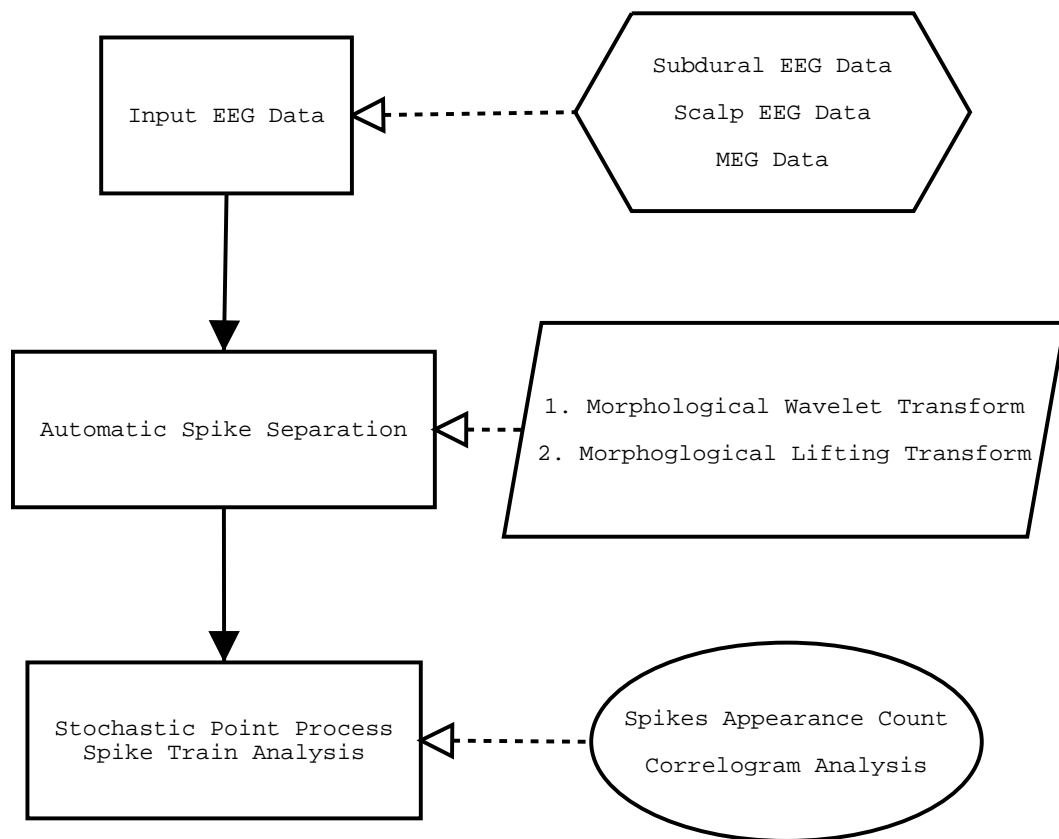


**Figure 5.1** Summary of Automatic Transient Spike Separation and Interictal Spike Train Analysis

## 5.2 Morphological Filtering in Wavelet Packet Decomposition

The wavelet packet transform is implemented by using a low-pass filter and a high-pass filter. The decomposed coefficient sets consist of scaling coefficients with lower frequency components and the wavelet packet coefficients with higher frequency components, both have coarser resolution than the original signal. The coefficients are repeatedly decomposed to the next scale level. The wavelet transform essentially divides a signal into subband frequency components. But the sharp spiky patterns in the epileptic EEG data are not well recognized by using wavelet packet decomposition alone. The reason is that the two components in the EEG data have overlapped frequency components.

Mathematical morphology gives a nonlinear method based on the set algebra and integral geometric analysis applied to signals. Morphological operations utilize one or more structuring elements defined a priori, which is chosen as a circular disc with radius equal to one. With this structuring element, morphological operators, such as opening and closing, are constituted to form a morphological filter which enables the detection of the modeled spiky pattern from the wavelet decomposition of the epileptic EEG data.

The duration of epileptic spikes are in the range of five data points to seventeen data points compared to 20 to 70 msec duration with a sampling rate of 250 Hz. The spikes are modeled as a pattern of triangular shape. It has a sharply rising and falling peak point in the middle. We have chosen a structuring element as a circular disc of a fixed radius, then structuring element is chosen because a circle has a constant curvature, while may measure the curvature variation of the background activity. Approximately, the background activity has constant curvature locally, which matches

the structuring element. The morphological filter smoothed portion of the signal where the morphological characteristics are different from the triangular transients. The residues between the signal and smoothed portion are taken as the “spiky” transients. Combining a specific morphological filtering and the wavelet packet decomposition, we have developed a new method to separate spiky transients and background activity in the EEG data. The wavelet bases used is the biorthogonal wavelet with compact support. We found that using biorthogonal wavelet gave better results.

The summation of two components is equal to original so that the integrity of the original signal dose not change. The wavelet decomposition and morphological classification can be repeated to the next levels. The stopping criterion depends on the minimum scope covering three points and the length of decomposition filter of the wavelet transform. For the duration of spiky transients of 6 sampling points, at the coarser scale the first-level decomposition will approximately reduce the spike span to 3 points. The morphological filter will have the best coverage to detect this spiky transient at this resolution level. For spiky transients with longer duration, it will need the second level decomposition to reduce to 3-point coverage at a coarser level. For spikes duration of 5-17 sampling points, the stopping level is three, where the spikes of longest duration can be the best detected. The supported length of biorthogonal filter integrates the local information and keeps the peak point in the coarser levels. In the end, one can regroup the separated components at final level by their morphological characteristics. The smooth and residue components are formed to be the background activity and the spiky transient, respectively.

The span of the circular disc covers three points at each level scale level. The three samples are the point to be processed and its adjacent neighbors. It covers the minimum area to detect a sharp spikes where the peaked point is in the middle. Using

a structuring element with fixed size, the morphological filter can detect and extract such a local geometric shape at the scale level. Using multiresolution decomposition, this structuring element adapts to spike patterns of different size. Instead of providing many different structuring elements for different types of transients, this developed method separates the targeted patterns from the EEG only using one structuring element.

Visual inspection of the separated background activity shows similar shapes to the original EEG without sharp spikes which are shown in the transient component. However, small ripples occur in the areas where large spikes located. The sharp spikes are correctly separated from the raw EEG signal. Some small, fast fluctuations are blended in the separated transients which are assumed as high frequency noise and highly discernible from the spikes. In practical application, these noises are not significant and can be eliminated.

The wavelet bases used in this paper have chosen to be the biorthogonal wavelet which is FIR filter with compact support and multiresolution representation. The biorthogonal filter is symmetric and the phase of the filter will not be distorted. We have compared the separated results by using the orthogonal wavelet transform. It found that the biorthogonal transform gave a better results. Even the morphological operations are known as non-linear processes, this method can identically separate two exact spikes with different directions (the upward and downward spikes) with only a sign difference. It is because the chosen structure element, circular disc, has symmetric shape. The symmetry property treats the directional signal equally. The detail descriptions have been included in appendix E.

### 5.3 Morphological Filtering in Lifting Scheme

The second morphological method of signal separation uses a morphological lifting scheme. The lifting scheme also decomposed a signal into two coefficient set: approximation coefficient and detail coefficient. The lifting scheme is easier to implement and its flexible structure may be embedded in other nonlinear operators in a multiresolution process. This developed method of the morphological lifting scheme separates a signal into two components which are the background activity and transient. The morphological lifting scheme contains three stages: split, predict and update. The first split stage simply divides a signal into two smaller sets of data by using even-and-odd indexed data points. The predict stage of the lifting scheme is realized with the morphological erosion which amounts to predict a signal using its geometrical shape. The update stage is an average operator designed to find the upward (downward) spikes. The morphological filter classifies the decomposition coefficients at each scale in recognition of their morphological characteristics.

This method has been tested on the epileptic EEG data as separation in chapter 4. The EEG was decomposed to the scale level three. The approximation coefficients at lower scales were reconstructed into the background and the detail coefficients at each level were regrouped and reconstructed to form the spike transients. When compared to result obtained by morphological filtering in wavelet packet transform, the lifting method produced similar background and spiky activity except peaks in the background appeared sharper visually. There appeared no small ripples in the separated background activity.

The separated background activity of the subdural EEG data detained by using the morphological lifting method occasionally looked sharper than that obtained by using morphological filter in wavelet packet transform. It happened where the

background activity has larger amplitude change over a longer interval than spikes patterns. The reason for this is that because the decomposition of morphological lifting scheme used three points to predict the coefficient in the next scale level. Unlike the morphological filter in the wavelet transform, it used the biorthogonal basis to do the decomposition, which the basis is longer than three points, for example the biorthogonal wavelet has a supported width of 17 points for the decomposed filter. The short support morphological filter tends to keep the peak sharper. The longer support of the predict and update filters can be added to smooth the background activity. The sharp spiky waveforms need less neighboring coverage, the morphological lifting filter well separates these patterns.

The developed morphological lifting scheme is different from the max-lifting method (35). The process of max-lifting takes the maximum amplitude of the two even-indexed points to predict the odd point. The errors of the prediction are used to update the lower level decomposition coefficients. The maximum operator is related to the morphological dilation. The proposed new morphological lifting scheme is adjusted for the special structure of the triangular shaped spike model. The sharp waveforms have salient peaks which are an important factor in spike recognition. In order to best recognize this characteristic, we involve the peak point in the design of the morphological filter. Instead of only using the even indexed points to predict the odd indexed point, we used both the even-indexed and odd-indexed points to achieve the best prediction of the peak. The morphological filter needs to judge this middle point to classify whether it is a spiky transient or not. The advantage of this way is that one can have more control about the spike detection, and the disadvantage is that one needs to store extra information for the perfect reconstruction. This tradeoff for better recognition of the spike patterns is not a problem because it only temporar-

ily stores this extra information. Once the spike has been recognized, all of these intermediate information can be thrown away. The storage required for final separated components for the morphological lifting scheme is the same as that for the morphological wavelet packet transform. The developed scheme gives a perfect reconstruction, but the decomposition process in the morphological lifting does not satisfy linear superposition. As explained before, it is because the morphological prediction of the odd-indexed points depends not only on the even-indexed points, but also the centered point itself, thus the linearity can not be maintained. By comparing model of the morphological filtering in wavelet transform and the method of morphological lifting scheme, the first method involves linear composition with a nonlinear threshold to give two components and the second method is a nonlinear process involving an additional points to reduce the prediction error. The first method adjusts the smoothness criterion to separate the two components. The second method is adapted to the model characteristics of the spike in its prediction.

Other issues of the morphological lifting method, like the structuring element and how many levels that one needs to best separate target signals, are similar to those in the method of morphological filtering in wavelet packet transform, as already discussed in the previous section.

## 5.4 Statistical Point Process of Spike Trains

The statistical analysis of these separated spiky trains is applied for epilepsy diagnose. These spikes represent the status of the abnormal brain activity. The defective neuro cells create some sharply peaked signal seen in the epileptic EEG data. The complexity of the interactions of neurons in the human brain makes a direct observation of their activities impossible. The recorded EEG data represents integrated

information from many brain cells which can be considered as a random process. The peak occurrence time of each spike is recognized as a random variable, hence the statistical point process may be used as model to describe one aspect of the statistical characteristics of a spike train.

Epileptic spikes recorded in one electrode reveal the activity of the nearby neurons in the brain. If spike appears from a group of neurons, the electrode near these neurons will collect stronger information and far away electrodes may record weaker signals. The spiky transient will decay as the traveling distance increases. The larger spike appearance in an electrode reflects the higher chance that the brain cells near this area have some abnormal activity. The frequency of spikes occurrence is a simple measure for a global view of the epilepsy state. Neurologists can manually classify spikes into different categories the strength at peaked points. The higher amplitude of a spike represents more severe response of the brain activity, in the area near that electrode possibly indicating a focus of the epilepsy in the area near that electrode. The lower amplitude spikes may be interpreted as the spread of an abnormal signal traveling across the brain. In our case, the frequency of spike appearance of EEG recorded from one epilepsy patient is measured for hour long data. The number is collected for every hour and compared the results between hours show they are very consistent indicating some electrodes in the frontal and temporal area of the brain having a higher spike appearances.

The stochastic point processes is more elegant way for the spike train analysis. The idea of this point process is to find the correlations of the appearance time of the events (spikes) be separated from two spike trains. Each hour long data is considered. Here, only the timing information of spikes is used while other measures of these transients, such as amplitudes, are not considered. The cross-correlogram

between two point process indicates the timing correlation between the events in two spike trains obtained from two electrodes. If one cell near an electrode generates an abnormal spiky transient, it will influence other cells in other areas to generate abnormal activities, too. The cross-correlogram between two electrodes will reveal this influence. Using a large amount of spiky transients, the correlations between these transients can be used to catch the dynamical interactions between neurons, which generate abnormal spiky transients. If a neuron generates a spike, it will travel through the brain to cause other neurons to generate abnormal signals. The timing information between two observed spiky transients from two different electrodes can be caught by the cross-correlogram of two corresponding point processes. By analyzing all cross-correlograms of all electrodes, physicians will have a global observation of the interactions among brain cells in different areas. The most interactive area is the possible focus of the epilepsy (which causes seizure). Combining with other clinical diagnoses, this will aid neurologists to arrive at a better decision for treating a patient.

In our study, we have taken the hour long EEG recordings for automatic extraction of spike trains which are used in the stochastic point process analysis. Our results are more reliable than using only smaller segments of EEG data.

## 6.0 CONCLUSIONS

In this study, we have developed two methods for separation of spiky transients from the background EEG data. The methods investigate a specific morphological filtering in multiresolutions. One method uses the morphological filtering in wavelet packet decomposition, and the other uses a morphological lifting scheme. Both have been shown experimentally to provide reliable extraction of spikes in long recordings of EEGs, where the detected spike trains in multiple electrodes have been analyzed through cross-correlograms of stochastic point process in identifying epileptic foci trajectories.

### 6.1 Contributions

The major contributions of this thesis is summarized below.

The first contribution is the signal component separation method using morphological filtering in wavelet packet decomposition. This novel method detects and separates triangular shape short transients from the background EEG activity. Only a single circular disc structuring element is used in multiresolution decomposition. The morphological filter smooths and ,thus, detects both upward and downward triangular peaks from the decomposition coefficients at appropriate resolution levels which give the separated transient spikes after reconstruction. The method performed effectively in our experimentations.

The second contribution is the developed morphological lifting scheme for two separation. of transient spikes from the EEG background data. This method utilizes

a morphological prediction filter to detect the triangular shaped peaks. This method performed equally well as the former method.

These two methods provide automatic separation of spike trains in long recordings of epileptic EEG data from multiple electrodes. This enabled us to make an accurate cross-correlation analyzes of the associated statistical point process, leading to an inference of epileptic foci trajectories in particular cases. confirmed by expert neurologists. The successful analysis provides, in times, an indirect verification on the accessory of the signal separation.

## 6.2 Future Works

There are several problems worthy to be investigate in future research:

(1) Add new knowledge and physiological descriptors to modeling the transients so as to further improve the signal separation.

(2) The filters used in prediction and updating stages of the developed morphological lifting scheme have short supports. Explore the use of longer supports for achieving more accurate separation results.

(3) Investigate additional information, in addition to the maximum correlation, derived from cross-correlograms of spike trains for enhancing the determination of the epileptic foci.

## APPENDIX A

## APPENDIX A Data Acquisition of Subdural EEG Data

The EEG data used in the paper is recorded on 1998 at Children hospital, University of Pittsburgh, Pittsburgh, PA. The patient is a young epilepsy boy. He had a life-long epilepsy disease. The type to record this data set is called as subdural EEG data, which the sensors collecting the data are directly attached on the surface of the brain. In order to do that, a surgery has been operated to open the skull and attached these sensors on the surface of the brain. The data was collected for several days, then the physician took the sensors out and recovered the wound. During the recording time, the patient stayed in the hospital and under intense watch to make sure everything under control. The subdural EEG signal is a collected information of the potential activity from the surface of brain by using electronic instruments. The recorded potential is the responses from the thousand active neurons of the brain or noises generated from the muscle, eye blinks and artifacts. The EEG machine is the instrument tools with some adjustable parameters to record and store the data. Different setting of the parameters will affect the recorded EEG data. In order to get the best information for the epilepsy analysis, it needs to pre-process the EEG data carefully in order to get best quality data. The raw EEG data has been pre-processed before applied by the proposed separation methods.

There are total 102 data channels to collected the EEG, EKG and EMG signal from 102 electrodes. The first 64 electrodes are put on the frontal area of brain which 32 electrodes are on the left side and 32 electrodes are on the right side. The upper inter-center region of the brain has covered with 32 channels which each 16 electrodes are on the right and left sides. There are two electrodes were used to record EKG signal. The last 4 electrodes are used to record the EMG signal which contains muscle

activities and eye ball movements. The montage is shown on Fig. A-1 and label names of each channel can be found on table B-1 to B-4 in the appendix B. Note that the upper inter-center electrodes are not shown in correct positions; it draws lower than it should be. These electrodes are located on the very upper area of head and each right and left electrodes are adjacent to each other where they are attached on the right and left hemisphere of the brain.

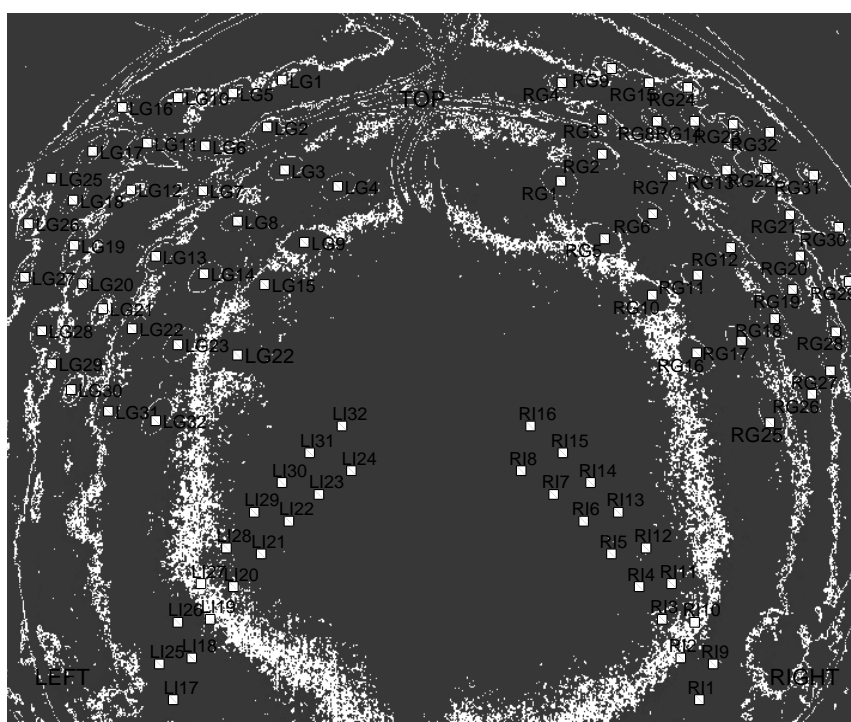


**Figure A-1** Montage of Subdural EEG. There are total 102 electrodes used to record the EEG data. In this figure, it only contains 94 channels and the rest of electrodes are used to record EKG and EMG data.

The EEG data is recorded as UNIQUANT file format which is designed from the NCI (Network Concepts, Inc.) (65). It has developed a transfer program to convert UNIQUANT file format to plain binary data. Two EEG machines are used to record these potentials of 102 channels, which each machine handled 51 channel separately. These two machines are made from the same manufacturer and have a identical

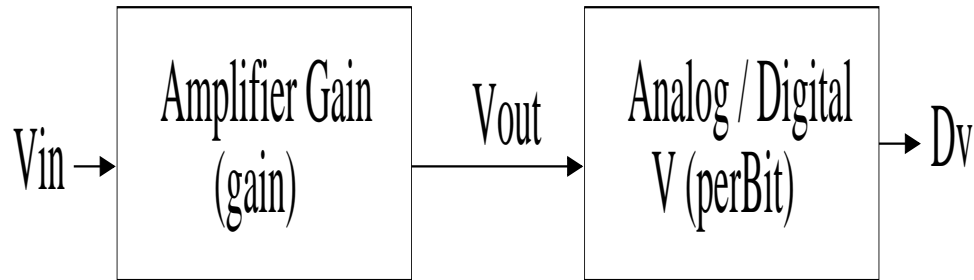


**Figure A-2** The Analog to Digital Conversion

configuration. Therefore, the amplifier and A/D converter are the same for both machine. The method used to record EEG signal is called bipolar recording, which the sensor can measure the differences between the target channel and a reference, see appendix C for different montage layout. The potential is an analog signal measured by the differences between the target channel and the reference point, where a A/D convertor transferred the analog signal to a digital format. The digital information will be the value stored in the storage device. In this case, the analog signal is converted as a 12-bit digital value and the conversion of A/D converter is between [0 4095] and its voltage range is between -625 and 625  $\mu$ . The conversion of analog signals to digital values involves two steps: One is amplifier gain and the other is analog to digital conversion (see Fig. A-2). The equations for the conversions are:

$$V_{out} = V_{in} \times gain, \quad (\text{A-1})$$

$$D_v = \frac{V_{out}}{V_{in}} + 2047 = \frac{V_{in} \times gain}{V_{perBit}} + 2047. \quad (\text{A-2})$$

To convert an offset binary digital value ( $D_v$ , 0-4095) to its original input potential ( $V_{in}$ ) one should use

$$V_{in} = \frac{(D_v - 2047) \times V_{perBit}}{gain}. \quad (\text{A-3})$$

The values for  $V_{perBit}$  (stored as  $\mu V$  per bit) and gain are stored in the EEG data file.

The two machines used to record the subdural EEG signal are not synchronized with each other. The sampling rate of both Each machine are 250 Hz, but each one is operated by its own clock to record data. The two recorded EEG data may have time shifting due to the synchronization problem. The analysis of EEG signal is very critical to the timing. The slight time shifting of two machine can cause a different results. A correction is given to perfectly align two EEG data sets. The two machines have monitored the EKG information separately, which are measured the same variation of heart activity. It gave a very accurate time index to measure the shifting between the two machines. It has examined the EKG data recording and found that the peak of heart beat can be aligned perfectly with two machine. However, between the peaks, the two EKG signals look different, because the two machines are using different references. The heart beat is a strong signal generating large amplitude pulse, which is affected less by the references.

We used least mean square error to find the minimum error of the peak-to-peak duration between the two EKG. Let the EKG data of the first machine be  $EKG_l$  and  $EKG_r$  be the second machine. Note the  $l$  and  $r$  are indexed as left and right.

$$LMS = \min_s ((EKG_l(t) - EKG_r(t + s))^2), \quad (\text{A-4})$$

where  $E$  is the error and  $s$  is the shift points. The minimum error  $LMS$  is found when  $EKG_r$  is shifted by  $s$  points. The method of least mean square error can find the optimal shift point which has the minimum peak-to-peak error between two EKG signals. If the error is being minimized, then  $EKG_r$  will be aligned together with  $EKG_l$  by moving  $s$  points. If the EKG has been synchronized, then the EEG data can be synchronized, too. It has been cross-examined the least mean square error method by using the correlation between two EKG data. After finding the optimal time shift  $s$ , it calculates the correlation between the well-alignment data. If the peak of the

correlation result is at center point, it means that it has largest similarity already and it is being aligned perfectly. After perfectly aligned, a visual examination show the EKG can use as good indication to measure the shift time. It is not common to have an alignment problems in the EEG recording. It happened because that the number of channels to record EEG data are larger than the capacity of a EEG machine and separated machines can not be synchronized with each other.

The other problem occurred this data set is the A/D conversion. During the conversions, if the amplitude of the potential is higher than the maximum range of A/D converter can handle, it will generate a saturation affection. If a saturation affection appearing, the convertor records the amplitude as its maximum digital number even it should be larger. The saturation affection also happened when the amplitude is lower than the minimum range of convertor. It is the same as the maximum saturation only it is opposite on the other direction. Because the physical limitation and setting of the EEG machine, the raw EEG data has a short flat line either on the top of positive spikes or the bottom of negative spikes. These artifacts are coming from the saturation affection. To correct this type of error, we have used the spline interpolation on the flat region to approximate the variation of spikes. It used the neighboring points near the flat saturation line to implement a linear interpolation to approximate the signal.

The bipolar recording need a reference point to record the differences between the electrodes and the reference. During the recording time, each machine had used different reference which caused a alias problem. Bipolar method can only recorded the potential differences between the channels and reference. If the references for each machine is not the same, then the difference recording on each machine will be varied by their reference points. The reference used on the first machine is the

montage “LG24” and the electrode “RG25” for the second one. The EEG data is recorded by two same model machines. It is assumed that the recording data are not affected by using these machines. But each EEG machine has used different reference and each reference have its own activity during the recording. The variation of the references make the recording EEG data changes time by time. If the EEG data changed dramatically, it is possible that the reference varied quickly and the remaining electrodes are not changed. The results of bipolar recording from the both machine could not really show the true activity of the brain.

Due to the bias caused from the reference, it tried to cut the affection of the varied reference. Let  $e_i(t)$  be the real potential of electrode  $i$  at the time  $t$  and  $e_r(t)$  be the actual potential of the reference. There are total  $n$  electrodes attached on the brain. The EEG machine recorded a potential value  $\hat{e}_i$  from the channel  $i$ . The  $\hat{e}_i(t)$  is measured from the differences between the potential of  $e_i(t)$  and  $e_r(t)$ .

$$\hat{e}_i(t) = e_i(t) + e_r(t), i = 1, \dots, n, \quad (\text{A-5})$$

where  $n$  indicates the channel number. If the average of the total measured potential  $\hat{e}_i(t)$ , it derived as

$$\begin{aligned} \frac{1}{n} \sum_{i=1}^n \hat{e}_i(t) &= \frac{1}{n} \sum_{i=1}^n (e_i + e_r)(t) \\ &= \frac{1}{n} \sum_{i=1}^n e_i(t) + \frac{1}{n} \sum_{i=1}^n e_r(t) \\ &= \frac{1}{n} \sum_{i=1}^n e_i(t) + e_r(t) \end{aligned} \quad (\text{A-6})$$

Equation (A-6) shows a linear function. It is assumed that human brain is an independent system and isolated from the outside world. The summation of potential from an this independent system is zero. The summation of the potential  $\hat{e}_i(t)$  is equal

to zero, shown as

$$\sum_{i=1}^n e_i(t) = 0. \quad (\text{A-7})$$

From equation A-6 and A-7, it can be derived

$$\begin{aligned} \frac{1}{n} \sum_{i=1}^n \hat{e}_i(t) &= \frac{1}{n} \sum_{i=1}^n e_i + e_r(t) = 0, \\ &= e_r(t). \end{aligned} \quad (\text{A-8})$$

The average potential of the reference electrode is equal to  $-e_r$ . One can derive

$$e_r(t) = \frac{1}{n} \sum_{i=1}^n \hat{e}_i(t). \quad (\text{A-9})$$

If the number of electrodes is large enough, equation (A-9) shows that the mean of bipolar measured potentials is equal to the potential of reference electrode.

The distortion of using separated references of the two machine can be eliminated by cutting the potential of the reference. To recover the real potential  $e_i$ , one can use the following method

$$\begin{aligned} e_i(t) &= \hat{e}_i(t) - \text{mean}(e_r(t)) \\ &= \hat{e}_i(t) - \frac{1}{n} \sum_{i=1}^n \hat{e}_i(t) \\ &= \hat{e}_i(t) - \text{mean}(\hat{e}_i(t)) \end{aligned} \quad (\text{A-10})$$

Equation (A-10) is called common-reference recording method. Theoretically, this method is a reference free method. To reduce the affection of the variation of references, it has been suggested that one can attach the reference on the ear in most cases. The ear has less neuro activity and the potential are varied relatively less than other area. Normally, the stability of the reference provides a better measurements.

The DC voltage will distort the natural of signal, such as mean value and energy or power. A good calibration can reduce the errors of DC affection, but it is normally

very hard to avoid it at all. If the amount of a signal is larger enough, the DC offset will show on the mean of the signal. The mean will be shifted with the DC offset. Because the human brain is an independent system, which the summation of all potentials is equal to zero. We have picked a segment of EEG data to calculate the mean value. Then the mean value of this segment is assumed as the DC offset of the machine. To get rid of the DC offset, this segment EEG data must minus the mean value. In the practical application, we have used one minute EEG data to be the length of each epoch. The sampling rate is 250 Hz, it means that one epoch contains total 15000 ( $250 \times 60$ ) sampling points. The mean of the potential measurement is based on the one minute long.

## APPENDIX B

## APPENDIX B Collection of EEG Data

The electroencephalography (EEG) is a the brain signal recorded either from the electrodes on surface of the human skull or the sensors directly attached on the brain. The second one is also called as subdural EEG signal. The subdural EEG signal provides better informations of brain activity. It is because it avoids the damping effect of the skull.

The subdural EEG data used in the paper is recorded at the end of October, 1998 at Children hospital, University of Pittsburgh, Pittsburgh, PA. There are total 102 channels used to collect EEG, EKG, muscle activities and eye ball movements. The first 64 electrodes are put on the frontal area of brain which 32 electrodes are on the left side and 32 electrodes are on the right side. The center region of the brain has put each 16 electrodes on the both right and left sides. The other two electrodes were used to record EKG. The last 4 electrodes are used to record the muscle activities and eye ball movements. The label of each channel can be found on table B-1 to B-4. The montage of these electrodes are shown on Fig. A-1. This montage is trying to collect the brain activity of the area of frontal lobe and temporal lobe. The EKG, muscle activity and eye ball movement are the extra information related the brain signal.

**Table B-1** Electrodes on the Frontal Area

Electrodes Name	Description	Electrodes Name	Description
LG1	Left Frontal	RG1	Right Frontal
LG2	Left Frontal	RG2	Right Frontal
LG3	Left Frontal	RG3	Right Frontal
LG4	Left Frontal	RG4	Right Frontal
LG5	Left Frontal	RG5	Right Frontal
LG6	Left Frontal	RG6	Right Frontal
LG7	Left Frontal	RG7	Right Frontal
LG8	Left Frontal	RG8	Right Frontal
LG9	Left Frontal	RG9	Right Frontal
LG10	Left Frontal	RG10	Right Frontal
LG11	Left Frontal	RG11	Right Frontal
LG12	Left Frontal	RG12	Right Frontal
LG13	Left Frontal	RG13	Right Frontal
LG14	Left Frontal	RG14	Right Frontal
LG15	Left Frontal	RG15	Right Frontal
LG16	Left Frontal	RG16	Right Frontal
LG17	Left Frontal	RG17	Right Frontal
LG18	Left Frontal	RG18	Right Frontal
LG19	Left Frontal	RG19	Right Frontal
LG20	Left Frontal	RG20	Right Frontal
LG21	Left Frontal	RG21	Right Frontal
LG22	Left Frontal	RG22	Right Frontal
LG23	Left Frontal	RG23	Right Frontal
LG24	Left Frontal	RG24	Right Frontal
LG25	Left Frontal	RG25	Right Frontal
LG26	Left Frontal	RG26	Right Frontal
LG27	Left Frontal	RG27	Right Frontal
LG28	Left Frontal	RG28	Right Frontal
LG29	Left Frontal	RG29	Right Frontal
LG30	Left Frontal	RG30	Right Frontal
LG31	Left Frontal	RG31	Right Frontal
LG32	Left Frontal	RG32	Right Frontal

**Table B-2** Electrodes on the Central Area of Brain

Electrodes Name	Description	Electrodes Name	Description
LI17	Left Middle	RI1	Right Middle
LI18	Left Middle	RI2	Right Middle
LI19	Left Middle	RI3	Right Middle
LI20	Left Middle	RI4	Right Middle
LI21	Left Middle	RI5	Right Middle
LI22	Left Middle	RI6	Right Middle
LI23	Left Middle	RI7	Right Middle
LI24	Left Middle	RI8	Right Middle
LI25	Left Middle	RI9	Right Middle
LI26	Left Middle	RI10	Right Middle
LI27	Left Middle	RI11	Right Middle
LI28	Left Middle	RI12	Right Middle
LI29	Left Middle	RI13	Right Middle
LI30	Left Middle	RI14	Right Middle
LI31	Left Middle	RI15	Right Middle
LI32	Left Middle	RI16	Right Middle

**Table B-3** Electrodes for Muscle and Eye Ball

Electrodes Name	Description	Electrodes Name	Description
LEMG	Left Muscle	REMG	Right Muscle
LOC	Left Eye Ball	ROC	Right Eye Ball

**Table B-4** Electrodes for EKG

Electrodes Name	Description	Electrodes Name	Description
LEKG	EKG	REKG	EKG

## APPENDIX C

## APPENDIX C The Montage of EEG Recording

The EEG data is recorded from EEG recording machine which can measure the potential variations (similar to voltage) generated from brain cells. It converts the biological brain signal into digital signal by using A/D (analog/digital) hardware acquisition method. In order to collect the signal, there are many electrodes attached on the human brain. The number of sensors is up to requirement. In our cases, it has been used 32 to 64 sensors. It could go up to more 100 hundred sensors. The EEG electrodes are often made with gold, having the size in the range in millimeters to about one centimeter. To measure the variation of potential generating from the neuro cells, it needs a circuit ground to form a close circuit. Depending on the ground reference, there are several montage methods to inspect the EEG potential. These methods are named as: referential montage, bipolar montage and common reference montage. These methods are described as follows:

1. The first EEG recording method is called as “referential montage”. In this method, every electrodes are measured the potential differences referred to a extra electrode which normally placed on a area with less neurons activity, such as ears. This EEG data recorded by referential method is called as raw EEG data in this paper.
2. The second methods called as “bipolar montage” which most clinical usages are based on this montage. The bipolar method is a calibration method revised from the referential recording. Bipolar montage is a user defined montage. Let electrodes  $e_1, e_2, \dots, e_n$  be raw value from the referential montage and the bipolar montage will be defined as  $e_1 - ref_1, e_2 - ref_2, \dots, e_n - ref_n$ , where  $ref_i$  could be any electrode recording  $e_k$ . There is no general rules to assign the

bipolar montage. It will depend on the clinical usage and need expert to modify them and sometimes several bipolar montages will be inspected simultaneously. The advantage of the bipolar montage is to promote an anti-phase relationship between the two electrode locations. Switching one montage to another montage may be very easy, but to find a best montage to show the status is a not an easy task.

3. The last montage is called as “common reference montage”. The common reference montage is very similar to the referential montage. Both montages are trying to referred the EEG recording into one electrode. But the common reference montage is referred from a computed (modified) reference point. The common reference montage is based on the assumption of the volume conductivity is total zero for the outside the volume.

The raw EEG data is normally collected by using referential recording method. All the channel is referred to one ground point which this point is placed on the surface of the human scalp such as ears or other places. The referential point has less brain activity because there are not many brain cells near this region. EEG machine then read the differences of the potential between the reference and sensors. But the reference is not absolutely no activity, it turns out that the ground point of the closed circuit is dynamically changed. Because the variation of ground activity, the raw EEG data is also changing depending the stability of the referential point. For example, if the generated brain activity of one sensor is similar to the activity of the referential area, the potential between them are zero and the EEG recording will be low. But it does not mean the brain cell is less active at the sensor region, it only indicates at that time, brain has relatively less differences. To reduce this effect, it can use the common

reference method to get the theoretical global ground of all the channels.

The mathematical description of these montage is shown as follows: Let the potential  $P_i$  is the real potential of channel  $i$  and voltage  $V_i$  is the measured voltage from a EEG recording machine between channel potential  $P_i$  and the potential of the reference ground. The reference channel is labeled as  $P_0$ . It has assumed that the EEG machine has no any artificial artifact and noise at all.

The measured voltage is

$$\begin{aligned}
 V_1 &= P_1 - P_0 \\
 V_2 &= P_2 - P_0 \\
 &\dots \\
 V_i &= P_i - P_0
 \end{aligned} \tag{C-1}$$

The common reference  $V_c$  is defined as the average of every channels' voltage:

$$\begin{aligned}
 V_c &= \frac{1}{N} \sum_{i=1}^N V_i \\
 &= \frac{1}{N} \sum_{i=1}^N (P_i - P_0) \\
 &= \frac{1}{N} \sum_{i=1}^N P_i - \frac{1}{N} \sum_{i=1}^N P_0 \\
 &= \frac{1}{N} \sum_{i=1}^N P_i - P_0
 \end{aligned} \tag{C-2}$$

The common reference voltage  $\tilde{V}_l$  of the channel is defined as:

$$\begin{aligned}
 \tilde{V}_l &= V_l - V_c \\
 &= (P_l - P_0) - \left( \frac{1}{N} \sum_{i=1}^N P_i - P_0 \right) \\
 &= P_l - \frac{1}{N} \sum_{i=1}^N P_i
 \end{aligned} \tag{C-3}$$

Picking any two new common reference voltage  $\tilde{V}_l$  and  $\tilde{V}_m$ , one can get a bipolar montage shown as:

$$\begin{aligned}\tilde{V}_l - \tilde{V}_m &= (P_l - \frac{1}{N} \sum_{i=1}^N P_i) - (P_m - \frac{1}{N} \sum_{i=1}^N P_i) \\ &= P_l - P_m\end{aligned}\tag{C-4}$$

The normal bipolar montage of channels  $l$  and  $m$  is

$$\begin{aligned}V_l - V_m &= (P_l - P_0) - (P_m - P_0) \\ &= P_l - P_m\end{aligned}\tag{C-5}$$

From Eq. (C-4) and (C-5), one can find that the bipolar montage is not related with the reference ground.

## APPENDIX D

## APPENDIX D International 10-20 System

The international 10-20 system (6) is widely used in EEG recording, see Fig. D-1. Each electrode are placed and named after the anatomical structure of the human brain. The name of electrodes begin with capital letter {F;C;P;T;O} which related with lobe of brain: Frontal, Central, Parietal, Temporal, Occipital. The extra one 'Fp' means Front polar. After the capital letter, it follows a numerical number to indicate exact location of the lobe. The electrodes placed on the brain are geometrically divided. The inter-electrode distance is defined as follows: the odd number 1,3,5,7,9 are on the left side which designate 10%, 20%, 30%, 40%, 50% of inion-nasion distance, and the even number 2,4,6,8,10 are used on the right side. The "10" and "20" refer to the 10% or 20% of the inter-electrode distance. Fig. D-2 shows the top and side view of the electrode placement of the international 10-20 system.

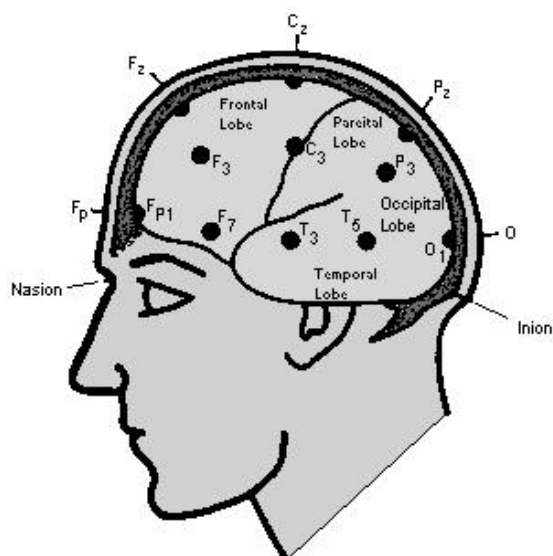
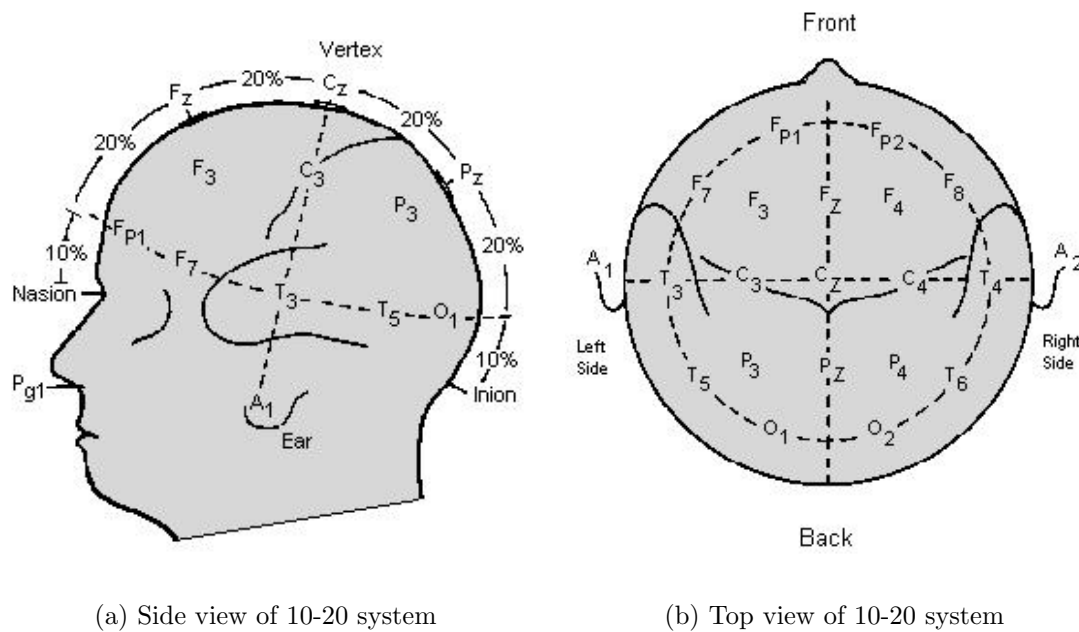


Figure D-1 International 10-20 system



(a) Side view of 10-20 system

(b) Top view of 10-20 system

**Figure D-2** The electrode placements of the 10-20 system

## APPENDIX E

## APPENDIX E The Bi-Directional Spike Detection in EEG Using Morphological Filtering in Wavelet Transform

Combining mathematical morphology and wavelet transforms, the proposed method successfully separates the background activity and transient phenomenon from epileptic EEG. The spikes have pointed peak toward positive or negative directions. Although the morphological operation is a non-linear process, we show that, with the selected structuring element, it has a ability to detect both directional spikes identically, except for a sign difference. If a function  $f(x)$  is a linear process, it obeys  $\Phi(af(x)) = a\Phi(f(x))$ , where  $a \in R$  and if  $\Phi$  is a linear operator. However, the morphological operation  $\Psi$  is a non-linear process which means  $\Psi(af(x)) \neq a\Psi(f(x))$ . If two pointed spikes are identical except their sign (“+” is for upward peaks and “-” for downward ones), it indicates the scalar  $a$  equal to  $-1$ . In this case the separations two identical spikes with different signs, the upward spikes should be no difference from the downward ones except for the sign difference. Generally, the nonlinear morphological process cannot reach this. But our structuring element has the ability to correctly extract the bi-directional spikes.

This multiresolution morphological separation method is capable of extracting identical spikes with different directions identically, except for their direction signs. It is because that the structuring element is symmetrical at the point of origin. The proof is shown as follows:

The morphological operations have the following properties (25):

**Definition 10.**  $\forall t \in R, t[f \oplus g] = tf \oplus tg,$

**Definition 11.**  $\forall t \in R, t[f \ominus g] = tf \ominus tg.$

The  $t$  is any real number and the morphological operators  $\oplus$  and  $\ominus$  are referred as the Minkowski addition and subtraction, see chapter 2. Let signal  $f(n) \subset \mathbb{E}$ , where  $\mathbb{E}$  represents the Euclidean spaces and  $n = 1, 2, \dots, N$ . Using the umbra concept, the morphological operations can be extended to a gray-level signal. The structuring element  $g \subset \mathbb{E}$  is a solid disk with unit length and its center is located at the origin. A reflection operation of the signal  $g$  is defined as  $\check{g}(n) = -g(-n)$  which it rotates  $180^\circ$  around the origin. The pre-requisite structuring element is symmetric with respect to the origin. Let  $g_c$  be the disk, It can be shown that  $\check{g}_c(n) = g_c(n)$ ,  $g_c(n) = g_c(-n)$ ,  $\check{g}_c(n) = g_c(-n)$ . Let the  $M_f^{g_c}(-f)$  be the proposed morphological filter processes the negative input signal  $-f$  and combining the property 10 and 11, we have:

$$\begin{aligned}
M_f^{g_c}(-f) &= (-f \circ g_c) \bullet g_c \\
&= ((((-f \ominus \check{g}_c) \oplus g_c) \oplus \check{g}_c) \ominus g_c) \\
&= (((-(f \ominus -\check{g}_c) \oplus g_c) \oplus \check{g}_c) \ominus g_c) \\
&= ((-((f \ominus -\check{g}_c) \oplus -g_c) \oplus \check{g}_c) \ominus g_c) \\
&= (-(((f \ominus -\check{g}_c) \oplus -g_c) \oplus -\check{g}_c) \ominus g_c) \\
&= -((((f \ominus -\check{g}_c) \oplus -g_c) \oplus -\check{g}_c) \ominus -g_c) \\
&= -((((f \ominus \check{g}_c) \oplus g_c) \oplus \check{g}_c) \ominus g_c) \\
&= -M_f^{g_c}(f) \tag{E-1}
\end{aligned}$$

The sign of signal  $f$  indicates the direction of the signal. If the positive sign represents the upward spike, then the minus sign represents the downward spike. Equation (E-1) shows that the bi-directional signal will not be affected using the morphological process with the selected structuring element except the direction sign. The reason is that the symmetrical disk plate located at the origin has no geometrical distortion on the input bi-directional signal.

## **BIBLIOGRAPHY**

## BIBLIOGRAPHY

1. Bender R., Schultz, A., and Pichlmayr, I., Testing the Gaussianity of the Human EEG During Anesthesia, Methods of Information in Medicine, vol. 31, pp. 56-59, 1992.
2. Bergeaud, F. and Mallat, S., Matching Pursuit: Adaptive Representations of Images and Sounds, Computational and Applied Mathematics, vol. 15, no. 2, Birkhauser, Boston, 1996.
3. Bertrand, O., Bohorquez J., and Pernier, J., Time-Frequency Digital Filtering Based on an Invertible Wavelet Transform: An Application to Evoked Potentials, IEEE Transactions on Biomedical Engineering, vol. 41, no. 1, Jan 1994, pp. 77-88.
4. Blanco, S., Quian Quiroga, R., Rosso, O. A., and Kochen, S., Time-Frequency Analysis of Electroencephalogram Series, Physical review E, vol. 51, no. 3, pp. 2624-2631, 1995.
5. Blanco, S., Kochen, S., Rosso Q. A., and Salgado, P., Applying Time-Frequency Analysis to Seizure EEG Activity, IEEE Engineering in Medicine and Biology, Jan/Feb, 1997, pp. 64-71.
6. Böcker, K. B. E., van Avermaete, J. A. G. and van den Berg-Lenssen, M. C., The International 10-20 System Revisited: Cartesian and Spherical Co-ordinates, Brain Topography, vol. 6, no. 3, pp. 231-235, 1994.
7. Bodenstern G., and Praetorius, H. M., Feature extraction from the electroencephalogram by adaptive segmentation, Proc. IEEE, vol. 65, pp. 642-652, 1977.
8. Calderbank, R. C., Daubechies, I., Sweldens, W. and Yeo B. L. Wavelet Transforms that Map Integers to Integers Applied and Computational Harmonic Analysis (ACHA), Vol. 5, Nr. 3, pp. 332-369, 1998.
9. Carrie, J. R. A., A hybrid Computer Technique for Detecting Sharp EEG Transients, Electroencephalography and Clinical Neurophysiology, vol. 33, pp. 336-338, 1972.
10. Cha, H., and Chaparro, L. F., Adaptive Morphological Representation of Signals: Polynomial and Wavelet Methods, Multidimensional Systems and Signal Processing, 8, pp. 249-271, 1997.
11. Chen, M. H., and Yan, P. F., A Multiscaling Approach based on Morphological Filtering, IEEE Transactions on Pattern Analysis and Machine Intelligence, vol. 11, no. 7, pp. 694-700, 1989.

12. Chen, C. S., Wu, J. L., and Hung, Y. P., Statistical Analysis of Space-Varying Morphological Opening with Flat Structuring Elements, IEEE Transactions on Signal Processing, vol. 44, no. 4, pp. 1010-1014, 1996.
13. Chen, C. S., Wu, J. L., and Hung, Y. P., Theoretical Aspects of Vertically Invariant Gray-Level Morphological Operators and Their Application on Adaptive Signal and Image Filtering, IEEE Transactions on Signal Processing, vol. 47, no. 4, pp. 1049-1060, 1999.
14. Choi, H. I., and Williams, W. J., Improved Time-Frequency Representation of Multicomponent Signals Using Exponential Kernels, IEEE Transactions on Acoustics, Speech, and Signal Processing, vol. 37., no. 6, pp. 862-871, 1989.
15. Chui, C. K., Wavelet Analysis and its Applications, New York: Academic Press, 1992.
16. Chatrian, G. E., Bergamini, L., Dondey, M., Klass, D. W., Lennox M., Buchthal, and I. Petersen, I., A Glossary of Terms Most Commonly used by Clinical Electroencephalographers, Electroencephalography and Clinical Neurophysiology, vol. 37, pp. 538-548, 1974.
17. Cohen, L., Time-Frequency Distributions - A Review, Proceedings of the IEEE, vol. 77, no. 7, pp. 941-981, 1989.
18. Crimmins, T. R., and Brown, W. M., Image Algebra and Automatic Shape Recognition, IEEE transactions on aerospace and electronic systems, vol. 21, pp. 60-69, 1985.
19. Crowe J. A., Wavelet transform as a potential tool for ECG analysis and compression, J. Biomed. Eng., vol. 14, 1992, pp. 269-272.
20. Daubechies, I., Sweldens, W., Factoring Wavelet Transforms into Lifting Steps, J. Fourier Anal. Appl., vol. 4, no. 3, pp. 247-269, 1998.
21. Dingle, A. A., Jones, R. D., Carroll, G. J., and Fright, W. R., A Multistage System to Detect Epileptiform Activity in the EEG, IEEE Transactions on Biomedical Engineering, vol. 40, pp. 1260-1268, 1993.
22. Donoho, D. L. and Johnstone I. M. , Ideal Spatial Adaptation by Wavelet Shrinkage, Biometrika, 81, pp. 425-455, 1994.
23. Florian G., and Pfurtscheller, G., Dynamic Spectral Analysis of Event-Related EEG Data, Electroencephalography and Clinical Neurophysiology, pp. 393-396, 1995.
24. Gath, I., Feuerstein, C., Pham, D. t., and Rondouin, G., On the Tracking of Rapid Dynamic Changes in Seizure EEG, IEEE Transactions on Biomedical Engineering, vol. 39, no. 9, pp. 952-958, 1992.

25. Giardian, C. R., Dougherty, E. R., Morphological Methods in Image and Signal Processing, Englewood Cliffs, N.J., Prentice-Hall, 1988.
26. Glover, J. R., Ktonas, P. Y., Raghavan, N., Uruñuela, J. M., Velamuri, S. S., and Reilly, E. L., A Multichannel Signal Processor for the Detection of Epileptogenic Sharp Transients in the EEG, IEEE Transactions on Biomedical Engineering, vol. 33, no. 12, pp. 1121-1128, 1989.
27. Glover, J. R., Raghavan, N. Jr., Ktonas, P. Y., and Frost, J. D. Jr., Context-Based Automated Detection of Epileptogenic Sharp Transients in the EEG: Elimination of False Positives, IEEE Transactions on Biomedical Engineering, vol. 36, no. 5, pp. 519-527, 1989.
28. Goetcherian, V., From Binary to Grey Tone Image Processing Using Fuzzy Logic Concepts, Pattern Recognition, vol. 12, pp. 7-15, 1980.
29. Gotman J., Automatic Recognition of Interictal Spikes, In: Long-Term Monitoring in Epilepsy, Supplement 37 to Electroencephalography and Clinical Neurophysiology, Edited by J. Gotman, J. R. Ives and P. Gloor, Elsevier, Amsterdam, New York: Elsevier, pp. 93-114, 1985.
30. Gotman, J., and Wang, L. Y., State-Dependent Spike Detection: Concepts and Preliminary Results, Electroencephalography and Clinical Neurophysiology, vol. 79, pp. 11-19, 1991.
31. Goutsias J., and Heijmans, H. J.A.M., Multiresolution Signal Decomposition Schemes. Part 1: Linear and Morphological Pyramids, IEEE Transactions Image Processing, 9 (11), Nov 2000, pp. 1862–1876.
32. Grieszbach, G., Schack, B., Putsche, P., Bareshova, E., and Bolten, J., Dynamic Description of Stochastic Signal by Adaptive Momentary Power and Momentary Frequency Estimation and its Application in Analysis of Biological Signals, Medical & Biological Engineering & Computing, vol. 32, pp. 632-637, 1994.
33. Hadwiger, H., Vorslesungen Über Inhalt, Oberfläche und Isoperimetrie, Springer, Berlin, 1957.
34. Heijmans, H. J. A. M., and Ronse, C., The Algebraic Basis of Mathematical Morphology I. Dilations and Erosions, Computer Vision, Graphics, and Image Processing, 50, 245-295, 1990.
35. Heijmans, Henk J.A.M., and Goutsias, J., Morphology-based perfect reconstruction filter banks, Proceedings of the IEEE-SP International Symposium on Time-Frequency and Time-Scale Analysis, Oct 6-9, 1998, Pittsburgh, PA, USA, pp. 353-356.

36. Heijmans, H. J. A. M., and Goutsias, J., Constructing Morphological Wavelets with the Lifting Scheme, Pattern Recognition and Information Processing, Proceedings of the Fifth International Conference on Pattern Recognition and Information Processing (PRIP 99), Minks, Belarus, May 18-20, 1999, pp. 65-72.
37. Heijmans, H. J.A.M. and Goutsias, J., Multiresolution Signal Decomposition Schemes: Part 2: Morphological Wavelets, IEEE Transactions Image Processing, 9 (11), Nov 2000, pp. 1897–1913.
38. Kenneth Hoffman, Linear Algebra, second edition, Prentic-Hall Inc. New Jersey, 1971.
39. Isaksson, A., Wennberg, A., and Zetterberg, L. H., Computer Analysis of EEG Signals with Parametric Models, Proceeding of the IEEE, vol. 69, no. 4, pp. 451-461, 1981.
40. Inouye, T., Iyama, A., Shinosaki, K., Toi, S., and Matsumoto, Y., Inter-Site EEG Relationships before Widespread Epileptiform Discharges, International Journal of Neuroscience, vol. 82, pp. 143-153, 1995.
41. James, C. J., Hagan, M. T., Jones, R. D., Bones, P. J., and Carroll, G. J., Multireference Adaptive Noise Cancelling Applied to the EEG, IEEE Transactions on Biomedical Engineering, vol. 44, no. 8, pp. 775-779, 1997.
42. Johnstone, I. M. and Silverman, B. W., Wavelet Threshold Estimators for Data with Correlated Noise, J. Roy. Statist. Soc. B, 59, pp. 319-351.
43. Jones, R. D., Dingle A. A., Carroll, G. J., Green, R. D., Black M., Donaldson, I. M., Parkin, P. J., Bones, P. J., and Burgess, K. L., A System for Detecting Epileptiform Discharges in the EEG: Real-Time Operation and Clinical Trial, Engineering in Medicine and Biology Society, 1996. Bridging Disciplines for Biomedicine., 18th Annual International Conference of the IEEE, vol. 3, 1997, pp. 948-949.
44. Khan, Y.U. and Tarassenko, L. Detection of interictal epileptic events in EEG using ANN, Artificial Neural Networks, Fifth International Conference on(Conf. Publ. No. 440), pp. 318-322, 1997.
45. Kobayashi, K., Ohtsuka, Y., Oka, E., and Ohtahara, S., Primary and Secondary Bilateral Synchrony in Epilepsy: Differentiation by Estimation of Interhemispheric Small Time Differences During Short Spike-Wave Activity, Electroencephalography and Clinical Neurophysiology, vol. 83, pp. 93-103, 1992.
46. Kreyszig, E., Introductory Functional Analysis with Applications, John Wiley & Sons. Inc. New York, 1978.

47. Ktonas, P. Y., Automated Spike and Sharp Wave (SSW) Detection, in Methods of Analysis of Brain Electrical and Magnetic Signals, EEG Handbook (revised series, vol. 1), A. S. Gevins and A. Remond, Eds. Amsterdam: Elsevier, pp. 211-241, 1987.
48. Lewis, A.S., and Knowles, G., Image Compression Using 2-D Wavelet Transform, IEEE Transaction on Image Processing, vol. 1, no. 2, pp. 244-250, Apr, 1992.
49. Li, C., Zheng, C., and Tai, C., Detection of ECG Characteristic points using Wavelet Transform, IEEE Transactions on Biomedical Engineering, vol. 42, no. 1, pp. 21-28, 1995.
50. Lopes da Silva, F. H., Dijk A., and Smith, H., Detection of Nonstationary in EEG Using the Autoregressive Model - An Application to EEGs of Epileptics, In: CEAN - Computerized EEG Analysis, Edited by Dolce Giuliano and Künkel Helmut, Gustav Fischer Verlag, Stuttgart, pp. 180-199, 1975.
51. F. H. Lopes Da silva, k. van Hulsten, J. G. Lommen, W. Storm van Leeuwen, C. W. M. van Veelen, and W. Vliegenthart, Automatic Detection and Localization of Epileptic Foci, Electroencephalography and Clinical Neurophysiology, vol. 43, pp. 1-13, 1977.
52. Mallat, S., Zero-Crossings of a Wavelet Transform, IEEE Transactions on Information Theory, vol. 37, no. 4, pp. 1019-1033, 1991.
53. Mallat, S., A Wavelet Tour of Signal Processing, Academic Press, MA, USA, 1998.
54. Maragos, P. and Schafer, R. W., Morphological Skelton Representaion and Coding of Binary Images, IEEE Transactions on Acoustics, Speech, and Signal Processing, vol. 34, no. 8, pp. 1228-1244, 1986.
55. Maragos, P. and Schafer, R. W., Morphological Filters - Part I: Their Set-Theoretic Analysis and Relations to Linear Shift-Invariant Filters, IEEE Transactions on Acoustics, Speech, and Signal Processing, vol. 35, no. 8, pp. 1153-1169, 1987.
56. Maragos, P. and Schafer, R. W., Morphological Filters - Part II: Their Relations to Median, Order-Statistic, and Stack Filters, IEEE Transactions on Acoustics, Speech, and Signal Processing, vol. 35, no. 8, pp. 1170-1184, 1987.
57. Maragos, P., A Representaion Theory for Morphological Image and Signal Processing, IEEE Transactions on Pattern Analysis and Machine Intelligence, vol. 11, no. 6, pp. 586-599, June 1989.

58. Martin, W., and Flandrin, P., Wigner-Ville Spectral Analysis of Nonstationary Process, IEEE Transactions on Acoustics, Speech, and Signal Processing, vol. 33, no. 6, pp. 1461-1470, 1985.
59. Matheron, G., Random Sets and Integral Geometry, John Wiley & Sons, Inc., New York, 1975.
60. Matsopoulos, G. K., and Marshall, S., Medical Applications of Mathematical Morphology, Morphological and Nonlinear Image Processing Techniques, IEE Colloquium on, 1993, pp. 8/1 -8/4.
61. Minkowski, H., Volumen and Oberfläche, Math. Ann., vol. 57, 1903, pp 447-495.
62. Michael D., and Houchin, J., Automatic EEG Analysis: A Segmentation Procedure based on the Autocorrelation Function, Electroencephalography and Clinical Neurophysiology, vol. 46, 1979, pp. 232-235.
63. Meste, O., Rix, H., Caminal, P., and Thakor, N. V., Ventricular Late Potentials Characterization in Time-Frequency Domain by Means of a Wavelet Transform, IEEE Transactions on Biomedical Engineering, vol. 41, no. 7, 1994, pp. 625-634.
64. Morales, A., and Acharya, R., Statistical Analysis of Morphological Openings, IEEE Transaction on Signal Processing, vol. 41, no. 10, Oct 1993, pp. 3052-3056.
65. NCI (Network Concepts, Inc.), UNIQUANT Data File Formats, NCI (Network Concepts, Inc.), WI, 1996.
66. Özdamar, O., Yaylali, I., Jayakar, P., and Lopez C. N., Multilevel Neural Network System for EEG Spike Detection, Computer-Based Medical Systems, 1991. Proceedings of the Fourth Annual IEEE Symposium, 1991, pp. 272 -279.
67. Perkel, D. H., Gerstein, G. L., and Moore G. P., Neuronal Spike Trains and Stochastic Point Processes I. The Single Spike Train, Biophysical Journal, vol. 7, no. 4, 1967, pp. 391-418.
68. Perkel, D. H., Gerstein, G. L., and Moore G. P., Neuronal Spike Trains and Stochastic Point Processes II. Simulataneous Spike Trains, Biophysical Journal, vol. 7, no. 4, 1967, pp. 419-440.
69. Peters, R. A. II, A New Algorithm for Image Noise Reduction Using Mathematical Morphology, IEEE Transaction on Image Processing, vol. 4, no. 5, May 1995, pp. 554-568.
70. Pola P., and Romagnoli, O., Automatic Analysis of Interictal Epileptic Activity Related to Its Morphological Aspects, Electroencephalography and Clinical Neurophysiology, vol. 46, pp. 227-231, 1979.

71. Pon, L-S., Sun M., Sciabassi, R.J., The Bi-Directional Spike Detection in EEG Using Mathematical Morphology and Wavelet Transform, Submitted to In Proc. IEEE/CIE 6th Int. Conf. On signal processing, Beijing, China, 2002.
72. Popescu, S., Trained Wavelets Used to Detect Epileptic Spikes, Proceedings of the IEEE-SP International Symposium on Time-Frequency and Time-Scale Analysis, October, pp. 285-288, 1998.
73. Praetorius, H. M., Bodenstern G., and Creutzfeldt, O. D., Adaptive Segmentation of EEG Records: a New Approach to Automatic EEG Analysis, Electroencephalography and Clinical Neurophysiology, vol. 42, pp. 84-94, 1977.
74. P. Rappelsberger and H. Petsche, Spectral Analysis of the EEG by Means of Autoregression, In: CEAN - Computerized EEG Analysis, Edited by Dolce Giuliano and Künkel Helmut, Stuttgart: Gustav Fischer Verlag, German, pp. 27-40, 1975.
75. Ronse, C., and Heijmans, H. J. A. M., The Algebraic Basis of Mathematical Morphology II. Opening and Closing, Computer Vision, Graphics, and Image Processing:Image Understanding, vol. 54, no. 1, July, 1991, pp 74-97.
76. Ruttimann, U.E., Unser, M., Rawlings, R.R., Rio, D., Ramsey, N.F., Mattay, V.S., Hommer, D.W., Frank, J.A., Weinberger, D.R., Statistical analysis of functional MRI data in the wavelet domain, IEEE Transactions on Medical Imaging, vol. 17, no 2, pp. 142-154, Apr 1998.
77. Saltzberg, B., Lustick, L. S., and Heath, R. G., Detection of Focal Depth Spiking in the Scalp EEG of Monkeys, Electroencephalography and Clinical Neurophysiology, vol. 31, pp. 327-333, 1971.
78. Sankar R., and Goldstein J., Computer-Aided Diagnosis of Epileptiform Transients in EEG, System Theory, 1988., Proceedings of the Twentieth Southeastern Symposium on, pp. 384 -387, 1989.
79. Schack, B., Bareshova E., Grieszbach G. and Witte H., Methods of Dynamic Spectral Analysis by Self-exciting Autoregressive Moving Average Models and Their Application to Analysing Biosignals, Medical & Biological Engineering & Computing, vol. 33, May, 1995, pp. 492-498.
80. Senhadji L., Carrault G. and Bellanger J. J., Detection et Cartographie Multi-Echelles en EEG, Wavelet Analysis and Applications, Y. Meyer and S. Roques. Frontiers, pp. 609-614, 1993.
81. L. Senhadji, J. L. Dillenseger, F. Wendling, C. Rocha, and A. Kinie, Wavelet Analysis of EEG for Three-Dimensional Mapping of Epileptic Events, Annals of Biomedical Engineering, vol. 23, pp. 543-552, 1995.

82. Serra, J., Image Analysis and Mathematical Morphology, 2nd ed., New York: Academic, 1982.
83. Skolnick, M. M., Application of Morphological Transformations to the Analysis of Two-Dimensional Electrophoretic Gels of Biological Materials, Computer Vision, Graphics, and Image Processing, 35, 306-332, 1986.
84. Smith, J. R., Automatic Analysis and Detection of EEG Spike, IEEE Transactions on Biomedical Engineering, vol. 21, no. 1, pp. 1-7, 1974.
85. Song, J. and Delp, E. J., The Analysis of Morphological Filters with Multiple Structuring Elements, Computer Vision, Graphics, and Image Processing, 50, 1990, pp. 308-328.
86. Sternberg, S. R., Biomedical Image Processing, Computer, vol. 16, no. 1, pp. 22-34, 1983.
87. Sternberg, S. R., Grayscale Morphology, Computer Vision, Graphics, and ImageProcessing, vol. 35, pp. 333-355, 1986.
88. Strang, G. and Nguyen, T., Wavelets and Filter Banks, Wellesley-Cambridge Press, Wellesley MA, USA, 1996.
89. Sun, M., and Sciabassi, R.J., Enhancing Weka Signal Components in Time-Frequency Distributions by Wavelet Pre-Processing, In Proc. IEEE ICASSP, 2: 673-676, 2000.
90. Suzuki, S., and Abe, K., New Fusion Operations for Digitized Binary Images and Their Applications, IEEE Transactions on Pattern Analysis and Machine Intelligence, vol. 7, pp. 638-651, 1985.
91. Sweldens, W., The Lifting Scheme: A new philosophy in biorthogonal wavelet constructions, In A. F. Laine and M. Unser, editors, Wavelet Applications in Signal and Image Processing III, pp. 68-79, Proc. SPIE 2569, 1995.
92. Sweldens, W., The Lifting Scheme: A Custom-Design Construction of Biorthogonal Wavelets, Journal of Applied and Computation Harmonic Analysis, 3(2), pp. 186-200, 1996.
93. Sweldens, W., Building your own wavelets at home, Wavelets in Computer Graphics, ACM SIGGRAPH Course Notes, 1996.
94. Trahanias, P.E., An approach to QRS Complex Detection Using Mathematical Morphology, IEEE Transactions on Biomedical Engineering, vol. 40, no. 2, pp. 201-205, Feb 1993.

95. Unser, M., Wavelets, statistics, and biomedical applications, Statistical Signal and Array Processing, 1996. Proceedings., 8th IEEE Signal Processing Workshop on (Cat. No.96TBI0004 , pp. 244-249, 1996.
96. Unser, M.; Aldroubi, A., A Review of Wavelets in Biomedical Applications, Proceedings of the IEEE, vol. 84, no. 4, pp. 626-638, Apr 1996.
97. Victor, J. D., and Canel, A., A Relation Between the Akaike Criterion and Reliability of Parameter Estimates, with Application to Nonlinear Autoregressive Modelling of Ictal EEG, Annals of Biomedical Engineering, vol. 20, pp. 167-180, pp. 167-180, 1992.
98. Wang J., and Wieser, H. G., Regional "Rigidity" of Background EEG Activity in the Epileptogenic Zone, Epilepsia, vol. 35 (3), 1994, pp. 495-504.
99. Webber, W. R. S., Litt B., Wilson K., and Lesser R. P., Practical Detection of Epileptiform Discharge (ED's) in the EEG using an Artificial Neural Network: A Comparison of Raw and Parameterized EEG data, Electroencephalography and Clinical Neurophysiology, vol. 91, pp. 194-204, 1994.
100. Wendling F., Shamsollahi, J. M., Bellanger J. J., Time-Frequency Matching of Warped Depth-EEG Seizure Observations, IEEE Transactions on Biomedical Engineering, vol. 46, no. 5, pp. 601-605, May 1999.
101. Werman M., and Peleg, S., Min-max Operators in Texture Analysis, IEEE Transactions on Pattern Analysis and Machine Intelligence, vol. 7, pp. 730-733, 1985.
102. Williams, W. J., Zaveri, H. P., and Sackellares, J. C., Time-Frequency Analysis of Electrophysiology Signals in Epilepsy, IEEE Engineering in Medicine and Biology, Mar/April, 1995, pp. 133-143.
103. Witte, H., Eiselt, M., Patakova, I., Petranek, S., Griessbach, G., Krajca, V., and Rother, M., Use of Discrete Hilbert Transformaion for Automatic Spike Mapping: a Methodological Investigation, Medical & Biological Engineering & Computing, vol. 29, pp. 242-248, 1991.